SYNTHESIS AND STUDY OF CRYSTALLINE HYDROGELS, GUIDED BY A PHASE DIAGRAM

Gang Huang, B.E., M.E.

Dissertation Prepared for the Degree of

DOCTOR OF PHILOSOPHY

UNIVERSITY OF NORTH TEXAS

December 2004

APPROVED:

Zhibing Hu, Major Professor
Paul Marshall, Committee Member
Angela Wilson, Committee Member
Teresa Golden, Committee Member
Bruce Gnade, Committee Member
Ruthanne D. Thomas, Chair of the Department of Chemistry
Sandra L. Terrell, Dean of the Robert B. Toulouse School of Graduate Studies

Huang, Gang, Synthesis and study of crystalline hydrogels, guided by a phase diagram. Doctor of Philosophy (Analytical Chemistry), December 2004, 127 pp., 4 tables and schemes, 31 illustrations, references, 114 titles.

Monodispersed nanoparticles of poly-N-isopropylacrylamide-co-allylamine (PNIPAM-co-allylamine) and PNIPAM-co-acrylic acid (AA) have been synthesized and used as building blocks for creating three-dimensional networks. The close-packed PNIPAM-co-allylamine and PNIPAM-co-AA nanoparticles were stabilized by covalently bonding neighboring particles at room temperature and at neutral pH; factors which make these networks amicable for drug loading and release. Controlled release studies have been performed on the networks using dextran markers of various molecular weights as model macromolecular drugs. Drug release was quantified under various physical conditions including a range of temperature and molecular weight. These nanoparticle networks have several advantages over the conventional bulk gels for controlling the release of biomolecules with large molecular weights.

Monodispersed nanoparticles of poly-N-isopropylacrylamide-co-allylamine (PNIPAM-co-allylamine) can self-assemble into crystals with a lattice spacing on the order of the wavelength of visible light. By initiating the crystallization process near the colloidal crystal melting temperature, while subsequently bonding the PNIPAM-co-allylamine particles below the glass transition temperature, a nanostructured hydrogel has been created. The crystalline hydrogels exhibit iridescent patterns that are tunable by the change of temperature, pH value or even protein concentration. This kind of soft and wet

hydrogel with periodic structures may lead to new sensors, devices, and displays operating in aqueous solutions, where most biological and biomedical systems reside.

The volume-transition equilibrium and the interaction potential between neutral PINPAM particles dispersed in pure water were investigated by using static and dynamic light-scattering experiments. From the temperature-dependent size and energy parameters, the Sutherland-like potential provides a reasonable representation of the inter-particle potential for PNIPAM particles in swollen and in collapsed phases. An aqueous dispersion of PNIPAM particles can freeze at both high and low temperatures. At low temperatures, the freezing occurs at a large particle volume fraction, similar to that in a hard-sphere system; while at high temperature, the freezing occurs at low particle concentrations, driven by the strong van der Waals attraction due to the collapsed microgel particles. The calculated phase diagram has been confirmed semi-quantitatively by experiments.

ACKNOWLEDGEMENTS

I would like to thank my advisor, Dr. Zhibing Hu, who introduced me into the wonderful world of hydrogels. Through his enthusiastic instruction and encouragement, I learned a lot and always was inspired by his dedication to science. I will benefit from this in my future work.

I also want to thank all my committee members, who take their precious time to read my dissertation and provide advice on my thesis.

The help and warm support of other graduate students in Dr. Hu's group is greatly acknowledged.

Special thanks are given to Dr. Jianzhong Wu, Professor of University of California, Riverside, for cooperation on the research of the interparticle potential and the phase behavior of temperature-sensitive microgel dispersions.

I am also grateful to the financial support from the National Science Foundation, under Grant DMR-0102468, the U.S. Army Research Office under Grant No. DAAD19-01-1-0596, the Texas Advanced Technology Program, and Access Pharmaceuticals, Inc.

At last, especially, I want to thank my wife, Xinlai Tu for her support of my study. So lucky with her love, I can fully devote myself to the research and finish this dissertation so smoothly. I also would like to thank my parents for their encouragement and support.

TABLE OF CONTENTS

Page

LIST OF TABLES AND SCHEMES

LIST OF ILLUSTRATIONS

CHAPTER 1

INTRODUCTION

A polymer gel, a three-dimensional network composed of polymer chains connected by multiple bonds, can contain a large fraction of solvent inside its structure. It has a very special property between solid and liquid. When the solvent is water, the polymer gel is named hydrogel. A hydrogel can undergo a large reversible volume transition in response to an environmental stimulus [1] such as temperature, pH value, ionic strength or an electric field. Because their water content simulates biological tissues, [2] hydrogels have many applications including artificial muscles, controlled drug release systems, and sensors. [3-10] Recently, intensive investigations have been focused on micro-scale hydrogels, or microgels, since they can respond to the environment much faster than the bulk gel. [11] In addition, they exhibit behavior ranging from that of polymer solutions to that of hard spheres, providing a model system for the study of the transition from the liquid to the crystal and from the supercooled liquid to the glassy state of atomic fluids.[12-16] In industry, microgels have been used in cosmetics, food, coatings, paints, rheological fluids and biomedical materials.[17-18]

Thermal responsive aqueous colloidal microgels form an interesting subset of polymer colloids, with N-isopropylacrylamide (NIPAM) being the major building block for temperature-sensitive microgels (see Figure 1.1). Since 1986, when Pelton and his student Chibante made the first NIPA-based microgels,[19] many publications about the preparation, characterization and application of these temperature responsive

microgels were published, indicating the current interest in "switchable" or "smart materials.[20-22] Poly-N-isopropylacrylamide has the temperature-sensitive phase behavior in water, with a lower critical solution temperature (LCST) at about 32 °C. Upon heating the gel, the gel shrinks by expelling water over a narrow temperature range, usually called the volume phase transition temperature. Below this temperature, PNIPAM is hydrophilic and swells in water, while above the temperature, it becomes hydrophobic and expels water, collapsing into a smaller volume. The synthesis of PNIPAM based microgels is obtained by using a precipitation polymerization method.[19] The schemetic set-up for the polymerization is shown in Figure 1.2. The pre-gel solution of the NIPA monomer was heated above the lower critical solution temperature (LCST), usually 60-70 °C, in order to generate free radicals by the decomposition of the persulfate initiator. The elevated temperature was also required so that growing PNIPAM chains phase separate to form colloidal particles. After several hours, narrowly distributed NIPA hydrogel particles were obtained with their swelling properties similar to those of the bulk NIPA gel. Many other water-soluble monomers could also be copolymerized with NIPAM to form thermo-sensitive microgels by using the same method. These include acrylic acid,[23-27] allylamine,[28-29] 2-hydroxyethyl acrylate[30-31] and N-acryloylglycine[32] (see Figure 1.1).

Another interesting phenomena about the PNIPAM based microgels is that they can form colloidal crystals at certain concentrations. Because of the electrostatic repulsion between the particles, originating from the sulfate groups introduced by the persulfate initiator, mono-dispersed NIPA particles can form an ordered array with a lattice spacing on the order of the wavelength of visible light. Iridescent colors from the

microgel dispersions have been observed due to the optical diffraction that follows Bragg's law. This kind of hydrogel opal can be applied to new biological or chemical sensors and optical filters.[33-34]

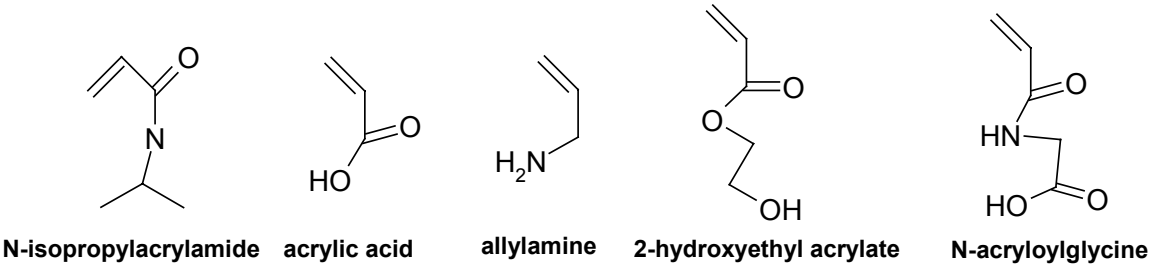

Figure 1.1: Monomers used in temperature responsive microgel synthesis

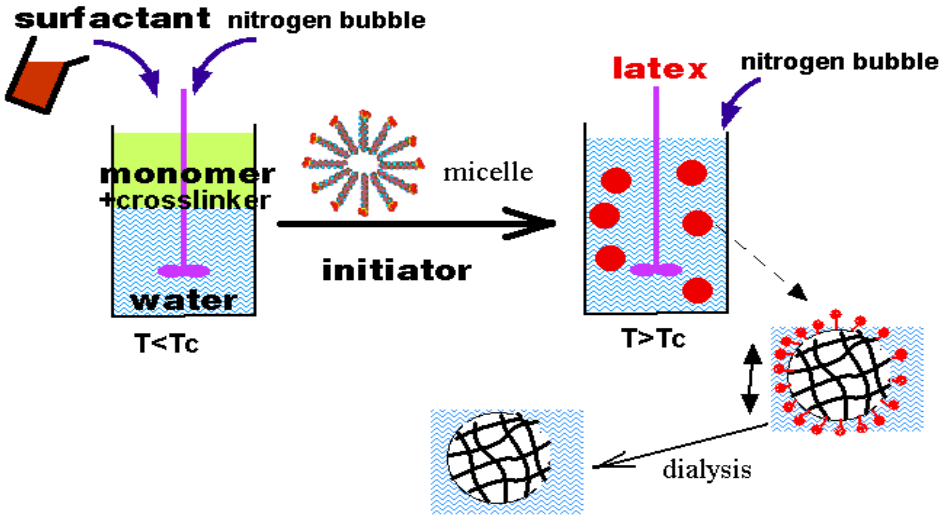

Figure 1.2: Synthesis process of Poly-NIPAM based nanoparticles.

Although gel nanoparticles react to external stimuli much faster, they are too small to be used in some practical applications. Recently, a new class of hydrogels with two levels of structural hierarchy has been developed by first making gel nanoparticles and then covalently bonding them together.[30] The primary network consists of crosslinked polymer chains inside each nanoparticle, while the second network is a crosslinked system of the nanoparticles. This structure has some unique properties, including entrapping and delivering drugs with different molecular weights between particles and in the particles.

This dissertation has been divided into seven chapters. Chapters 2-7 are briefly described as follows:

In Chapter 2, the theoretical background and the application of laser light scattering are briefly reviewed.[35-36] In polymer and colloid sciences, two laser light scattering measurements are usually used to provide information on the macromolecules in solutions such as the size, the molar mass and the conformation of the macromolecules. One technique is called static light scattering (SLS), which measures the time average intensity $<I>$ or photon counts $<n>$ of the scattered light. The other technique is dynamic light scattering (DLS), which measures the fluctuation of intensity of light $I(t)$ with time. From SLS, we can get the weight average molecule weight (M_w), the z- average root mean square radius of gyration $<R_g^2>^{1/2}$ (or simply R_g), and the second order virial coefficient A_2. By using DLS, the hydrodynamic radius R_h, the translation diffusion coefficient D, the relaxation rate Γ and the size distribution of the colloidal particles can be obtained.

In Chapter 3, we introduce a new kind of hydrogel network with two levels of structural hierarchy for controlled drug release. Temperature responsive hydrogels such as poly-N-isopropylacrylamide (PNIPAM) have become a well-studied class of systems in drug delivery research in the past few years.[37-44] Because of the volume phase transition property of PNIPAM, an on-off drug release can be achieved in the gels by a minor temperature change. The gels can be made in bulk or in nano- or microparticle form. Mono-dispersed nanoparticles were synthesized by copolymerizing NIPA with allylamine or acrylic acid. These nanoparticles have been stabilized at room temperature in neutral environment by covalently bonding neighboring particles using glutaric dialdehyde and adipic acid dihydrazide as cross-linking agents. The mesh size of the primary networks inside each particle ranges from 1-10nm, while the mesh size of the second network among the particles is in the range of 10-500nm. Dyed dextran markers with different molecular weights between 3,000 and 500,000 were used as a model drug system for the study of release kinetics in this nanoparticle network. It has been found that dextran entrapped between particle cavities in the nanoparticle network was released with a rate regulated by their molecular weights and the cavity size. In contrast, there is no release of dextran from the conventional bulk PNIPAM gel with high cross-linking density. For the PNIPAM-co-allylamine network, the release of dextran macro-molecules is temperature responsive, much faster at room temperature than at human body temperature. The PNIPAM-co-AA network showed a temperature independent release profile for different molecular weight markers. This kind of new nanoparticle network

could have several advantages over conventional gels for controlling the release of different bio-molecules.

In Chapter 4, we show a new route to the fabrication of bulk hydrogels with mesoscopical crystal structures. Since mono-dispersed PNIPAM nanoparticles can self-assemble into an ordered crystalline structure in water,[45-51] they could be used as templates for the fabrication of photonic crystals. A variety of methods used to stabilize the crystal structure have been developed. The central idea is similar to that of chapter three, covalently bonding the self-assembed PNIPAM-co-allylamine nanoparticles. Taking advantage of the fact that the thermally sensitive nanoparticles in colloidal glasses can be converted into ordered crystals via particle based volume transition as reported by Lyon and co-workers,[46-47] a crystalline hydrogel could be obtained by initiating the crystallization process near the colloidal crystal melting temperature, while subsequently bonding the PNIPAM-co-allylamine particles below the glass transition temperature. This can increase the polymer concentration, resulting in a crystalline hydrogel with higher mechanical strength. Furthermore, the allylamine contributes amino groups that can be covalently bonded in water at a neutral pH, this does not significantly affect the volume phase transition of the PNIPAM polymer. As a result, these novel materials, which contain up to 97% water, display a striking iridescent color, like a precious opal but soft and flexible. Creating such periodic 3D structures in materials allows us to obtain useful functionality not only from the constituent building blocks, but also from the long-range ordering that characterizes these structures.

In Chapter 5, we continued our study of the crystalline nanoparticle networks, but focused on potential applications such as the chemical and biological sensing.[52-60] This hydrogel with a periodic structure that has a spacing on the order of hundreds of nanometers, interacts strongly with visible and infrared light, leading to the optical diffraction that follows Bragg's law. Because the building blocks for these hydrogels are environmentally responsive PNIPAM colloidal spheres, they can show induced shifts in optical diffraction due to transformation of the hydrogel from a swollen hydrophilic network to a collapsed hydrophobic network. Their size, as well as the lattice spacing between the particles can be tunable by external stimuli. As a result, the crystalline hydrogel can serve as an optical sensor to visually inspect environmental changes.

By using UV-visible spectrometry, a blue shift of the Bragg peak has been observed in response to a temperature increase. The change of color is due to the shrinkage of the particle size with temperature, which causes a decrease of inter-particle spacing. In addition, due to the residues of basic (i.e. $-NH_2$) groups on the PNIPAM-allylamine building blocks, the swelling capacity of the resulting hydrogel can also be changed by controlling the pH value of the medium. The color of the hydrogels shifts from green to blue as the pH value of the surrounding environment increases. We also found that this kind of crystalline hydrogel could respond to the concentration change of protein solutions. Here we used bovine serum albumin (BSA) as a model drug. It is found that 0.05 wt % change on the concentration of BSA can be observed from the shift of the Bragg peak. This hydrogel with a periodic structure may lead to new sensors operating in aqueous solutions where most biological and biomedical systems reside.

Colloidal microgel dispersions provide model systems for studying the long-standing fundamental questions on the nature of liquids, solids, and glasses. Among numerous conventional colloids, aqueous dispersions of poly-N-isopropylacrylamide (PNIPAM) microgel particles are of special interest for studying phase transitions and for the fabrication of colloid-based advanced materials.[11, 61] The interaction potentials between microgel particles can vary from star-polymer-like to hard-sphere-like potential for short-range repulsion, from electrostatically neutral to highly ionizable for long-range electrostatic interactions, and from essentially no attraction to strong attraction for the van der Waals forces.[62-63] The versatility in the interaction potential makes PNIPAM microgel particles attractive for studying a broad variety of interesting phenomena in colloidal systems.[48, 64]

In Chapter 6, molecular-thermodynamic models in conjunction with experimental measurements are applied to correlate and predict the volume transition and structural ordering of poly-N-isopropylacrylamide (PNIPAM) microgel particles dispersed in water. The effective pair potential between neutral PNIPAM particles is represented by a Sutherland-like potential, where the size and energy parameters are correlated with particle radius and the solution osmotic second virial coefficients attained from static and dynamic light scattering experiments. Using a first-order perturbation theory for the fluid phase, and an extended cell model for the crystalline solid, the calculated phase diagram indicates that an aqueous dispersion of PNIPAM particles may freeze at both high and low temperatures. At low temperature, the freezing occurs at large particle volume fraction, similar to that in a hard-sphere system; while at high temperature, the freezing

occurs at low particle concentration, driven by the strong van der Waals attraction due to the collapsed microgel particles. The calculated phase diagram has been confirmed semi-quantitatively by experiments.

In Chapter 7, the main conclusions of the dissertation are summarized.

Chapter References

1. Tanaka, T. *Phys. Rev. Lett.* **1978**, 40, 820.
2. Peppas, N. A., Langer, R. *Science*, **1994**, 263, 1715.
3. Tanaka, T., Nishio, I., Sun, S. T., Ueno-Nishio, S. *Science* **1982**, 218, 467.
4. Siegel, R. A., Firestone, B. A. *Macromolecules* **1988***,* 21, 3254.
5. Osada, Y., Okuzaki, H., Hori, H. *Nature* **1992**, 355, 242.
6. Chen, G., Hoffman, A. S. *Nature* **1995,** 373, 49.
7. Osada, Y., Gong, J. P. *Adv. Mater.* **1998**, 10*,* 827.
8. Snowden, M. J., Murray, M. J., Chowdry, B. Z. *Chemistry & Industry* **1996**, 531.
9. Wang, C., Stewart, R. J., Kopecek, J. *Nature*, **1999**, 397, 417.
10. Lendlein, A., Kelch, S. *Angew. Chem. Int. Ed*. **2002**, 41, 2034.
11. Pelton, R. *Adv. Colloid Interface Sci.* **2000**, 85, 1.
12. Saunders, B. R.; Vincent, B. *Adv. Colloid Interface Sci*. **1999**, 80, 1.
13. Murry, M. J.; Snowden, M. J. *Adv. Colloid Interface Sci.* **1995**, 54, 73.
14. Senff, H.; Richtering, W. *J. Chem. Phys.* **1999**, 111, 1705.
15. Senff, H.; Richtering, W. *Langmuir* **1999**, 15, 102.
16. Bartsch, E.; Kirsch, S.; Lindner, P.; Scherer, T.; Stolken, S. *Ber. Bunsen-Ges. Phys. Chem.* **1998**, 102, 1597.
17. Everett, D. H. *Basic Principles of Colloid Science*, London **1998**.
18. Russel, W. B., Saville, D. A., Schowalter, W.R. *Colloidal Dispersions*, Cambridge University Press, Cambridge **1989**

19. Pelton, R. H., Chibante, P. *Colloids Surf*. **1986**, 20, 247.

20. Osada, Y., Ross-Murphy, S. B. *Sci. Am*. May **1993**, 82.

21. Galaev, I. Y. *Russian Chem. Rev*. **1995**, 64(5), 471.

22. Dagani, R. *C & E N*, **1997**, 26.

23. Jones, C.D., Lyon, L.A. *Macromolecules*, **2000**, *33*, 8301.

24. Jones, C.D., Lyon, L.A. *Macromolecules*, **2003**, *36*, 1988.

25. Xia, X., Hu, Z. *Langmuir,* **2004**; *20*(6), 2094

26. Hu, Z.B. , Xia, X. *Adv. Mater*., **2004**, 16(4), 305

27. Snowden, M.J., Chowdhrym B.Z., Vincent, B. *J. Chem. Soc., Faraday Trans*. **1996**, 92(24), 5013

28. Huang, G., Gao, J., Hu, Z.B. *J. Control. Release*, **2004**, 94, 303

29. Hu, Z.B., Huang, G. *Angew. Chem. Int. Ed*. **2003**, 42, 4799

30. Hu. Z.B., Lu, X., Gao, J. *Adv. Mater*. **2000**, 12, 1173

31. Hu, Z.B., Lu, X., Gao, J. *Adv. Mater*. **2001**, 13, 1708

32. Choi, H.S., Kim, J.M., Lee, K. *J. Appl. Polym. Sci*. **1998**, 69, 895

33. Weissman, J.M., Sunkara, H.B., Tse, A.S., Asher, S.A. *Science*, **1996**, 274, 959

34. Holtz, J.H., Asher, S.A. *Nature*, **1997**, 389, 829

35. Chu, B. *Laser Light Scattering*, 2nd edition; Academic Press, **1991**

36. Tanaka, T. Experimental Methods in Polymer Science; Academic Press, **2000**

37. Hoffman, A.S. *J. Controlled Release* **1987**, 6, 297

38. Bae, Y.H., Okano, T., Kim, S.W. *Pharm. Res*.**1991**, 8, 531.

39. Bae, Y.H., Okano, T., Kim, S.W. *Pharm. Res*. **1991**, 8, 624.

40. Okano, T., Bae, Y.H., Jacobs, H., Kim, S.W. *J. Controlled Release* **1990**, 11, 255.

41. Gutowska, A., Bae, Y.H., Feijen, J., Kim, S.W. *J. Controlled Release* **1992**, 22, 95.

42. Okuyama, Y., Yoshida, R., Sakai, K., Okano, T., Sakurai, Y. *J. Biomater. Sci. Polym. Ed.* **1993**, 4, 545.

43. Wang, C., Stewart, R.J., Kopecek, J. *Nature* **1999**, 397,417.

44. Qiu, Y., Park, K. *Advanced Drug Delivery Reviews* **2001**, 53, 321.

45. H. Senff, W. Richtering, *Langmuir* **1999**, 15, 102.

46. Debord, J.D., Lyon, L.A. *J. Phys. Chem*. **2000**, 104, 6327.

47. Debord, J.D., Eustis, S., Debord, S.B., Lofye, M.T., Lyon, L.A. *Adv. Mater.* **2002**, 14, 658

48. Hellweg, T., Dewhurst, C.D., Bruckner, E., Kratz, K., Eimer, W. *Colloid and Polymer Science* **2000**, 278, 972.

49. Gao, J., Hu, Z.B. *Langmuir* **2002**, 18, 1360

50. Wu, J.Z., Zhou, B., Hu, Z.B. *Phys. Rev. Lett*. **2003**, 90, 048304.

51. Wu, J.Z., Huang, G., Hu, Z.B. *Macromolecules* **2003**, *36*, 440.

52. Asher, S. A.; Alexeev, V. L.; Goponenko, A. V.; Sharma, A. C. *J. Am. Chem. Soc*. **2003**, 125, 3322.

53. Asher, S. A.; Sharma, A. C.; Goponenko, A. V.; Ward, M. M. *Anal. Chem*. **2003**, 75, 1676.

54. Lee, K.; Asher, S. A. *J. Am. Chem. Soc*. **2000**, 122, 9534.

55. Sharma, A.C., Jana, T., Kesavamoorthy, R., Shi, L., Virji, M.A., Finegold, D.N., Asher, S. A. *J. Am. Chem. Soc*. **2004**, 126, 2971.

56. Reese, C.E. Mikhonin, A.V., Kamenjicki, M., Tikhonov, A. Asher, S.A. *J. Am. Chem. Soc.* **2004**, 126, 1493.

57. Lee, Y.; Braun, P. V. *Adv. Mater*. **2003**, 15, No. 7-8, 563.

58. Lee, Y. Pruzinsky, S. A., Braun, P. V. *Langmuir* **2004**, 20, 3096.

59. Nakayama, D., Takeoka, Y., Watanabe, M., Kataoka, K. *Angew. Chem. Int. Ed*. **2003**, 42, 4197.

60. Cassagneau, T.; Caruso, F. *Adv. Mater*. **2002**, 14, No.22, 1629.

61. Saunders, B. R.; Vincent, B. *Advan Colloid Interface Sci* **1999**, *80*, 1.

62. Kawaguchi, H. *Prog Polym Sci* **2000**, *25*, 1171.

63. Fernandez-Nieves, A.; Fernandez-Barbero, A.; Vincent, B.; de las Nieves, F. J. *Macromolecules* **2000**, *33*, 2114.

64. Hu, Z. B.; Wang, C. J.; Chen, Y. Y.; Zhang, X. M.; Li, Y. *J Polym Sci B-Polym Phys* **2001**, *39*, 2168.

CHAPTER 2

PRINCIPLES AND APPLICATIONS OF LASER LIGHT SCATTERING

2.1 Introduction

When a beam of monochromatic, coherent light passes through a non-absorbing dilute macromolecule solution or colloid dispersion, the incident electromagnetic field induces an oscillating dipole at each point along its path. [1-3] The electrons are accelerated in oscillating dipoles and thus radiate light as a secondary source of light waves. Since the refractive indices of the solvent molecules and solute are different in most of the cases, the secondary waves mutually interfere, resulting in scattered light in all directions. This scattered light contains information about the macromolecules in solution such as the size, the molar mass and the conformation of the macromolecules in solutions. By placing a detector (e.g., a photon multiplier tube) at a distance and focusing it to a small volume of scattered medium, one can obtain information about the macromolecules in solution from two different measurements: measurements of the time-average scattered intensity <I> or photon counts <n> and the fluctuation of I(t) or n(t) with time. In polymer and colloid science, these two measurements are respectively referred to as static (elastic, i.e., no absorption) and dynamic (quasi-elastic) laser light scattering (LLS).

If all the macromolecules or particles were stationary, the scattered light intensity at each direction would be constant, which is independent of time. Actually, all the scatterers in solution are undergoing constant Brownian motion and this Brownian motion leads to both the fluctuation of the intensity pattern on the detection plane and the

fluctuation of I(t) with time if the detection area is small enough. The fluctuation rate can be related to relaxation processes, such as diffusion (translation and rotation) and internal motion of the macromolecules. The faster the relaxation process, the faster the fluctuation of I(t) will be. While the static LLS measures the time-average scattered intensity, dynamic LLS measures the intensity fluctuation. That is where the word "dynamic" comes from. Its essence may be explained as follows if we take a translation relaxation as an example: Because of the Doppler effect, when the incident light is scattered by a moving macromolecule or particle, the frequency of the scattered light will be slightly higher or lower than that of the original light, depending on whether the particle moves towards or away from the detector. Thus, for a macromolecular solution or a colloid dispersion, the frequency distribution of the scattered light is slightly broader than that of the incident light. This is why dynamic LLS is also called quasi-elastic light scattering (QELS). The frequency broadening ($\sim 10^5$-10^7 Hz) is so small in comparison with the incident light frequency ($\sim 10^{15}$ Hz) that it is very difficult, if not impossible, to detect it in the frequency domain. However, it can be effectively recorded in the time domain through a time correlation function. For this reason, dynamic light scattering is sometimes known as photon correlation spectroscopy (PCS).

In 1869, J. Tyndall made the first experimental investigation of light scattering. He observed the scattering of natural light when it passed through a colloid dispersion. The scattered light showed a light bluish color and was partially polarized if the incident light was polarized. In 1881, L. Rayleigh, the director of the Cavendish Laboratory at Cambridge University of British, successfully derived at the conclusion, based on the

Maxwell theory of electromagnetic field, that the intensity of the scattered light by the non-absorption, non-interaction and optically isotropic small particles is inversely proportional to the fourth power of the incident wave length. In 1944, Debye measured the molecular weight of macromolecules from a dilute solution using the light scattering method. In 1948, Zimm[4] proposed the famous Zimm plot by extrapolating both concentration and measuring angle to zero value at a single coordinate. Since then, static light scattering as a classic and absolute analytical method has been widely used to characterize both synthetic and natural macromolecules. Before the development of the laser, light scattering was limited to measuring scattered intensity at different angles and concentration, from which three parameters of macromolecules, namely the weight-averaged molecular weight (M_w), z-average root-mean-square radius of gyration ($<R_g^2>^{1/2}$, simply R_g) and the second-order virial coefficient (A_2) can be obtained. In the last two decades, thanks to advances in stable laser sources, ultra-fast electronics and personal computers, LLS, especially dynamic LLS, has evolved from a very special instrument for physicists and physical chemists to a routine analytical tool in polymer laboratories, LLS is even used as a daily quality-control device in production lines. Dynamic LLS provide the information about the translational diffusion coefficient (D), relaxation rate (Γ), and hydrodynamic radius (R_h) of the macromolecule solution. Commercially available LLS instruments are normally capable of making both static and dynamic measurements simultaneously to study colloidal particles or macromolecules in solutions, as well as in gels and viscous media.

2.2 Static Laser Light Scattering[5-6]

In a static LLS system two kinds of interference should be considered. One is the inner interference arising from different parts of a larger (dimension >λ/10) particle, whereas the intra-particle interference from small particles (dimension < λ/10) may be neglected. The other one is the interference from different particles. For dilute solutions, the inter-particle interference could be neglected.

The Rayleigh ratio is a very important factor in static LLS, defined as

$$R = \frac{Ir^2}{I_0} \qquad (2-1)$$

where I is the the scattered intensity per unit scattering volume, I_0 is the incident light intensity, and r is the average distance between the scatterers and the observer. Thus, the dimension of the Rayleigh ratio R is the reciprocal of the dimension of length. Based on the electromagnetic principle and concentration fluctuation theory, we can derive the excess Rayleigh ratio of the dilute solution (R_{excess}):

$$R_{excess} = \frac{I_{excess} r^2}{I_0} = \frac{4\pi^2 n^2}{\lambda_0^{\,4}} \left(\frac{dn}{dC}\right)^2 \frac{kTC}{\partial \Pi / \partial C} \qquad (2-2)$$

Where I_{excess} ($=I_{solution}-I_{solvent}$) is the net scattering intensity of the solute by subtracting the intensity of solvent from that of the solution, and n, λ_0, C, k, T, Π are the colloidal solution refractive index, the incident light wavelength, the solute concentration, the Boltzmann constant, the absolute temperature and the osmotic pressure, respectively.

For dilute macromolecule or particle solutions, the relationship of the osmotic pressure and colloidal concentration can be written as

$$\frac{\Pi}{C} = \frac{N_0 kT}{M}(1 + A_2 CM + \ldots) \qquad (2-3)$$

Thus $$\frac{\partial \Pi}{\partial C} = \frac{N_0 kT}{M}(1 + 2A_2 CM + \ldots) \qquad (2-4)$$

where N_0, M, and A_2 are Avogadro's number, the weight-average molecular weight, and the second –order virial coefficient, respectively.

By substitution of equation (2-4) into equation (2-2), we can get the excess Rayleigh ratio:

$$R_{excess} = \frac{4\pi^2 n^2}{\lambda_0^{\,4} N_0}(\frac{dn}{dC})^2 \frac{CM}{1 + 2A_2 CM + \ldots} \qquad (2-5)$$

R_{excess} is the net scattering intensity of the solute by subtracting the intensity of solvent from that of the solution. By defining $K = 4\pi^2 n^2 (dn/dC)^2 /(N_0 \lambda_0^{\,4})$, we get

$$\frac{KC}{R} = \frac{1}{M} + 2A_2 C + \ldots \qquad (2-6)$$

where we have omitted the footnote "excess" in R_{excess}. For larger macromolecules or colloidal particles, a construction factor must be introduced. Here, P(θ) is defined as an angular scattering function

$$P(\theta) = \frac{R(\theta)}{R(0)} = 1 - \frac{1}{3} q^2 < R_g^{\,2} > \qquad (2-7)$$

where $q = (4\pi n/\lambda_o)\sin(\theta/2)$ is the magnitude of the scattering vector, $<R_g^2>$ is the mean square of the radius of gyration. Thus,

$$\frac{KC}{R(\theta)} = \frac{1}{MP(\theta)} + 2A_2 C \qquad (2-8)$$

when the concentration C→ 0,

$$R(\theta) = KCMP(\theta) = KCM\left[1 - (1/3)q^2 < R_g{}^2 >_z + \ldots\right]$$

$$\frac{R(\theta)}{KC} = M_w(1 - \frac{1}{3}q^2 < R_g{}^2 >_z + \ldots) \qquad (2-9)$$

When $q^2<R_g^2>$ <<1, omitting the higher order (>2) terms in series, we get

$$\frac{KC}{R(\theta)} = \frac{1}{M}[1 + \frac{1}{3}q^2 < R_g{}^2 >_z] + 2A_2C \qquad (2-10)$$

This is the basic equation of static LLS which is frequently shown in the literature.[7-9] The molar mass in the equation, $M_w = \sum_i C_i M_i / \sum_i C_i$, is weight-average; and the mean square radius of gyration, $< R_g{}^2 >_z = \sum_i C_i M_i R_{g,i}{}^2 / \sum_i C_i M_i$ is z-average.

It shows that with R(θ) measured for a series of C and q, we are able to determine $<R_g^2>_z$ from the slope of $[KCR(\theta)]_{C\to 0}$ versus q^2; A_2 from the slope of $[KC/R(\theta)]_{\theta\to 0}$ versus C; and M_w from $[KCR(\theta)]_{C\to 0,\theta\to 0}$. The Zimm plot, i.e., KC/R(θ) versus (q^2+kC) with k being an adjustable constant, allows both q and C extrapolations to be made on a single coordinate plane.[4] It should be noted that Equation (2-10) is valid under the restriction that the polymer solution exhibits no adsorption, no fluorescence, and no depolarized scattering. In practice, the Rayleigh ratio is determined by a relative method; namely, by measuring the scattering intensity of a standard such as benzene or toluene, we can calculate the Rayleigh ratio of a given solution by

$$R_{vv}(\theta) = R_{vv}^0(\theta)\frac{I(\theta)_{solution} - I(\theta)_{solvent}}{I(\theta)_{standard}}(\frac{n_{solvent}}{n_{standard}})^{\gamma} \qquad (2-11)$$

where the subscript "νν" means both the incident and the scattered light are vertically polarized; I and n are, respectively, the time-average scattering intensity and the

refractive index. The term $(n_{solvent}/n_{standard})^{\gamma}$ is a refraction correction for the scattering volume and γ is a constant between 1 and 2, depending on the detection geometry of the light scattering instrument, because we should compare the same scattering volume from the solution and the reference standard.

2.3 Dynamic Laser Light Scattering

In dynamic light scattering, we are interested in determining the motion of the particles.[10-11] The motion includes translational, rotational and internal motion. The particle motion results in two effects: frequency distribution and the scattered intensity fluctuates. The frequency shift is caused by random movement of the particles due to the Doppler effect and is only about one hundred millionth that of the incident frequency. Therefore, it is very difficult to precisely detect the frequency shift even with a Fabry-Perot interferometer. However, in the time domain, the fluctuation of the scattered intensity is intimately related with frequency broadening can be detected, if the detector is sensitive enough and can sample the scattered signals fast enough. It is equally efficient to determine either the fluctuation of the scattered intensity or the frequency broadening because the two effects are related each other. We exclude the less commoncases in which the fluctuation of scattered intensity is caused by a change in the number of the macromolecules or colloid particles in an extremely dilute system. The most commonly used method in quasi-elastic light scattering (QELS) is the digital technique of photon correlation spectroscopy (or optical mixing), which measures the intensity fluctuation of scattered light in the time domain. There are two basic forms of

optical mixing: heterodyne and homodyne (self-beating). By heterodyne mixing we refer to mixing the scattered light with a reference beam (local oscillator) un-shifted or shifted in frequency from the incident light beam. In self-beating optical mixing the scattered wave is not mixed with a reference signal, but is directly detected. Here we only discuss the self-beating intensity-intensity time correlation spectroscopy.

The Siegert relation is a very important equation in dynamic LLS. When the scattered field is a Gaussian random process, the correlation functions $g^{(1)}(t)$ and $g^{(2)}(t)$ are connected through the Siegert relation.

$$g^{(2)}(t) = 1 + \left|g^{(1)}(t)\right|^2 \qquad (2-12)$$

where $g^{(1)}(t) \equiv \left[< E(0)E^*(t) > / < E(0)E^*(0)\right]$ and $g^{(2)}(t) \equiv [< I(0)I(t) > / < I(0) >^2]$ are the normalized field-field and normalized intensity-intensity autocorrelation functions, respectively. Thus, the intensity time autocorrelation function

$$G^{(2)}(t) =< I(0)I(t) >=< I(0) >^2 \; g^{(2)}(t) =< I(0) >^2 \; [1 + \left|g^{(1)}(t)\right|^2] \qquad (2-13)$$

the significance of introducing $g^{(2)}(t)$ and $G^{(2)}(t)$ lies in that $G^{(2)}(t)$ and <I(0)> can be measured experimentally. In practice, the detection area can not be zero no matter how small it is. Therefore, the scattered light detected can not be purely coherent and an instrument parameter, β (<1), is introduced in equation (2-13):

$$G^{(2)}(t) = A(1 + \beta\left|g^{(1)}(t)\right|^2) \qquad (2-14)$$

where A ($\equiv< I(0) >^2$) is the baseline, t is the delay time, β is a parameter depending on the coherence of the detection optics, and $I(t)$ is the detected scattered intensity or photon

counts at time t, which includes contributions both from the solvent and from the solute. Therefore,

$$G^{(2)}(t) =< [I_{solvent}(0) + I_{solute}(0)][I_{solvent}(t) + I_{solute}(t)] >$$

and equation (2-14) becomes

$$G^{(2)}(t) = A\left\{1 + \beta[\frac{I_{solvent}}{I_{solution}}\left|g^{(1)}_{solvent}(t)\right| + \frac{I_{solute}}{I_{solution}}\left|g^{(1)}_{solute}(t)\right|]^2\right\} \qquad (2-15)$$

where all the cross terms disappear since the light scattered by solvent molecules and solute particles are not correlated. It should be noted that $\left|g^{(1)}_{solvent}(t)\right|$ decays much faster than $\left|g^{(1)}_{solute}(t)\right|$ because small solvent molecules diffuse much faster than larger particles do. Thus, after a very short delay time, equation (2-15) becomes

$$G^{(2)}(t) \equiv A[1 + \beta(\frac{I_{solute}}{I_{solution}})^2\left|g^{(1)}_{solute}(t)\right|^2] = A[1 + \beta_{app}\left|g^{(1)}_{solute}(t)\right|^2] \qquad (2-16)$$

where $\beta_{app} = \beta(I_{solute} / I_{solution})^2$. For a dilute solution, the scattered intensity from solvent molecules can become appreciable, i.e., $I_{solute} \leq I_{solution}$, so that the apparent coherence β_{app} would be even lower, i.e., $G^{(2)}(0)$ apperars to have lower value than expected. We should be aware of this situation, especially for weakly scattering dilute and low molar mass polymer solution. For example, if $I_{solute}=I_{solvent}$, $\beta_{app}=\beta/4$. It should be noted that β is constant for each particular optical geometry of the scattering instrument. I_{solute} can be estimated from β_{app} (certainly I_{solute} could be measured in static LLS by comparing the scattered intensity of solution and solvent). The values of β at different scattering angles

have been pre-calibrated with a narrowly distributed latex standard whose scattering intensity is much stronger than water (solvent), as first demonstrated by Sun *et al*..[12]

Generally, the relaxation of $\left|g^{(1)}(t)\right|$ includes both diffusion (translation and rotation) and internal motions. Let us only consider the translational diffusion relaxation of the particles. For monodispersed spherical scatters, $\left|g^{(1)}(t)\right|$ is theoretically represented as an exponential decay function:

$$\left|g^{(1)}(t)\right| = Ge^{-\Gamma t} \qquad (2-17)$$

where G and Γ are the factor of proportionality and the line-width, respectively and $\Gamma^{-1}=\tau_c$, the characteristic decay time representing the rate of dynamic relaxation in self-beating. For a poly-dispersed polymer sample with a continuous distribution of molar mass M, equation (2-17) may be generalized as

$$\left|g^{(1)}(t)\right| = \int_0^\infty G(\Gamma)e^{-\Gamma t}d\Gamma \qquad (2-18)$$

where $G(\Gamma)$ is called the line-width distribution and $G(\Gamma)d\Gamma$ is the statistic weight of the particles or macromolecules which possess line-width Γ. By using a Laplace inversion program, CONTIN,[13-14] the normalized distribution function of the characteristic line width $G(\Gamma)$ was obtained. For a dilute solution, Γ measured at a finite scattering angle is related to C and q by

$$\frac{\Gamma}{q^2} = D(1+k_dC)(1+fq^2 < R_g^2 >_z) \qquad (2-19)$$

where D is the translational diffusion coefficient of the solute molecule at $C\rightarrow 0$, k_d is the diffusion second virial coefficient, and f is a dimensionless parameter depending on

polymer chain structure and solvent (for polymers with flexible chains in a good solvent, f is between 0.1 and 0.2). Hence, for small C and q, $D \approx \Gamma/q^2$. It should be noted that by the definition of $\left|g^{(1)}(t)\right|$, $G(D)=q^2G(\Gamma)$, the translational diffusion coefficient distribution, is an intensity distribution. Since $\left|g^{(1)}(t)\right|$ approaches unity as $t \to 0$, we have

$$\left|g^{(1)}(t \to 0)\right| = \frac{\langle E(0)E^*(t \to 0)\rangle}{\langle E(0)E^*(0)\rangle} = \int_0^\infty G(\Gamma)d\Gamma = \int_0^\infty G(D)dD = 1 \qquad (2-20)$$

where <D> is the average diffusion coefficient defined as

$$< D >= \int_0^\infty G(D)DdD \qquad (2-21)$$

Further, the translational diffusion coefficient D may be related to the molecular friction factor f through the Stokes-Einstein relation

$$D = k_B T / f \qquad (2-22)$$

where k_B and T are the Boltzmann constant and the absolute temperature, respectively. For a hard sphere with a radius of R, $f=6\pi\eta R$, where η is the viscosity of the solvent. For a polymer coil, R is replaced by its hydrodynamic radius R_h, so that

$$R_h = \frac{k_B T}{6\pi\eta D} \qquad (2-23)$$

In dynamic light scattering, translational motion of macromolecules or particles within a size range of 1-1,000 nm can be measured. The characteristic time of dynamic relaxation in self-beating (τ_c), which include translational, rotational, and internal motion, could vary from tens of nanoseconds to seconds.

Dynamic LLS plays a very important role in particle sizing. In a dilute dispersion, if the colloidal particles are spherical, or in other words, in the absence of rotational and internal motions, $G(\Gamma)$ can be converted to the hydrodynamic size distribution $f(R_h)$. All the parameters required are either well-known constants or precisely measurable by other methods. Therefore, particle sizing on the basis of dynamic LLS can be considered as an absolute method without calibration. This is why dynamic LLS is so successful in particle sizing and many commercial instruments have been developed using the dynamic LLS principle.

2.4 LLS Instrumentation

A modern commercial light scattering spectrometer consists of the light source, the optics, the cell holder and the detector. An ALV/DLS/SLS-5000 equipped with an ALV-5000 digital time correlator is used in our lab. The spectrometer is shown in Figure 2.1. The light source is a Helium-neon (He-Ne) laser with a wavelength of 632.8nm and an output power of 22 mW. The incident light was vertically polarized with respect to the scattering plane and the light intensity was regulated with a beam attenuator (Newport M-925B). The scattered light is transmitted through a very thin(~ 40 μm in diameter) optical fiber leading to an active, quenched, avalanche photo diode (APD) as the detector. As a result, the coherent factor β in dynamic laser light scattering is approximately 0.98. The avalanche photo diode has sensitivity 100 times higher than that of a normal photo multiplier (PM) tube, while the dark count increases no more than 10 times. Thus, a 22-mW laser can have a measured count rate similar to a 400 mW laser for a normal PM

tube. For DLS experiments in this dissertation, the standard deviation of every measurement of hydrodynamic radius (R_h) can be automatically calculated and is below 1%. The schematic setup of the LLS is given in Figure 2.2.

Figure 2.1: A commercial ALV/DLS/SLS-5000 laser light scattering (LLS)

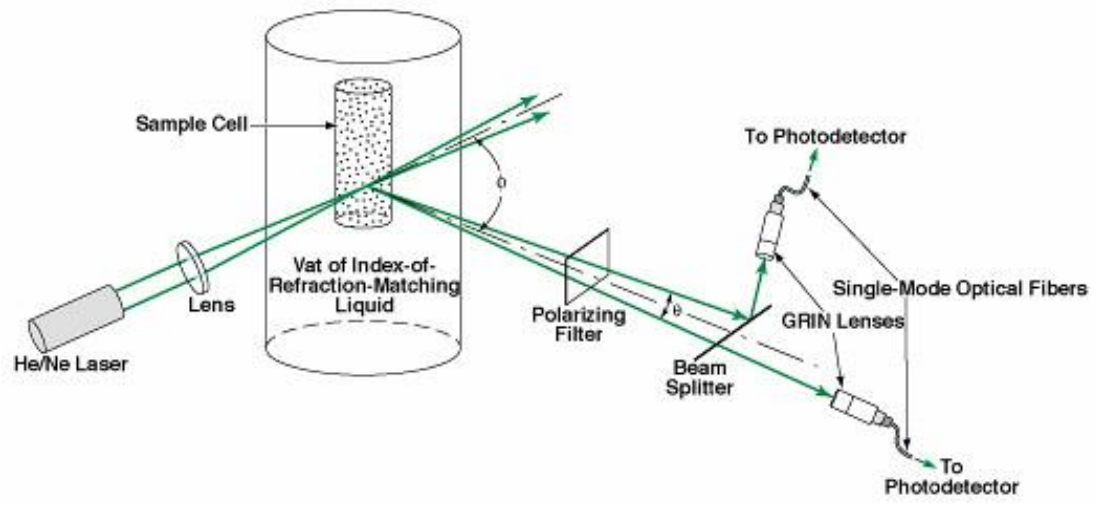

Figure 2.2: Schematic setup of laser light scattering instrument

Chapter References

1. Abbiss, J.b., Smart, A.E. *Photon correlation Techniques and Applications*. **1988**, OSA Proceedings.
2. Ostrowsky, N., Sornette, D., Parker, P., Pike, E.R. *Opt. Acta*., **1981**, 28, 1059.
3. Hallett, F.R., Watton, J., Krygsman, P.H. *Biophys. J*., **1991**, 59, 357.
4. Zimm, B.H. *J. Chem. Phys*. **1948**, 16, 1099.
5. Tanaka, T. *Experimental Methods in Polymer* S*cience*; Academic Press. **2000**
6. Chu, B. *Laser Light Scattering*, 2nd Edition, Academic Press, **1991**
7. Wu, J.Z., Huang, G., Hu, Z.B. *Macromolecules* **2003**, *36*, 440
8. Wu, C. Chan, K.K., Xia, K.Q. *Macromolecules* **1995**, 28, 1032.
9. Zhang, G., Wu, C. *J. Am. Chem. Soc*. **2001**, 123, 1376
10. Berne, B.J., Pecora, R. *Dynamic Light Scattering*, John Wiley & Sons Press: New York, **1976**
11. Brown, W. *Dynamic Light Scattering*, Oxford University Press, Oxford, **1993**
12. Sun, S.T., Nishio, I., Swislow, G., Tanaka, T.J. *J. Chem. Phys*. **1980**, 73, 5971.
13. Provencher, S.W. *Biophys. J*. **1976**, 16, 29
14. Provencher, S.W. *Makromol. Chem*. **1979**, 180, 20

CHAPTER 3

CONTROLLED DRUG RELEASE FROM HYDROGEL NANOPARTICLE NETWORKS*

3.1 Introduction

Hydrogels are three-dimensional macromolecular networks that contain a large fraction of water within their structure, do not dissolve and are soft and pliable. These properties are similar to natural tissue and, therefore hydrogels are particularly useful in biomedical and pharmaceutical applications.[1] Some hydrogels can reversibly swell or shrink up to 1000 times in volume based in response to a variety of external stimuli.[2-6] Temperature responsive hydrogels, such as N-isopropylacrylamide (PNIPAM) are a well-studied class of systems in drug delivery research.[7-14] Specifically, PNIPAM hydrogel undergoes the volume phase transition at a critical temperature (T_c) of 34 ^{0}C.[3] Below T_c, it is hydrophilic and swells in water, while above T_c, it becomes hydrophobic and expels water, collapsing into a smaller volume. Using the temperature responsive properties of the PNIPAM hydrogel, pulsatile drug delivery may be intelligently triggered by a minor temperature change. An on-off drug release profile in response to a stepwise temperature change has been observed in PNIPAM and its derivatives.[7-12]

Hydrogels can be prepared by the co-polymerization of two different monomers, [8-9] by forming interpenetrating polymer networks[14] or by creating networks with microporous structures.[15] They can be made in bulk or in nano- or micro-particle form. The bulk gels are easy to handle, but usually have very slow swelling rates. Gel

* Reproduced with permission from [Huang, G., Gao, J., Hu, Z.B., John, J.V., Ponder, B.C., Moro, D. *J. Controlled Release*; **2004**, 94, 303] Copyright [2003] Elsevier B.V.

nanoparticles react quickly to an external stimulus, but may be too small for some practical applications. Recently, PNIPAM nanoparticles have been stabilized into bulk form by bonding PNIPAM nanoparticles, to form a network.[16] This approach to linking particles is limited by harsh reaction conditions, either an aqueous solution with pH 12, or an organic solvent that may encumber the loading of hydrophilic drugs.

Here the synthesis of nanoparticles of PNIPAM-co-allylamine and PNIPAM-co-AA is described. These nanoparticles, as building blocks, have been chemically inter-connected in the presence of dextran, to form three-dimensional macroscopic gels at room temperature and neutral pH. The gels have two levels of structural hierarchy[16]: the primary network, consisting of crosslinked polymer chains inside each nanoparticle, while the secondary network is a crosslinked system of the nanoparticles. The mesh sizes of the primary and the secondary networks are in the range of ca. 1–10 and 10–500 nm, respectively. This structure provides some unique capabilities, including entrapping and releasing drug between particles. In this report, the dextran release patterns at two different temperatures, below and above the gel collapse temperature, are examined and compared to that of a PNIPAM gel. The newly structured gels allowed temperature-controlled release of dextran.

3.2 Experimental

3.2.1 Materials

N-Isopropylacrylamide (NIPAM) and N, N'-methylene-bis-acrylamide were purchased from Polyscience Co. and Bio-Rad Co., respectively, and used as received. Potassium persulfate, sodium dodecyl sulfate, glutaric dialdehyde, acrylic acid, and allylamine were obtained from Aldrich Company. Dextrans conjugated with Texas Red dye, with the molecular weight (MW) ranging from 3000 to 70,000 and fluorescent dextran of MW 500,000 were purchased from Molecular Probes, Eugene, OR. 1- Ethyl-3-(3-dimethylaminopropyl) carbodiimide hydrochloride and adipic acid dihydrazide were supplied by Access Pharmaceuticals Inc. Water for all reactions, solution preparation, and polymer purification was distilled and purified to a resistance of 18.2 MΩ cm using a MILLIPORE system, and filtered through a 0.22 μm filter to remove particulate matter.

3.2.2 Sample preparation

3.2.2.1 Synthesis of precursor nanoparticles

PNIPAM-co-allylamine nanoparticles were prepared by precipitation polymerization.[17] NIPAM monomer (3.8 g, 33.6 mmol), allylamine (0.2 g, 3.4 mmol, 10 mol% of NIPAM monomer), different amounts of sodium dodecyl sulfate and N,NV-methylene-bis-acrylamide (0.067 g, 0.44 mmol, 1.3 mol% of NIPAM monomer) in water (230 ml) at room temperature were purged with nitrogen and stirred for 30 min, and then heated to 70 ^{o}C. Potassium persulfate (0.166 g) in 20 ml water was added to the reactor to initialize polymerization. The reaction was maintained at 68–70 ^{o}C under nitrogen for 4 h. After cooling to room temperature, the resultant nanoparticles were dialyzed for 1

week to remove surfactant and unreacted molecules. The dialysis water was changed three times every day. The cut off molecular weight of the dialysis membrane was 13,000.

PNIPAM-co-AA nanoparticles were prepared and purified using the same procedures, except that allylamine was replaced by acrylic acid (0.24 g, 3.33 mmol, 10 mol% of NIPAM monomer).

3.2.2.2. Drug loading and synthesis of gel nanoparticle networks

A. PNIPAM-co-allylamine nanoparticle network.

The dialyzed particle dispersion was condensed by evaporation of water at room temperature directly to a polymer concentration of 10 wt.%. Then defined amounts of dextran, with a given molar mass, were mixed with the dispersion. Glutaric dialdehyde (0.04 g, 25 wt.%) solution was added to 1.0 g of the dispersion containing dextran, which was vortex mixed and centrifuged to remove air bubbles. A covalently crosslinked network of nanoparticles formed in 2 h at room temperature.

B. PNIPAM-co-AA nanoparticle network.

1-Ethyl-3-(3-dimethylaminopropyl) carbodiimide hydrochloride (EDC) (0.032 g, 0.17 mmol) in 0.2 g water and then adipic acid dihydrazide (0.015 g, 0.085 mmol) in 0.2 g water were added to 1.0 g of the PNIPAM-AA nanoparticle dispersion (10 wt.%) containing dextran. The excess of diimide and dihydrazide (containing two -NH_2 group per molecule) were calculated to react with all carboxyl groups (~5.8 mg, 0.08 mmol) in 1.0 g of the 10 wt.% dispersion. EDC, also called zero-length crosslinking reagent, could be used to mediate the formation of an amide linkage between a carboxylate and an

amine with no additional chemical structure introduced between the two conjugating molecules. Its water solubility allows for direct addition to a reaction without prior organic solvent dissolution. N-substituted carbodiimides can react with a carboxyl group on particles to form highly reactive O-acylisourea intermediate. These reactive species then react with a nucleophile such as adipic acid dihydrazide to form an amide bond. [18] The process of the cross-linking reaction is shown in scheme 3.1.

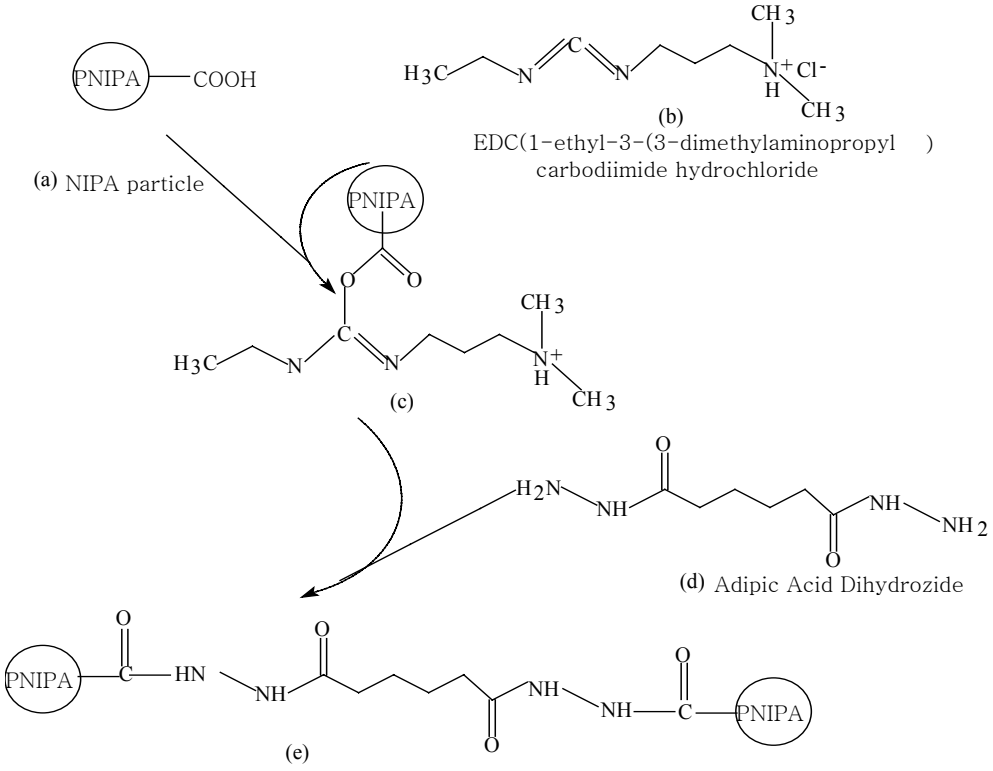

Scheme 3.1: The carboxyl (COOH) groups on the PNIPAM-co-AA nanoparticles reacting with EDC and adipic acid dihydrozide to form a network in water.

3.2.2.3. Synthesis of the PNIPAM bulk gel loaded with dextran

N-Isopropylacrylamide(1.56 g), N, N'-methylenebis-acrylamide (0.2 g, 1.3 mmol, 9.4 mol% of NIPAM monomer), and tetramethylethylenediamine (48 μl) were dissolved

in 20 ml water containing 20 ppm dextran. The solution was purged with nitrogen for 20–30 min to remove dissolved oxygen. Polymerization was initiated by addition of ammonium persulfate (8 mg) at 4 ^{o}C.

3.2.2.4. Controlled drug delivery experiments

Nanoparticle networks containing dextran were removed from the test tube by injecting water into the bottom of the reaction vessel using a syringe. For dextran release measurements at 21 ºC, the networks were directly immersed in water and aliquots were periodically removed. The concentration of dextran in the solution was determined using a UV–visible spectrophotometer (Agilent 8453). The aliquots were returned to the solution after analysis. The absorption maximum of Texas Red dextran with molecular weights ranging from 3000 to 70,000 was 594 nm, while the absorption peak for the fluorescent dextran with molecular weight 500,000 was 497 nm. For measurements at 37 ºC, the network was first heated to 37 ºC in air to shrink the gel volume. The shrunken network was then washed with 37 ºC water to remove surface contaminants and finally immersed in water at 37 ºC.

3.3. Results and Discussions

3.3.1 Precursor PNIPAM derivative nanoparticles.

Figure 3.1 compares hydrodynamic radius distributions of nanoparticles of PNIPAM co-polymerized with 10 mol % allyamine and with 10 wt % PAA in water, respectively. PNIPAM-co-allyamine nanoparticles exhibit a similar volume phase transition behavior as homo-PNIPAM nanoparticles, as shown in Figure 3.1 (a). The poly-N-isopropylacrylamide-co-allylamine (PNIPAM-co-allylamine) nanoparticles were

in the swollen state with <R_h> about 186 nm at 21°C and in the collapsed state with <R_h> about 72 nm at 37 °C. On the other hand, the hydrodynamic radius of PNIPAM-co-PAA nanoparticles shrank much less, from 320 nm to 210 nm, as the temperature increased from 21 to 37 °C, shown in Figure 3.1 (b). It is known that the volume phase transition temperature of an ionic PNIPAM gel is shifted to a higher temperature as the ionic concentration increases. This is a result of the increase of osmotic pressure due to static electric interaction among ions in the network. In this case of PNIPAM particles with 10 mol % PAA at neutral pH, the AA was completely ionized; as a result, the phase transition occurs at a broader and higher temperature range and less shrinkage of AA co-polymerized gel was observed at 37 ºC.

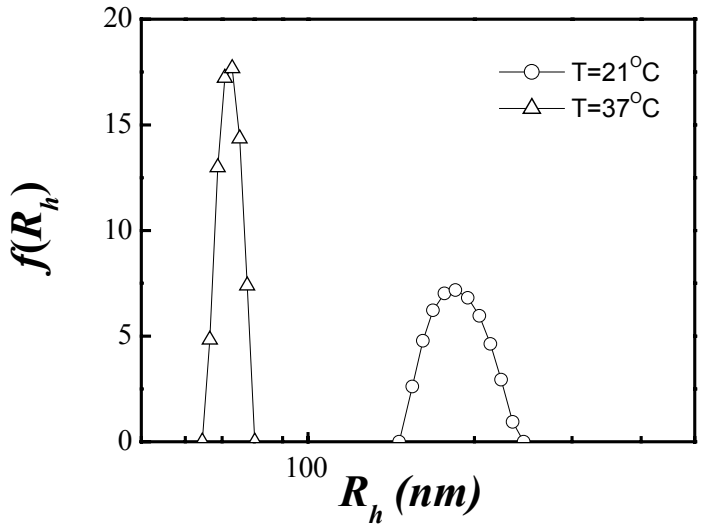

(a)

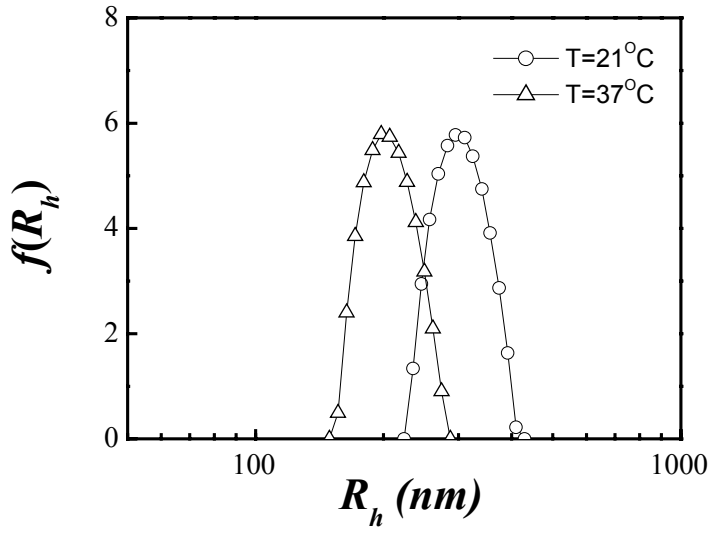

(b)

Figure 3.1: The hydrodynamic radius distribution of particle dispersions in water at 25 ^{o}C and 37 ^{o}C, respectively. (a) PNIPAM-co-allylamine particles, and (b) PNIPAM-co-AA particles.

Figure 3.2 compares the temperature dependent hydrodynamic radii of the PNIPAM-co-allylamine and homo-PNIPAM particles between 20 and 40 ºC. The PNIPAM-co-allylamine exhibit a similar phase transition as homo-PNIPAM particles with the volume phase transition temperature at 35 ^{o}C, about 1 ^{o}C higher than that of homo-PINIPAM particles. This is understandable because amine groups are hydrophilic at a neutral pH, independent of temperature. Incorporating amine groups makes the gel nanoparticle more hydrophilic with a higher transition temperature.

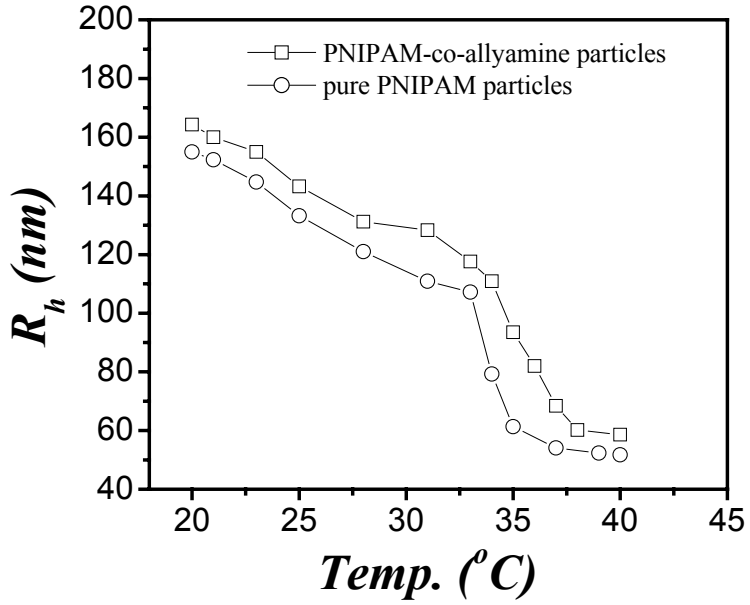

Figure 3.2: The temperature dependent hydrodynamic radii of PNIPAM-allylamine and homo-PNIPAM particles in water. The light scattering angle is at 30 º.

The PNIPAM-co-allylamine particles with different hydrodynamic radii were obtained by introducing different amounts of the surfactant (sodium dodecyl sulfate) in the polymerization processes. As the surfactant concentration increases from 0.012 to 0.05g/100ml, $<R_h>$ decreases from 350 to 120 nm as shown in Figure 3.3. The trend is similar to that in emulsion polymerization of styrene. Fig. 3.3 a further shows that gel particles of different sizes all exhibit narrow size distribution.

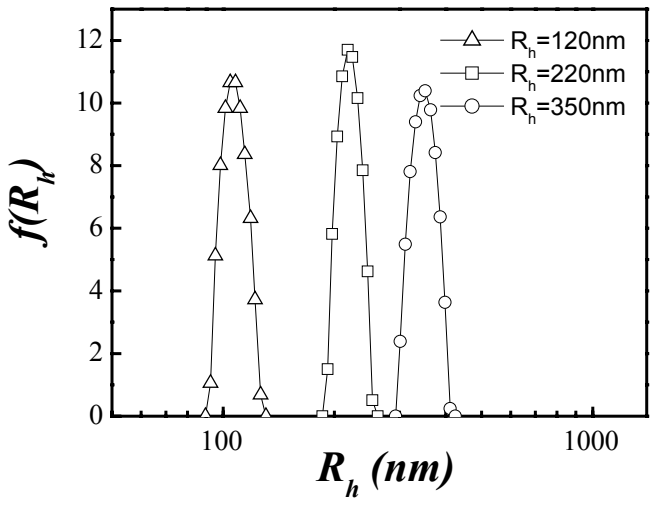

(a)

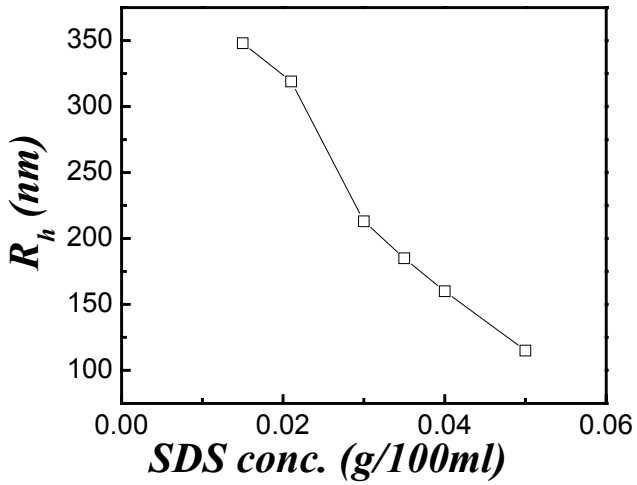

(b)

Figure 3.3: The PNIPAM-allyamine particles with different sizes have been prepared by varying surfactant concentration during polymerization processes. (a) Hydrodynamic radius distributions of PNIPAM-allylamine particles at 21 ^{o}C in water. (b) The hydrodynamic radius is plotted against concentration of sodium dodecylsulfate.

3.3.2 Hydrogel nanoparticle networks.

Figure 3.4 shows the temperature-dependent volume change of the PNIPAM-co-allylamine nanoparticle network in water. Since the particles are linked together by covalent bonding, the network retains its shape in water. At room temperature, the gel shows iridescent colors (Fig. 3.4 a), in contrast to conventional gels, which are colorless. The colors of the samples arise from selective Bragg diffraction from ordered colloidal structures as revealed by UV-visible spectroscopy.[19] Because the inter-particle distance can vary depending on either concentration or precursor particle size, the colors of the samples can change accordingly. When the temperature was increased to 37 ^{o}C (Fig.3. 4 b), that is, above the volume phase transition temperature (Tc = 35 ^{o}C) of the PNIPAM-co-allylamine gel, the network shrank substantially and exhibited a white color due to non-selective light scattering by microdomains formed during the volume transition.[20]

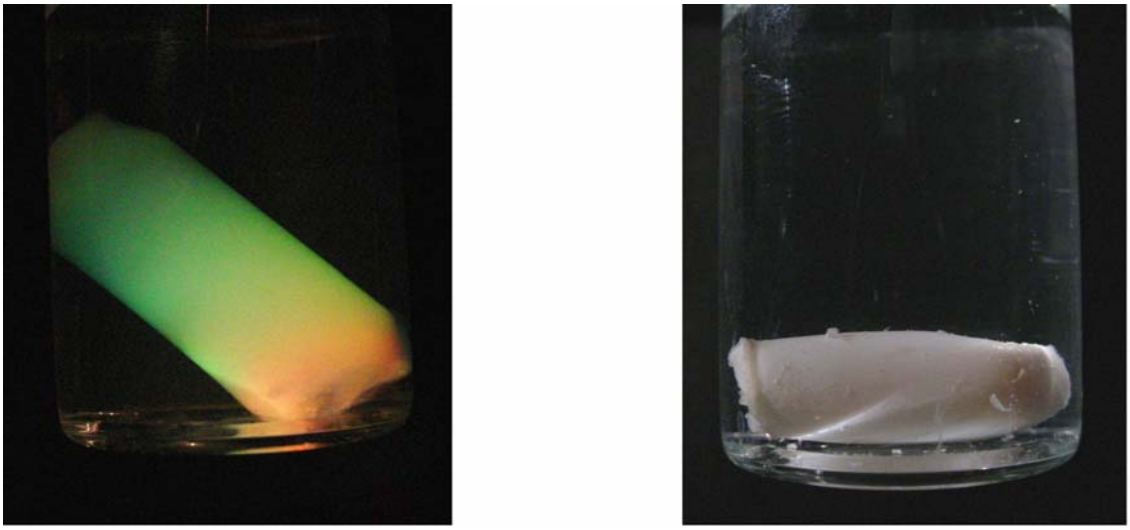

(a) (b)

Figure 3.4: Photographs of the PNIPAM-co-allylamine nanoparticle network in water at 21 and 37 °C, respectively. The diameter of the vial in the pictures is 2.73 cm. The average hydrodynamic radius of the building block in water at 21 °C is 186 nm.

By performing static light scattering measurements on the samples used in Fig. 3.1 (a), the weight-average molecule mass (M_w) of the nanoparticles was determined to be 4.8×10^8 g/mol. Using the equation $M_w/N_A=\rho(4/3)\pi<R_h>^3$, the solid densities ρ of the particle spheres in their swelling (at 21 °C) and shrinking state (at 37 °C) were estimated to be 0.030 and 0.51 g/cm^3, respectively. In comparison, the solid densities of the nanoparticle network at 21 and 37 °C were 0.024 and 0.12 g/cm^3, respectively. The solid density of the nanoparticle network was smaller than that of the particles, indicating that there were cavities between particles in the nanoparticle network.

The shrinking ratio ($V_{21\,°C}/V_{37\,°C}$) between the gel volumes at 21 and 37 °C for the nanoparticle network was ~5, which is much smaller than that (~17) for the particles. This again indicates that the nanoparticle network contained cavities between the particles. These cavities may be attributed to the more hydrophilic feature in the surface layers of the particles, because hydrophilic groups tend to stay on the surface during the polymerization process. After inter-sphere crosslinking, the total average density of the nanoparticle network became smaller, because these cavities occupy some space. This density difference between inside spheres and inter-sphere cavities may be suitable for drug loading and release and is worth further investigation.

3.3.3 Controlled drug release

In model studies, dextrans of different chain lengths were entrapped both inside the primary polymer chain networks of the PNIPAM bulk gels with a total crosslink (*N*,*N*'-methylene-bis-acrylamide) density of 9.4 mol% and in the cavities between the particles of PNIPAM-co-allylamine nanoparticle networks with total crosslink (*N*,*N*'-

methylene-bis-acrylamide and glutaric dialdehyde) density of 11.3 mol%. Dextran was labeled either with a Texas Red dye or with fluorescent groups.

The two gels were immersed in water at room temperature or 37 °C and the time dependent drug release was monitored by UV–visible spectroscopy. At room temperature, the cumulative release of dextrans MW 3000–500,000 from the bulk gel was very small (Fig. 3.5 a). After 28 h, the cumulative released dextran was lower than 25% of the load. In contrast, dextrans entrapped in the cavities of PNIPAM-co-allylamine gel nanoparticle networks were released much faster (Fig. 3.5 b). The release rate of dextrans with a low molecular weight (3000 and 10,000) was roughly constant within the time range investigated, and the total dextran released after 9 h was 50% and 60% of the original loads, respectively.

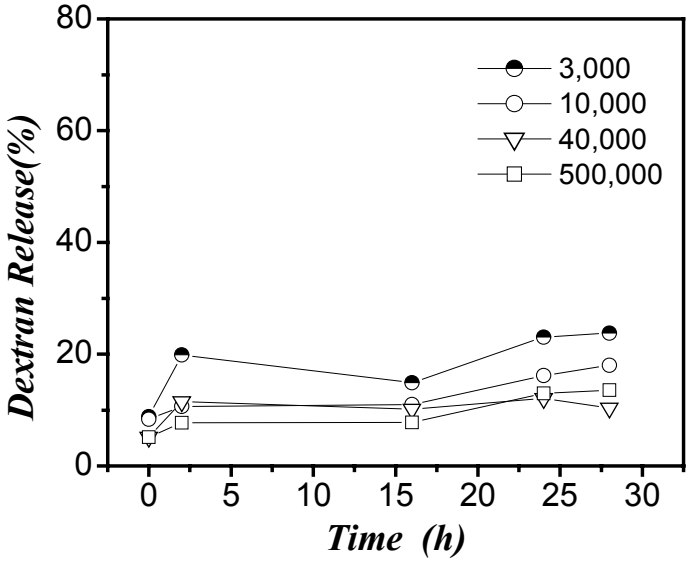

(a)

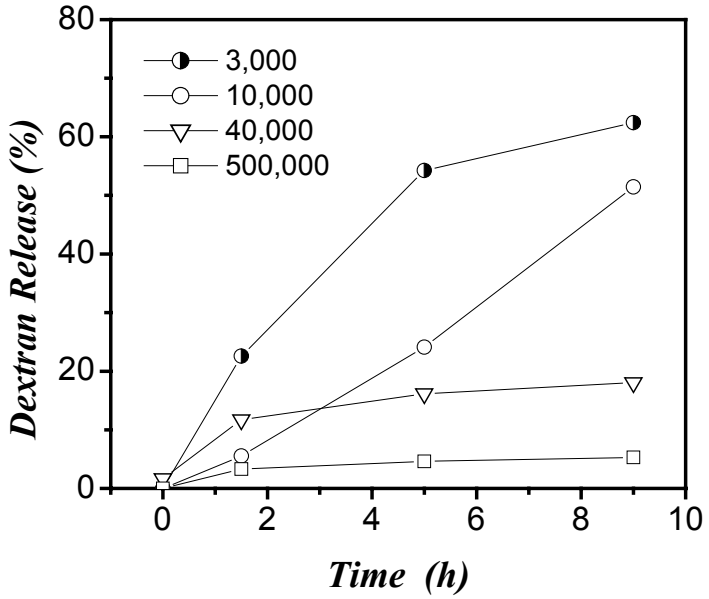

(b)

Figure 3.5: The time dependent dextran release at room temperature monitored by UV/Vis spectroscopy: (a) from a PNIPAM bulk gel, (b) from PNIPAM-co-allylamine nanoparticle network. The dyed or fluorescent dextrans have nominal molecular weights of 3,000 (black and white semi-circles), 10,000 (open circles), 40,000 (downward triangles) and 500,000 (squares).

It is known that, the average linear polymer molecular segment between two neighboring crosslinking knots in a bulk gel, can be defined as the mesh size, which depends on the molar ratio of the crosslinker to the monomer, and is usually around 1–10 nm. In the present case, the molar ratio is ~1:10. Based on a C---C bond length of 1.54 Å, and a bond angle is 109°, the polymer segment length of ten C---C bonds between two crosslinking points, is about 1 nm. This is small even for the diffusion of dextran with lowest molecular weight of 3000.

In contrast, the mesh size between particles in the nanoparticle network depends on the volume fraction and the size of the particles. In the current case, the particles are closely packed with a volume fraction of approximately 0.74. As a result, the mesh size is primarily determined by the particle radius and is about 120 nm at room temperature. Consequently, this network can selectively control the diffusion rate of dextrans with different molecular weights. The release of dextran, Mw 500,000 is almost zero, compared to the fast release of dextran, Mw 3000. Porous bulk gels previously have been employed for delivery of large molecules.[15] However, the pore size distribution of a porous gel is expected to be much broader than the mesh size distribution of a uniformly packed nanoparticle network, because the particle size can be well-controlled, with a size variation of less than 5%.

PNIPAM and its derivatives have been used to obtain an on–off drug release profile in response to a stepwise temperature change.[7-12] Creating the PNIPAM-co-allylamine nanoparticle network allows one to obtain a temperature-induced volume phase transition not only for the constituent building blocks but also for the close-packed particle structure. Fig. 3.6 shows release profiles of dextran with different molecular weights from the nanoparticle network at 21 and 37 °C, respectively. It can be seen that the release of dextran at 21 °C is much faster than at 37 °C. This is due to the collapse of the nanoparticle network at 37 °C, hindering the diffusive release of dextran. Such an on–off release profile was observed for dextrans with MW of 70,000, 40,000, and 10,000, as shown in Fig. 3.6 a–c.

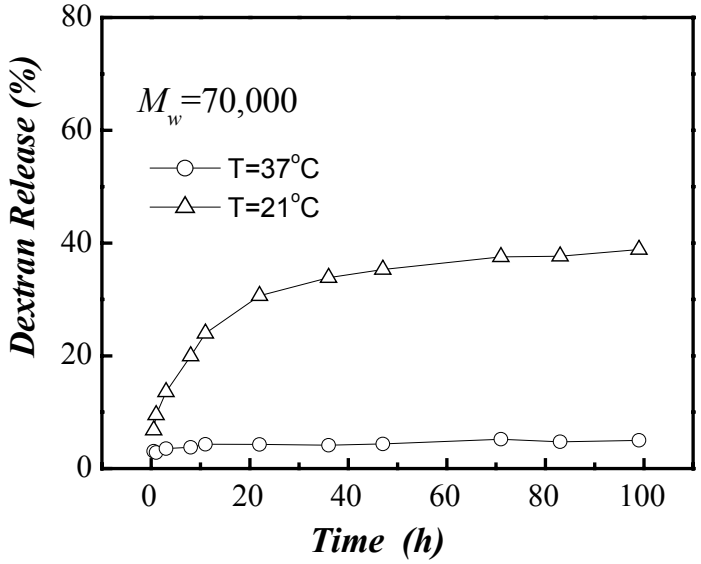
80
60
40
20
0
M_w=70,000
T=37°C
T=21°C
Dextran Release (%)
0
20
40
60
80
100
Time (h)

(a)

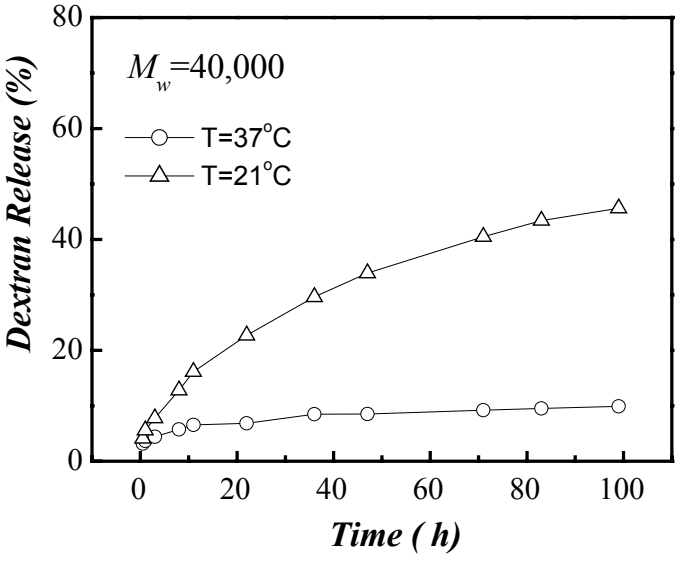
80
60
40
20
0
M_w=40,000
T=37°C
T=21°C
Dextran Release (%)
0
20
40
60
80
100
Time (h)

(b)

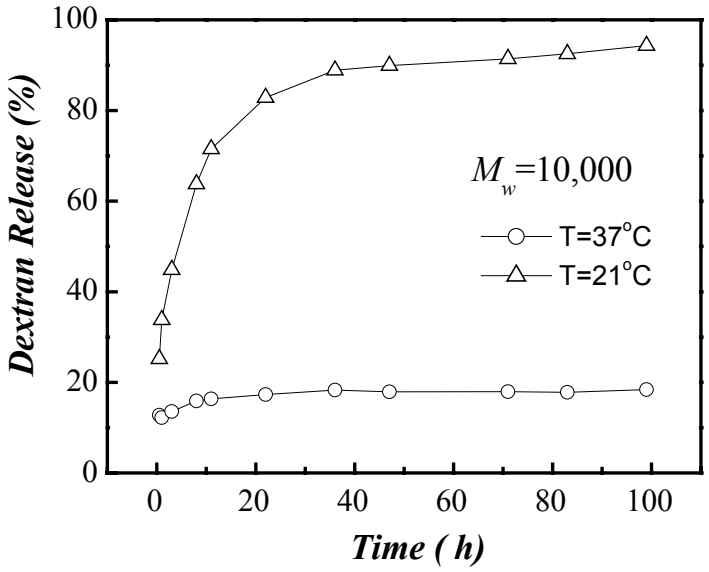

(c)

Figure 3.6: Cumulative release of Texas Red dye labeled dextrans from PNIPAM-co-allylamine nanoparticle network at 21 and 37 °C with dextrans of molecular weight (a) 70,000; (b) 40,000; and (c) 10,000.

In contrast, the PNIPAM-co-acrylic acid (PNIPAM-co-AA) nanoparticle network exhibited a temperature-independent release profile for dextran. As shown in Fig. 3.7, the cumulative release profiles of dextran, MW 10,000 at 21 and 37 °C were very similar, the difference being within the error range (about 15%) for repeated measurements. Here, complete release of dextran was 100%. This is understandable because the volume phase transition temperature of the copolymer is higher than 37 °C. Without a substantial collapse of the gel network, the mesh size does not change much. Release of dextran with a higher MW of 70,000 from the same PNIPAM-co-PAA nanoparticle network at 37 °C

is shown in Fig. 3.7. Again, dextran with a higher molecular weight was released more slowly.

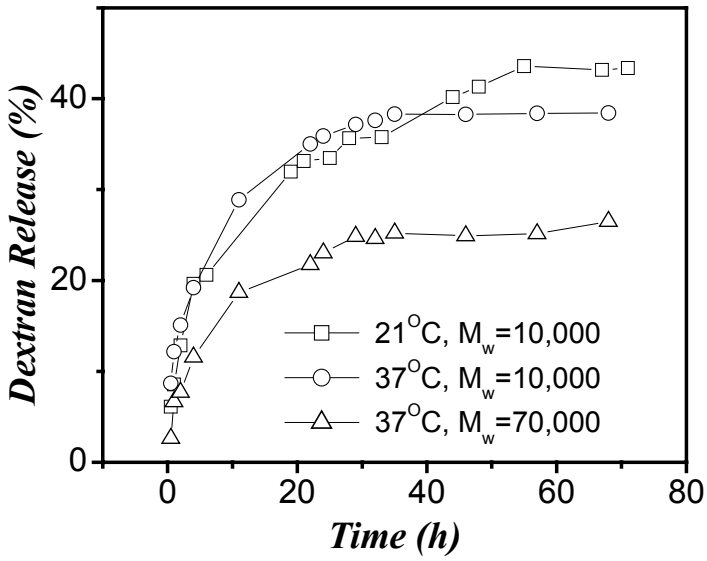

Figure 3.7: Cumulative release of dextrans with different molecular weights from PNIPAM-co-AA nanoparticle network: dextran 10,000 at 21 °C (squares), dextran 10,000 at 37 °C (circles), and dextran 70,000 at 37 °C (triangles).

Although the same comonomer mixing ratio was used for preparation of PNIPAM-co-allylamine and PNIPAM-co-acrylic acid gels, the relative reactivity of the two comonomers for polymerization is different, resulting in a different functional group density on the nanoparticle surfaces. This may, in turn, influence the crosslinking between nanoparticles, the mesh size of secondary structure, and the dextran release patterns, depending on the molecular weight. However, since the PNIPAM-co-allylamine nanoparticle network exhibited the volume change below 37 °C, while PNIPAM-co-AA

does not, the relative reactivity of allylamine and AA may not significantly affect the thermally responsive release properties.

3.4 Conclusions

Monodispersed nanoparticles of PNIPAM-co-allylamine and PNIPAM-co-AA were synthesized and used as building blocks to create three-dimensional networks. The close-packed PNIPAM-co-allylamine and PNIPAM-co-AA nanoparticles were stabilized by covalently bonding neighboring particles using glutaric dialdehyde and adipic acid dihydrazide as crosslinking agents, respectively. Both crosslinking reactions were carried out at room temperature and in a neutral or slightly acidic environment. Dyed or fluorescent dextran macromolecules with different molecular weights, between 3000 and 500,000, were used as a model drug system for the study of release kinetics. It is found that, dextran entrapped between particle cavities in the nanoparticle network was released with a rate regulated by their molecular weights and the cavity size; no release from a conventional bulk PNIPAM gel with high crosslinking density was observed. The release of dextran macromolecules from the PNIPAM-co-allylamine network was much faster at room temperature than that at human body temperature. In contrast, the PNIPAM-co-AA network showed a temperature-independent release profile for dextran macromolecules with relatively low molecular weights. Creating the PNIPAM derivative nanoparticle networks allowed useful functionality for controlled drug release not only from the constituent building blocks but also from their close-packed particle structures.

Chapter References

1. Peppas, N. A., Langer, R. *Science* **1994**, 263, 1715.
2. Tanaka, T. *Phys. Rev. Lett*. **1978**, 40, 820.
3. Hirotsu, S., Hirokawa, Y., Tanaka, T. *J. Chem. Phys*. **1987**, 87, 1392.
4. Siegel, R. A., Firestone, B. A. *Macromolecules* 1988, 21, 3254.
5. Osada, Y., Okuzaki, H., Hori, H. *Nature* **1992**, 355, 242.
6. Hu, Z. B., Zhang, X., Li, Y. *Science* **1995**, 269, 525; Hu, Z. B., Chen, Y., Wang, C., Zheng, Y., Li, Y. *Nature* **1998**, 393, 149.
7. Hoffman, A. S. *J. Controlled Release* **1987**, 6, 297.
8. Bae, Y.H., Okano, T., Kim, S.W. *Pharm. Res*. **1991**, 8, 531.
9. Bae, Y.H., Okano, T., Kim, S.W. *Pharm. Res*. **1991**, 8, 624.
10. Okano, T., Bae, Y.H., Jacobs,H., Kim, S.W. *J. Controlled Release* **1990**, 11, 255.
11. Gutowska, A., Bae, Y.H., Feijen, J., Kim, S.W. *J. Controlled Release* **1992**, 22, 95.
12. Okuyama, Y., Yoshida, R., Sakai, K., Okano, T., Sakurai, Y. *J. Biomater. Sci. Polym.* **1993**, Ed. 4, 545.
13. Wang, C., Stewart, R. J., Kopecek, J. *Nature* **1999**, 397, 417.
14. Qiu, Y., Park, K. *Advanced Drug Delivery Reviews* **2001**, 53, 321.
15. Kabra, B. G., Gehrke, S. H., Spontak, R. J. *Macromolecules* 1998, 31, 2166; Gehrke, S. H., in: Amidon, G.L., Lee, P.I., Topp, E.M. (Eds.), *Marcel Dekker,*

New York, 2000, 473.

16. Hu, Z. B., Lu, X., Gao, J., Wang, C. *Adv. Mater*. **2000**, 12, 1173; Hu, Z. B., Lu, X. H., Gao, *J. Adv. Mater*. **2001**, 13, 1708.

17. Pelton, R. H., Chibante, P. *Colloids and Surfaces* **1986**, 20, 247.

18. Hermanson, G. T. *Bioconjugate Techniques*, 1996, Academic Press: San Diego.

19. Gao, J., Hu, Z. B. *Langmuir* **2002**, 18, 1360.

20. Hu, Z. B., Wang, C. J., Chen, Y. Y., Zhang, X. M., Li, Y. *J. Polym. Sci., Part B: Polym. Phys.* **2001**, 39, 2168.

CHAPTER 4

A NEW ROUTE TO CRYSTALLINE HYDROGELS AS GUIDED BY A PHASE DIAGRAM*

4.1 Introduction

Monodispersed colloidal systems have been used as models for the study of phase transitions and as templates for the fabrication of photonic crystals.[1-7] Most investigations on colloids are primarily focused on hard-sphere-like particles such as polymethylmethacrylate, silica or polystyrene.[7] It has been found recently that wet and soft poly-N-isopropylacrylamide (PNIPAM) nanoparticles can self-assemble into a crystalline array in water.[8-14] However, the use of PNIPAM colloidal dispersions based on their crystalline structure is limited because the structure can be easily destroyed by any external disturbance such as small vibrations. To solve this problem, Asher and co-workers have developed a method for embedding a polystyrene colloidal crystalline array inside a PNIPAM gel.[7, 14] Hu et al. have demonstrated that the crystalline structure of PNIPAM nanoparticles can be stabilized by bonding particles into a network.[15-16] The later approach has a limit that the particle-linking reaction had to be carried out under a harsh environment (pH 12) that could encumber loading protein drugs. Furthermore, the mechanical strength of the bonded particle assembly was weak due to its low polymer concentration. Here we show a new route towards the fabrication of crystalline hydrogels

* Reproduced with permission from [Hu, Z.B., Huang, G. *Angew Chem Inter. Ed*., **2003**, 42, 4799] Copyright [2003] Wiley-VCH Verlag GmbH & Co. KgaA, Weinheim

following a phase diagram. The central idea is to synthesize monodispersed nanoparticles of PNIPAM-co-allylamine and measure the phase diagram of their water dispersion. Taking advantage of the fact that the thermally sensitive nanoparticles in colloidal glasses can be converted into ordered crystals via particle based volume transition as reported by Lyon and co-workers,[11] a crystalline hydrogel could be obtained by initiating the crystallization process near the colloidal crystal melting temperature while subsequently bonding the PNIPAM-co-allylamine particles below the glass transition temperature. This can increase the polymer concentration, resulting in a crystalline hydrogel with higher mechanical strength. Furthermore, the allylamine contributes amine groups that can be covalently bonded in water at a neutral pH but does not significantly affect the volume phase transition of the PNIPAM polymer. Hydrogels are well known for their unique hydrophilic and environmentally responsive properties that lead to fascinating applications including controlled drug delivery, artificial muscles, devices and sensors.[17-25] Tailoring hydrogels with periodic structures under mild synthesis conditions could open a new avenue for these applications.

4.2 Experimental Section

4.2.1. Synthesis of hydrogel nanoparticles:

3.845 g NIPA monomer, 0.2 g (10% molar ratio) allylamine monomer, and 0.1315 g methylene-bisacrylamide as crosslinker, 0.0755 g sodium docecyl sulfate as surfactant, and 230 ml deionized water were mixed in a reactor. The solution was heated

up to 60 ^{o}C under nitrogen bubbling for about 40 min, and 0.155 g potassium persulfate dissolved in 20 ml of deionized water was added to initiate the reaction. The reaction was carried out at 60 ^{o}C for 5h. The resulting particle dispersions were dialyzed for 7 days to remove small molecules and surfactants.

4.2.2. UV-visible characterization:

The PNIPAM-co-allylamine particle dispersions have been condensed using an ultracentrifuge with the speed of 40,000 rpm for 2 h. The polymer concentration of a dispersion was obtained by completely drying the dispersion at 60 ^{0}C and then weighing it. The turbidity of the PNIPAM-allylamine nanoparticle dispersions was measured as a function of the wavelength using a UV-Visible Spectrophotometer (Agilent 8453).

4.2.3. Synthesis of crystalline hydrogels:

PNIPAM-allylamine particle dispersion of 4.0 wt % was heated from 23 ^{0}C to 40 ^{0}C and then cooled back to 23 ^{0}C with a rate about 0.4 ^{0}C/min. We then added glutaric dialdehyde (0.04 g 25 wt % for 1 g dispersion) as a crosslinker to the top of the dispersion. This chemical agent diffused through the dispersion and covalently bonded the particles together in neutral pH as illustrated in Scheme 4.1. The particle assembly with a crystalline structure was stabilized by the crosslinking reaction in about two days, and removed from the test tube by injecting water to the bottom of the tube using a syringe.

4.3 Results and Discussions

Monodispersed N-isopropylacrylamide (PNIPAM)-co-allylamine colloidal spheres were synthesized using a percipitation polymerization method.[26] These particles showed the phase behavior similar to that of pure PNIPAM gel [27] with a slightly higher volume phase transition temperature around 35 ^{o}C. The average hydrodynamic radius of the particle is about 140 nm at 23 ^{o}C and shrinks to about 80 nm at 36 ^{o}C.

The dispersions with polymer concentrations ranging from 2 wt-% to 4 wt-% exhibit iridescent colors as shown in Fig. 4.1 (a), indicating that the particles self-assemble into an ordered arrangement. As the polymer concentration increases, the crystalline grain size decreases and the color shifts to shorter wavelengths. When the concentration is above 4.5 wt-%, the crystals are too small to be observed and the assemblies are in a glass phase. When the concentration is below 1.8 wt-%, the dispersions become cloudy because the particles are well separated, and scatter light randomly.

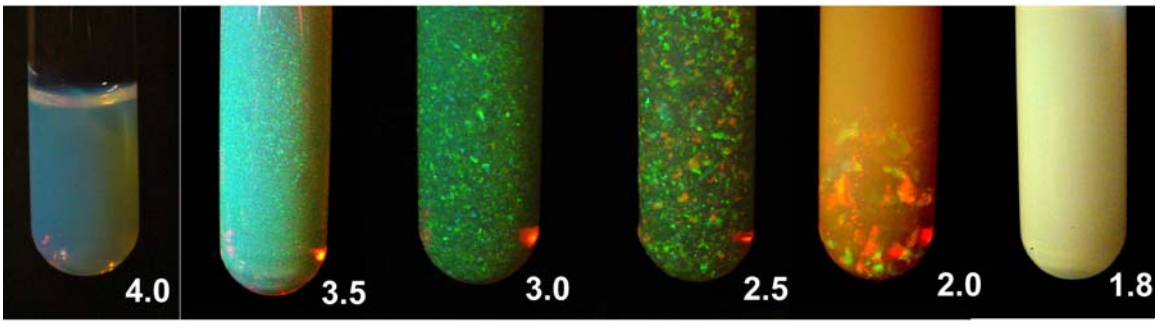

(a)

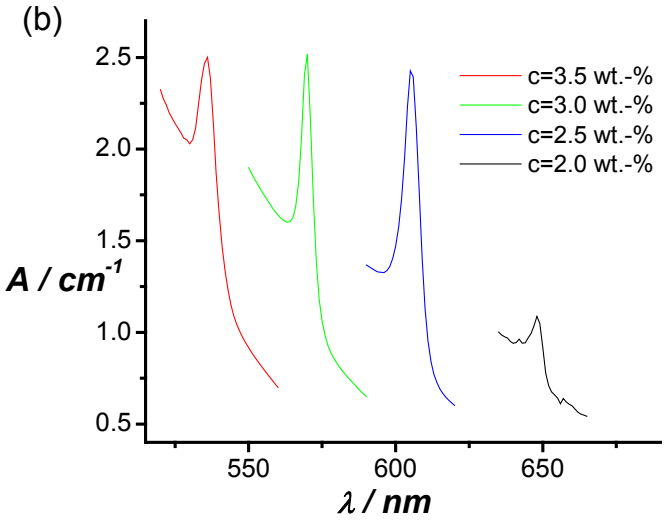

Figure 4.1: (a) Photographs of PNIPAM-allylamine nanoparticle dispersions at various polymer concentrations at 23 ^{o}C. From left to right: 4.0, 3.5, 3.0, 2.5, 2.0 and 1.8 wt. %. Here the average hydrodynamic radius of the particles in water at 23 ^{o}C is 140 nm. The diameters of the tubes are 1 cm. (b) The turbidity versus wavelength curves measured using a UV-visible spectrophotometer. The Bragg diffraction peak shifts to lower wavelength as the polymer concentration increases. From left to right: 3.5, 3.0, 2.5, and 2.0 wt.%.

The color observed in the dispersions is due to diffraction from the ordered colloidal arrays with a lattice spacing on the order of the wavelength of visible light according to the Bragg's law: $2nd\sin\theta = m\lambda$, where n is the mean refractive index of the dispersion, θ is the diffraction angle, d is the lattice spacing, m is the diffraction order, and λ is the wavelength of diffracted light.[8] Figure 4.1 (b) shows the turbidity of the PNIPAM-allylamine nanoparticle dispersions as a function of the wavelength. The sharp peak is from the Bragg diffraction and shifts from 640 nm to 530 nm as the

polymer concentration increases from 2.0 wt% to 3.5 wt%. This shift is due to the decrease of the inter-particle distance with higher polymer concentration.

Figures 4.2 (a) and (b) show the temperature dependent turbidity of the PNIPAM-allylamine colloidal dispersions at 2.5 wt. % and 3.0 wt. %, respectively. When the temperature is increased above room temperature, the intensity of the Bragg peak initially increases, indicating that heating can facilitate the formation of an ordered structure. As the sample is heated further, the Bragg peak becomes broader, shifts to shorter wavelength and eventually disappears at a melting temperature, T_m. The value of T_m increases as polymer concentration increases. This phase behavior is summarized in a diagram as shown in Figure 4.2 (c). Here T_c (dashed line) is the volume phase transition temperature of PNIPA-allylamine particles, T_m (solid squares) is the melting temperature and T_g (open circles) is the glass transition temperature.

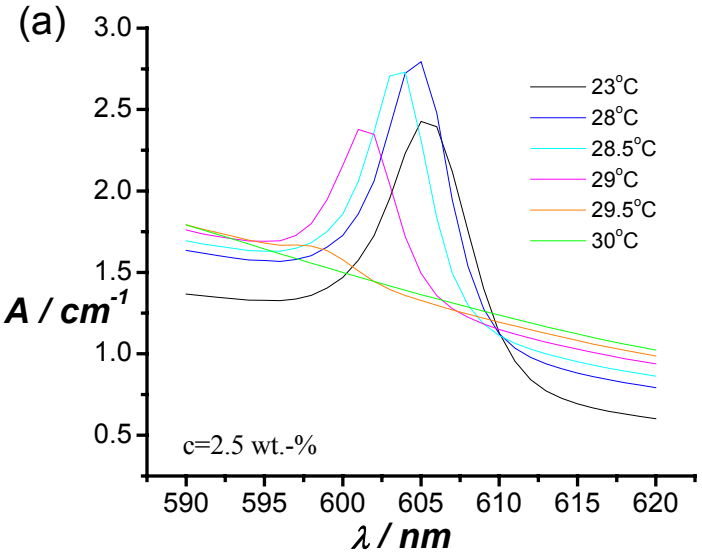

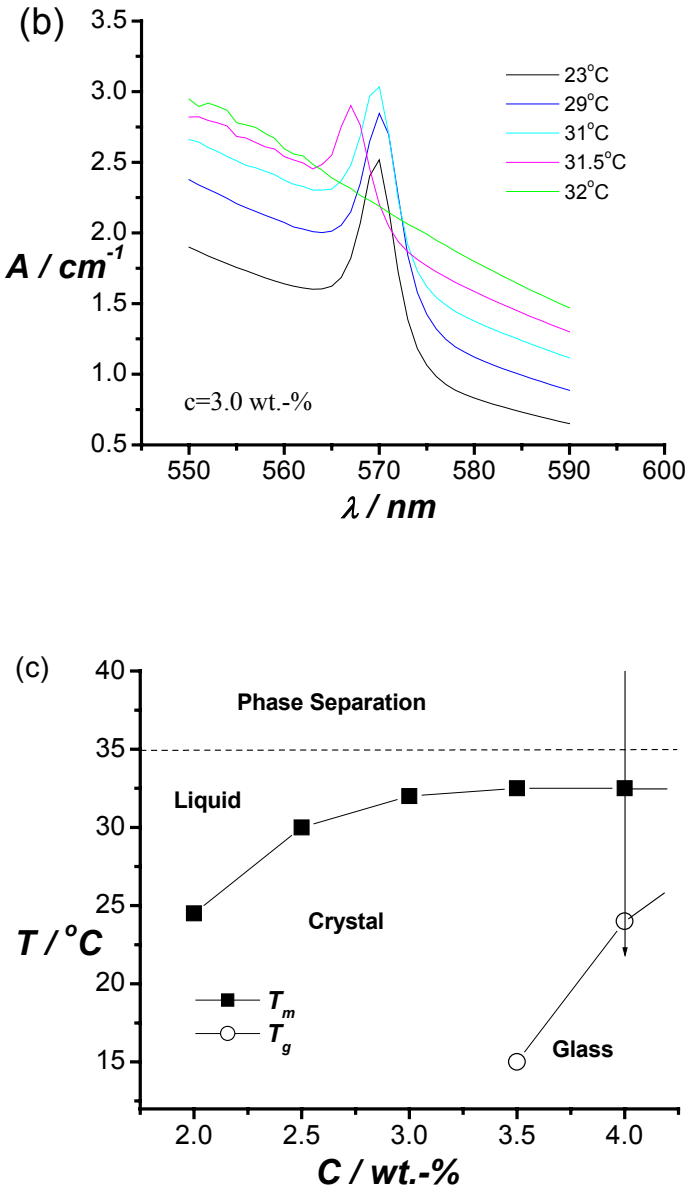

Figure 4.2: Temperature-dependent phase behavior of the PNIPAM-allylamine nanoparticle dispersions. (a) The turbidity versus wavelength curves at various temperatures for C=2.5 wt.% dispersion. (b) for C=3.0 wt.% dispersion. (c) The phase diagram: the dashed line (T_c) indicates the volume phase transition of the PNIPAM-allylamine particles, the solid square represents the melting temperature, T_m, and the open circle represents the glass transition temperature, T_g.

Guided by this diagram, we have engineered a crystalline hydrogel with higher polymer concentration. We started with a PNIPAM-allylamine particle dispersion of 4.0 wt % at which the viscosity is too high to allow the particles to form a periodic structure at room temperature. This system was heated from 23 ^{0}C to 40 ^{0}C and then cooled back to 23 ^{0}C with a rate about 0.4 ^{0}C/min. As shown by an arrow in Fig. 4.2 (c), when the sample was cooled below T_m, the crystallization started. Here the dispersion had low viscosity since the particles were only partially swollen. This allowed the spheres to have enough freedom to self assemble into an ordered array. When the sample was cooled further to below T_g, the particle size and viscosity increased considerably. As a result, the crystalline structure formed at the higher temperature was "frozen", or preserved. Then, the particle assembly with a crystalline structure was fully stabilized by the crosslinking reaction in neutral pH as illustrated in Scheme 4.1 in about two days. Due to the higher mechanical strength of this crystalline hydrogel, it is easier to remove it from the tube than the previous sample formed at room temperature in a high pH aqueous solution.[16] It is apparent that a combination of the covalent bonding process and the heating-cooling process yields a crystalline structure at a high polymer concentration and can significantly improve the mechanical strength of a crystalline hydrogel.

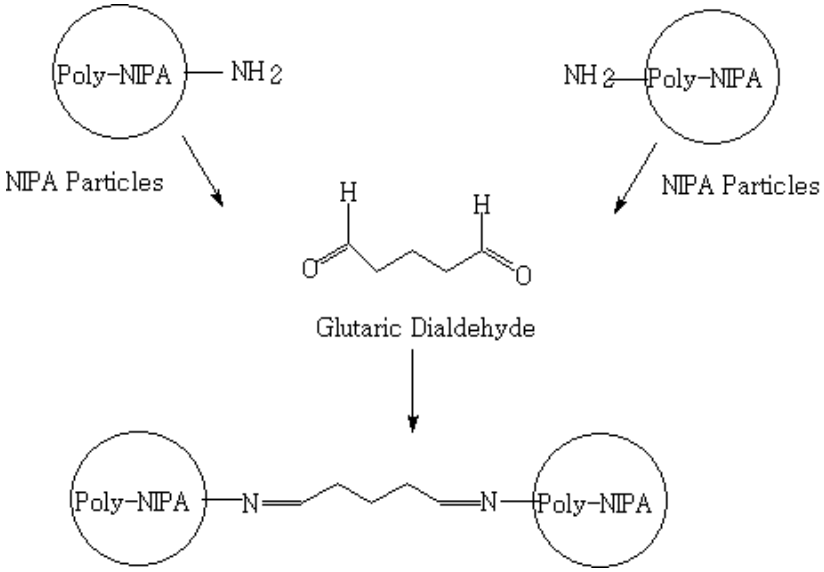

Scheme 4.1: The amine (NH_2) groups on the PNIPAM-allylamine nanoparticles react with glutaric dialdehyde to form a network in water under a neutral pH and room temperature.

This fabrication process leads to the formation of crystalline hydrogels with different iridescent color patterns. Figure 4.3 shows blue, green, and red iridescent hydrogels that have corresponding polymer concentrations at 5.4, 4.0 and 3.5 wt%, respectively. Upon the increase of the polymer concentration, the inter-particle distance decreases, causing a blue-shift in iridescent color. Here, we have not only made soft and wet crystalline hydrogels that have an iridescent pattern as that of a precious hard opal, but we have also developed a way to engineer different iridescent colors.

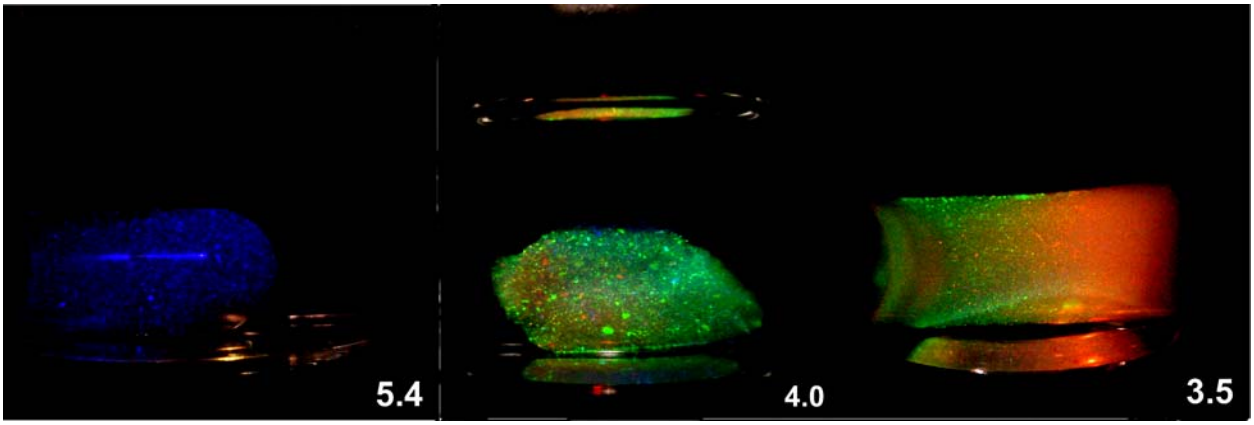

Figure 4.3: Iridescent colors of the PNIPAM-allylamine crystal hydrogels made via Scheme 4.1 change with polymer concentration in water at pH 7. From left to right: 5.4, 4.0, and 3.5 wt%. The average hydrodynamic radii for the three samples in water at 23 ^{o}C are about 140 nm. The diameter of the vial is 2.73 cm.

Creating crystalline hydrogels allows us to obtain useful functionalities not only from the periodic structure but also from the constituent building blocks. Because the building blocks here are environmentally responsive colloidal spheres, their sizes as well as the lattice spacing should be tunable by external stimuli. As a result, the crystalline hydrogel can serve as an optical sensor to visually determine environmental changes. One of the examples is shown in Figure 4.4 (a). The crystalline hydrogel at room temperature displays a bright green color. With the increasing temperature, the color of the gel changes from green to blue at 34 ^{o}C, and eventually to milky white at 35 ^{o}C, just above the volume phase transition temperature of the particles. When the temperature is decreased to room temperature again, the gel returned its original color and volume. This process is fully reversible. The change of color is due to the shrinkage of particle size with the temperature, which causes the decrease of inter-particle spacing. It is noted here

that the current hydrogel has iridescent speckles, indicating the existence of large crystalline domains, in contrast to previous thermally tunable hydrogels that have only a uniform color. [16]

Due to the residues of basic (i.e. $-NH_2$) groups on the PNIPAM-allylamine building blocks, the swelling capacity of the resulting hydrogel can be changed by controlling the pH value of the medium. As shown in Figure 4.4 (b), the color of the hydrogel shifts from green to blue as the pH value is changed from 7 to 11. The amine groups on the particles are partially ionized in water at a neutral pH, causing swelling of the particles. At a higher pH, the ionization of the basic groups is inhibited, causing the shrinkage of the particles. This change of the building block size at different pH values causes the lattice spacing to decrease, resulting in the color change.

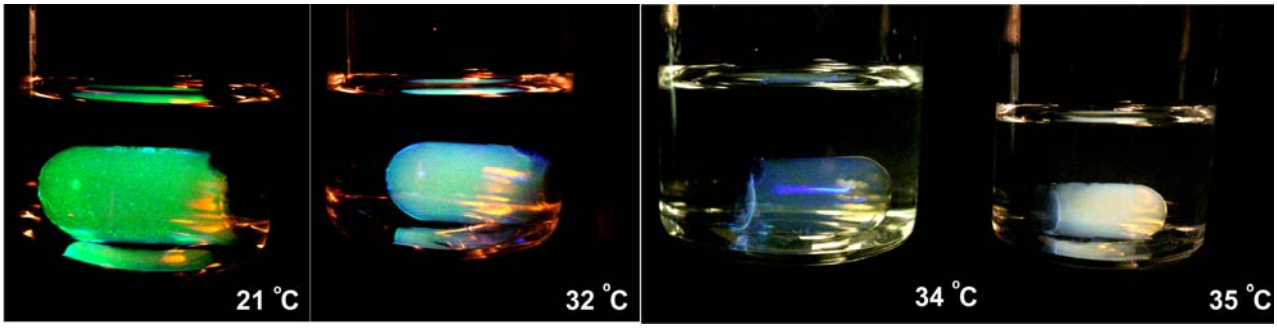

(a)

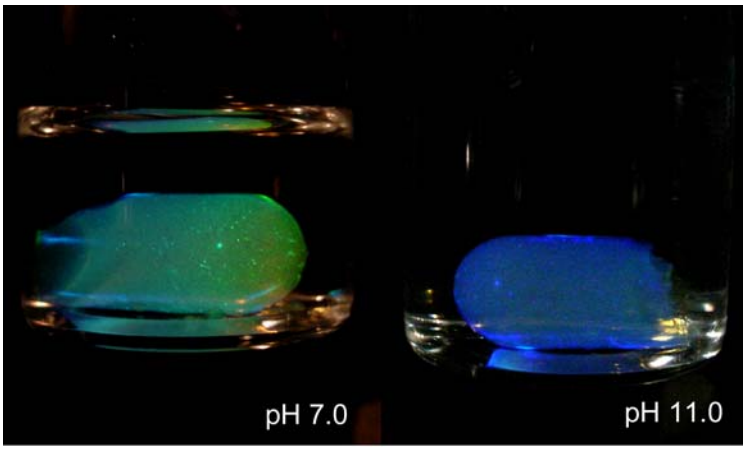

(b)

Figure 4.4: (a) The PNIPAM-allylamine crystal hydrogel changes its iridescent colors with the temperature. The diameter of the vial is 2.73 cm. From left to right: 21, 32, 34 and 35 ^{o}C. (b) pH responsive property of the PNIPAM-allylamine crystalline hydrogel. From left to right: pH 7 and pH 11.

4.4 Conlcusions

In summary, monodispersed PNIPAM-co-allylamide colloidal spheres have been synthesized by precipitation polymerization. The phase diagram of this system is determined using a UV-visible spectrophotometer. Following the phase diagram, a new route to make a crystalline structure with high polymer concentration is discovered by initiating crystallization near T_f but stabilizing the crystalline structure below T_g. The stabilization is achieved by bonding the PNIPAM-allylamine spheres using glutaric dialdehyde as the crosslinker at room temperature under a neutral pH. The hydrogel with a higher polymer concentration has a better mechanical strength, while a mild synthesis condition at pH 7 makes this material particularly useful for biomedical applications, including loading biomolecules between the particles for controlled drug

delivery. The crystalline hydrogels exhibit iridescent patterns that are tunable by the change of temperature or pH. This kind of soft and wet hydrogels with periodic structures may lead to new sensors, devices, and displays operating in aqueous solutions where most biological and biomedical systems reside.

Chapter References

1. Pusey, P. N. in *Liquid, Freezing, and the Glass Transition*, edited by Les Houches, Levesque, J. P. H. D., Zinn-Justin, J. Elsevier, Amsterdam, **1990**.
2. Blaaderen, A. V., Ruel, R., Wiltzius, P. *Nature* **1997**, 385, 321.
3. Cheng, Z., Russel, W. B., Chaikin, P. M. *Nature* **1999**, 401, 893.
4. Jiang,P., Bertone, J. F., Colvin, V. L. *Science* **2001**, 291, 453.
5. Jethmalani, J. M., Sunkara, H. B., Ford, W. T., Willoughby, S. L., Ackerson, B. J. *Langmuir* **1997**, 13, 2633.
6. Lellig, C., Hartl, W., Wagner, J., Hempelmann, R. *Angew. Chem. Int. Ed*. 2002, 41, 102.
7. Xia, Y., Gates, B., Yin, Y., Lu, Y. *Adv. Mater*. **2000**, 12, 693; Xia, Y. *Adv. Mater*. **2001**, 13, 369.
8. Weissman, J. M., Sunkara, H. B., Tse, A. S., Asher, S. A. *Science* **1996**, 274, 959.
9. Senff, H., Richtering, W. *Langmuir* **1999**, 15, 102.
10. Debord, J. D., Lyon, L. A. *J. Phys. Chem*. **2000**, 104, 6327; Debord, J. D., Eustis, S., Debord, S. B., Lofye, M.T., Lyon, L. A. *Adv. Mater.* **2002**, 14, 658.
11. Hellweg,T., Dewhurst, C. D., Bruckner, E., Kratz, K., Eimer, W. *Colloid and Polymer Science* **2000**, 278, 972.
12. Gao, J., Hu, Z. B. *Langmuir* **2002**, 18, 1360.
13. Wu, J. Z., Zhou, B., Hu, Z. B. *Phys. Rev. Lett*. **2003**, 90, 048304. ; Wu, J. Z., Huang, G., Hu, Z. B. *Macromolecules* **2003**, *36*, 440.

14. Holtz, J. H., Asher, S. A. *Nature* **1997**, 389, 829.

15. Hu, Z. B., Lu, X. H., Gao, J., Wang, C. J. *Adv. Mater.* **2000**, 12, 1173.

16. Hu, Z. B., Lu, X. H., Gao, J. *Adv. Mater.* **2001**, 13, 1708.

17. Peppas, N. A., Langer, R. *Science* **1994,** 263, 1715.

18. Tanaka, T., Nishio, I., Sun, S. T., Ueno-Nishio, S. *Science* **1982**, 218, 467.

19. Siegel, R. A., Firestone, B. A. *Macromolecules* **1988***,* 21, 3254.

20. Osada, Y., Okuzaki, H., Hori, H. *Nature* **1992**, 355, 242.

21. Chen, G., Hoffman, A. S. *Nature* **1995,** 373, 49.

22. Osada, Y., Gong, J. P. *Adv. Mater.* **1998**, 10*,* 827.

23. Snowden, M. J., Murray, M. J., Chowdry, B. Z. *Chemistry & Industry* **1996**, 531.

24. Wang, C., Stewart, R. J., Kopecek, J. *Nature*, **1999**, 397, 417.

25. Lendlein, A., Kelch, S. *Angew. Chem. Int. Ed*. **2002**, 41, 2034.

26. Pelton, R. H., Chibante, P. *Colloids Surf.* **1986**, 20, 247.

27. Hirotsu, Y., Hirokawa, T., Tanaka, T. *J. Chem. Phys*. **1987**, 87, 1392.

CHAPTER 5

TUNABLE OPAL HYDROGEL SENSORS

5.1 Introduction

The self-assembly of colloidal microgels became a topic of growing interest in recent years.[1-12] Due to the electrostatic repulsion between monodispersed particles, colloids can form an ordered array. This periodic hydrogel structure has a spacing of the order of hundreds of nanometers, therefore interacting strongly with visible and infrared light, leading to optical Bragg diffraction.[13] The optical diffraction may be shifted due to transformation of the hydrogel from a swollen hydrophilic network to a collapsed hydrophobic network. These gels are especially interesting because they can respond to a variety of physical and chemical stimuli by changing their dimensions. Unfortunately, these wet colloidal crystal dispersions are not robust so they can be easily destroyed by an external disturbance such as shock or heating, which could cause irreversible disruption of the ordered structure. Asher and co-workers entrapped a three-dimensional crystalline colloidal array (CCA) of monodispersed, highly charged polystyrene latex particles in a hydrogel. The volume phase transition of the hydrogel causes a change in the CCA lattice spacing, which changes the diffraced wavelength of light. Such hydrogels have been used as metal ion, sugar and pH sensors.[14-18] Braun et al. [19-20] and Watanabe et al.[21-22] have developed an inverse opal hydrogel by polymerization of Poly-N-ispropylacrylaimde (PNIPAM) or 2-hydroxyethylmethacrylate (HEMA) hydrogel within the interstitial space of a colloidal crystal template either with polystyrene or with silica,

followed by removing the template. These gels have been used as glucose or pH sensors by incorporating different functional groups in the networks. Hu and Huang demonstrated that the crystalline structure of PNIPAM nanoparticles can be stabilized by bonding particles into a network with higher mechanical strength using a heating–cooling process.[23] Due to the change of the lattice spacing between the particles, this kind of nanoparticle network change its color in response to the change of the temperature, pH or concentration of the microgels. Here, we describe the method of using UV-visible Spectroscopy to quantitively characterize the crystalline hydrogel networks and to apply these networks for sensor applications.

5.2 Experimental Section

5.2.1 Materials:

N-isopropylacrylamide (NIPA) was bought from Polyscience Co and used as received. Cross-linking agent N, N'-methylene-bis-acrylamide (MBAAm) was purchased from Bio Rad Co. Potassium persulfate (KPS), sodium dodecyl sulfate (SDS), glutaric dialdehyde, and allylamine were all purchased from Aldrich Chemical Company.

5.2.2 Synthesis of PNIPAM-co-allylamine nanoparticles.

The new kind of N-isopropylacrylamide (NIPA) derivative nanoparticles was synthesized using a precipitation polymerization method.[24] 3.845g NIPA monomer, 0.2g (10% molar ratio) allylamine monomer, and 0.1315g methylene-bisacrylamide as crosslinker, 0.0755g sodium docecyl sulfate as surfactant, and 230ml deionized water were mixed in a reactor. The solution was heated up to 60 ^{o}C under nitrogen bubbling for

about 40min, 0.155g potassium persulfate dissolved in 20ml of deionized water was added to initiate the reaction. The reaction was carried out at 60 ^{o}C for 5h. After cooling the solution to room temperature, the final reaction dispersion was exhaustively dialyzed in a dialysis tube for 7 days while the deionized water (conductivity<1 μ S.cm^{-1}) outside the tube was changed three times a day.

5.2.3 Synthesis of crystalline hydrogels.

Allylamine can provide free amine functional groups on the surface of the particles for further crosslinking sites. After using ultra-centrifuge with the speed of 40,000 rpm for 2h, we obtained condensed particle dispersions. The microgels in the dispersions self-assembled into ordered structural arrays at different concentrations when dispersions were heated from 23 ^{0}C to 40 ^{0}C and then cooled back to 23 ^{0}C with a rate of approximately 0.4 ^{0}C/min. glutaric dialdehyde (0.04 g 25 wt % for 1 g dispersion) was added as a crosslinker to the top of dispersions. This chemical agent diffused through dispersions and covalently bonded the particles together in a neutral pH solution. The particle assembly with a crystalline structure was stabilized by the crosslinking reaction in about two days, and removed from the test tube by injecting water to the bottom of the tube using a syringe.

5.2.4 UV-visible characterization.

The polymer concentration of a dispersion was obtained by completely drying the dispersion at 60 ^{0}C and then weighing it. The turbidity of the PNIPAM-co-allylamine nanoparticle dispersions was measured as a function of the wavelength using a UV-

Visible Spectrophotometer (Agilent 8453). The light source was deuterium and the wavelength ranged from 200 to 900 nm.

5.3 Results and Discussions

5.3.1 Physical properties of nanoparticles

Static light scattering was carried out for PNIPAM microgel dilute dispersions with concentration from 2.5×10^{-6} to 5×10^{-6} to 1×10^{-5}. Figure 5.1 (a) and (b) show the Zimm plots at 23 and 35 ^{o}C respectively. From the extrapolation of $KC/R_{vv}(q)$ in equation 2-10 to the zero angle and zero concentration, the second virial coefficient A_2, and the radius of gyration $\langle R_g \rangle$ were obtained and summarized in Table 5.1. The positive A_2 at 23 ^{o}C shows that water is a good solvent for the PNIPAM-co-allylamine microgel, while the negative value of A_2 at 35^{o}C shows that water becomes a poor solvent when the temperature is above the LCST (about 34 ^{o}C). By combining DLS and SLS results, we can find that $R_g/R_h=0.713$ is lower than $0.774=(3/5)^{1/2}$ at 23 ^{o}C, indicating that there are some pendant PNIPAM segments on the microgel surface. While at 35 ^{o}C, $R_g/R_h=0.747$ is close to the theoretical value of $(3/5)^{1/2}$ for the uniform hard spheres, which means uniform dense spheres for PNIPAM-co-allylamine microgels at the temperatures higher than the LCST.

Temp. (ºC)	R_h (nm)	R_g (nm)	A_2 ($mol.dm^3/g^2$)	M_w (g/mol)
23	128	91.3	8.404×10^{-9}	7.08×10^{8}
35	75	55.7	-1.911×10^{-8}	3.67×10^{8}

Table 5.1: Static and Dynamic light scattering results of the PNIPA-co-allylamine particles in the water dispersion

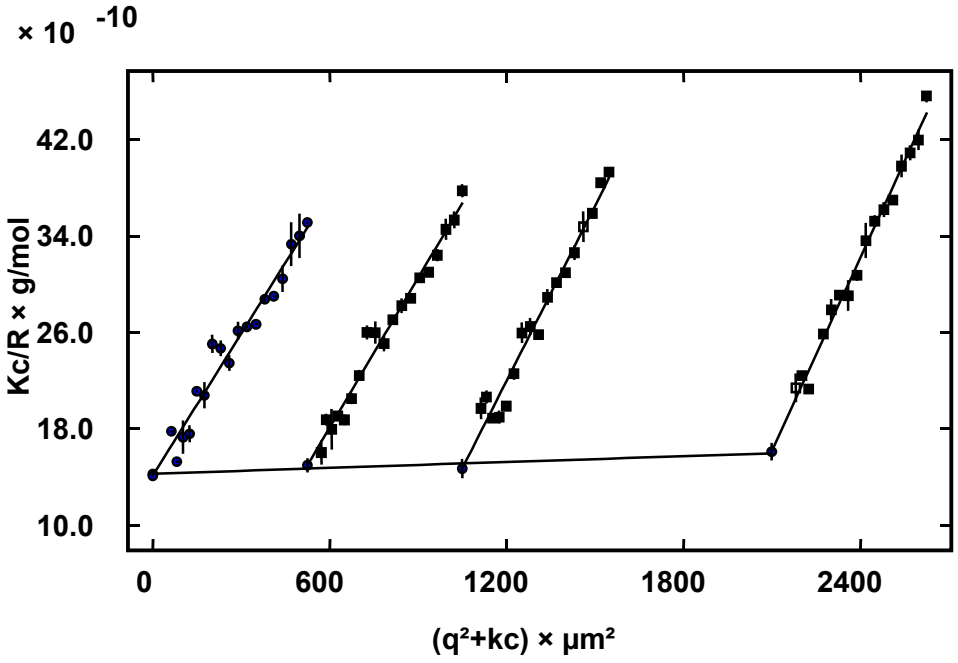

(a)

.

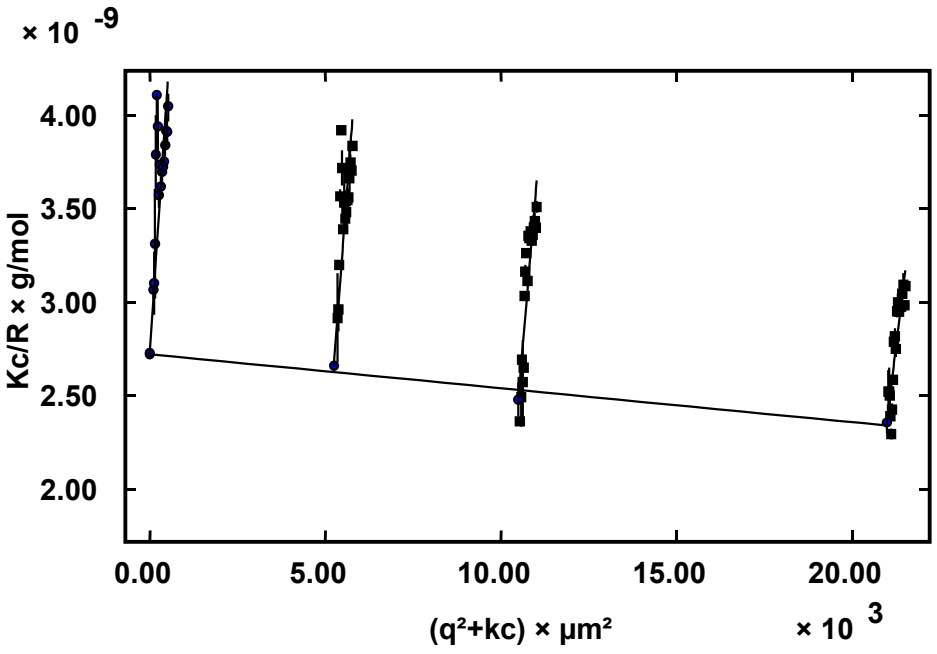

(b)

Figure 5.1: Zimm plots of the PNIPAM-co-allylamine microgel particles dispersed in water at various temperatures (a) 23.0 ^{o}C and (b) 35.0 ^{o}C, where the concentration ranges from 2.5×10^{-6} to 1.0×10^{-5} g/g.

5.3.2 Phase behavior of microgel dispersions

Figure 5.2 shows the schematic phase diagram of PNIPAM-allylamine microgel solutions with the different concentrations. From 2 wt-% to 4 wt-%, the nanoparticles self-assembled into a colloidal crystal phase with a long-range order. The crystal grain size decreased with increasing concentration. The crystal color also shifts from blue to green, and then to red. When the concentration was approximately 4.0 wt-%, the crystals were too small to be observed, and nanoparticles self-assembled into a glass phase with short-range order. When the concentration was approximately 1.8 wt-%, the dispersion

became cloudy because the microgel spheres are well separated, and scattered light randomly.

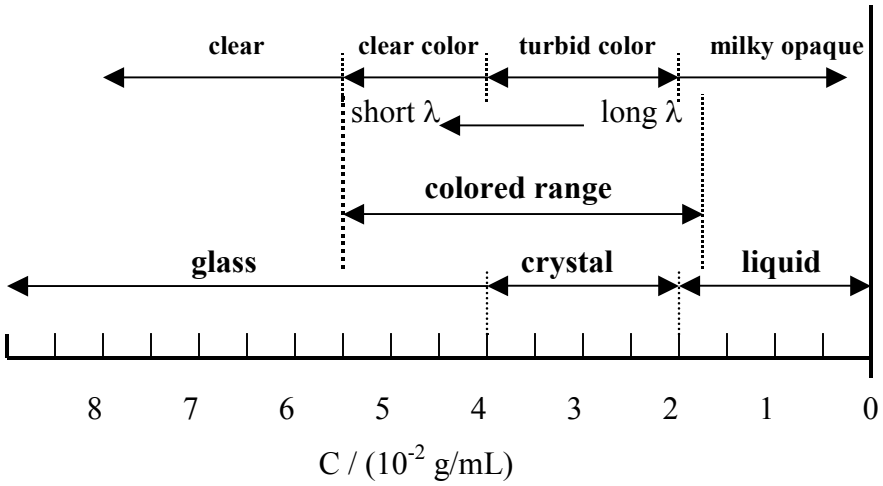

Figure 5.2: Schematic phase diagram of PNIPA-co-allylamine microgel dispersions as a function of *C*/wt % at 23 ^{o}C.

Figure 5.3 (a-b) shows the iridescent color patterns of PNIPAM-co-allylamine nanoparticle solutions with concentrations from 3.5 wt-% to 2 wt-% at 21 and 29 ^{o}C, respectively. It is difficult for the particles in dispersions with polymer concentrations ranging from 3.0 to 3.5 wt% to self-assemble into a crystalline structure at 21 ^{o}C because the viscosity is too high. However, when the temperature was raised to 29 ^{o}C, the particles began to shrink and squeeze more water out. This made the dispersion more dilute. As a result, the particles have more freedom to self-assemble into an ordered array. This experiment demonstrated that the crystalline phase can form at higher polymer concentration upon the increase of the temperature.

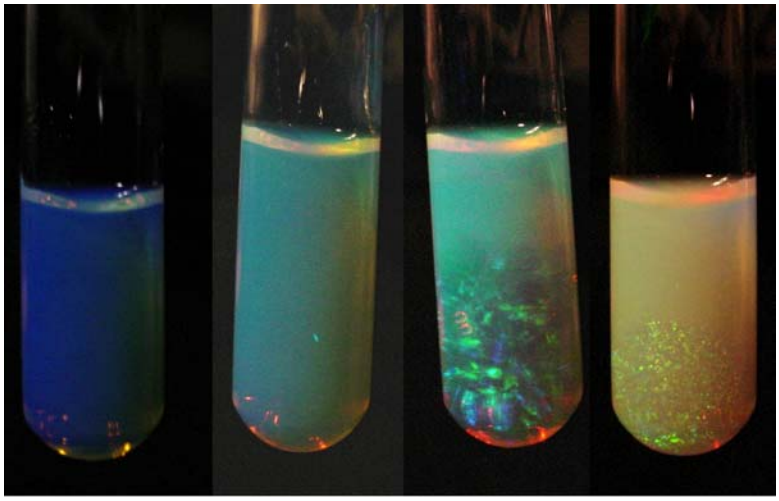

(a)

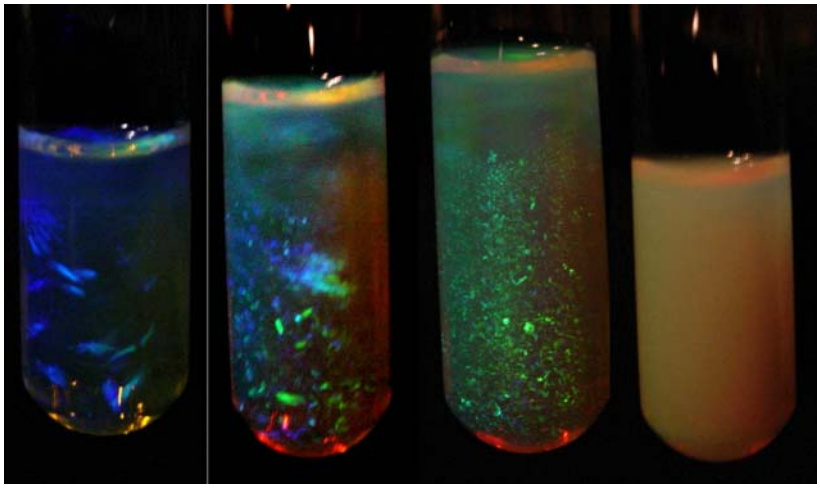

(b)

Figure 5.3: Photographs of PNIPAM-allylamine nanoparticle dispersions at various polymer concentrations at (a) 21 and (b) 29 ^{o}C, respectively. From left to right: 3.5, 3.0, 2.5, 2.0 wt. %. Here the average hydrodynamic radius of the particles in water at 23 ^{o}C is 140 nm. The diameters of the tubes are 1 cm.

The colors of the dispersions originated from the optical interference that relates to the interparticle distance. Because the interparticle distance is determined by the particle concentration, this interference is also related to the concentration. According to the Bragg diffraction equation, $m\lambda=2nd\sin\theta$ and the concentration equation C=m/V, the wavelength should be linearly related to the $C^{-1/3}$, where λ is the wavelength of diffracted light, θ is the diffraction angle, n is the mean refractive index of the dispersion. Figure 5.4 shows a linear relationship by plotting λ vs. $C^{-1/3}$ ($\lambda = -2.5145+821.88\times C^{-1/3}$). The wavelength λ_c is the Bragg peak position of the dispersion.

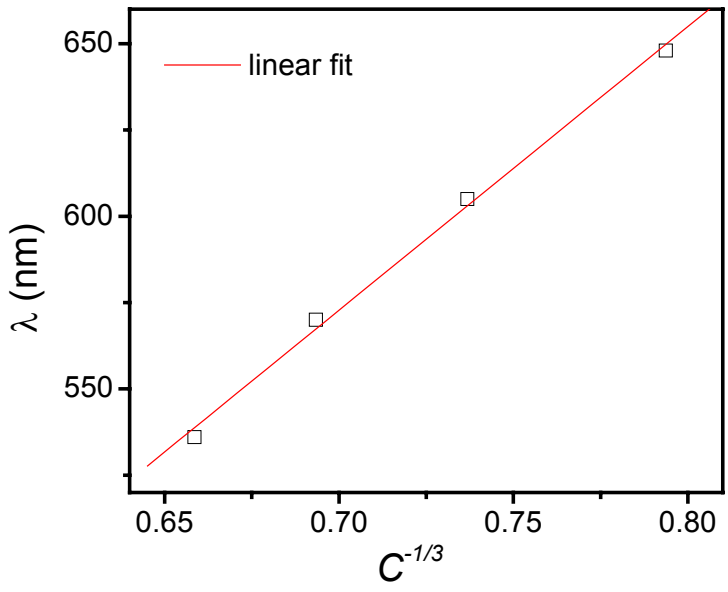

Figure 5.4: The linear relationship between wavelength of Bragg peak (λ_c) and $C^{-1/3}$, C is the concentration of the microgel dispersions.

5.3.3 Mechanical strength of nanostructured hydrogels

Because the mechanical strength of these nanostructured hydrogels is relatively strong, we have measured the shear modulus of the gels at different conditions. The shear modulus is obtained from uniaxial compression measurements.[31] The elastic shear modulus G is determined from the slope of linear dependence

$$\sigma = f / S_0 = G(\lambda - 1/\lambda^2) \qquad (5\text{-}1)$$

where f is the value of an exerted force, S_0 is the cross-section of the undeformed swollen crystal hydrogels, and λ is the relative deformation of the specimen. Figure 5.5 (a) showed the shear moduli of the crystal networks with different polymer concentrations. The particle sizes of these three networks are the same and are about 140nm. When the concentrations of the crystalline hydrogels changed from 4.0 to 5.0 wt.-%, the shear modulus increased from 0.534×10^4 to 1.323×10^4 dyn/cm^2. This shear modulus for gels formed by a heating-cooling process is clearly higher than that of the crystalline gels formed at lower temperatures. Figure 5.5 (b) showed the shear moduli of crystalline nanoparticle networks with different particle sizes, but the same concentration of 4.5 wt.-%. When the particle size increased from 140 to 180nm, the shear modulus decreased from 0.715×10^4 to 0.504×10^4 dyn/cm^2. Because as the interparticle distance increased, particles were arranged not as dense as smaller particles, the bonds between the particles could be easily destroyed by an external stress.

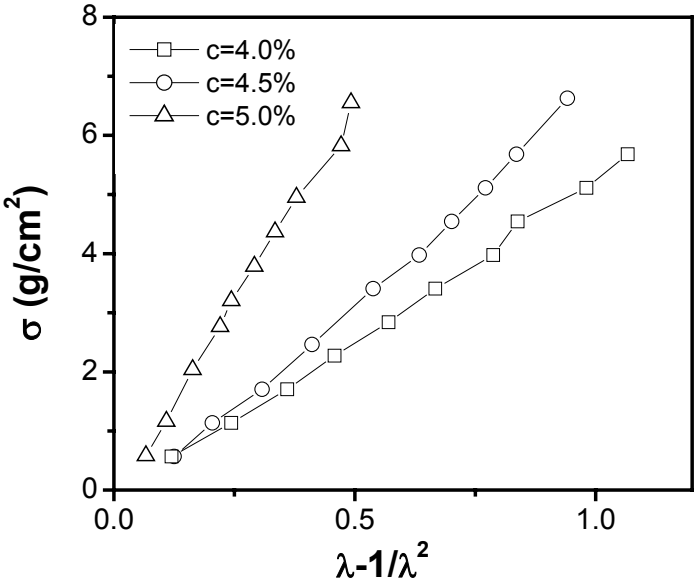

(a)

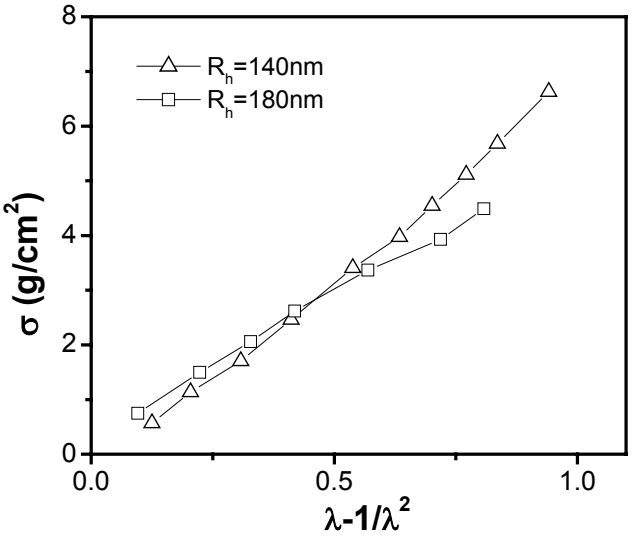

(b)

Figure 5.5: (a). the shear modulus of the PNIPAM-allylamine crystal hydrogels with different concentrations. (b) The shear modulus of the PNIPAM-allylamine crystal hydrogels with different particle sizes.

5.3.4 The sensor applications

Creating crystalline hydrogels allows us to obtain useful functionalities not only from the periodic structure but also from the constituent building blocks. Because the building blocks are environmentally responsive colloidal spheres, their sizes as well as the lattice spacing should be tunable by external stimuli. As a result, the crystalline hydrogel can serve as an optical sensor to visually inspect environmental changes.

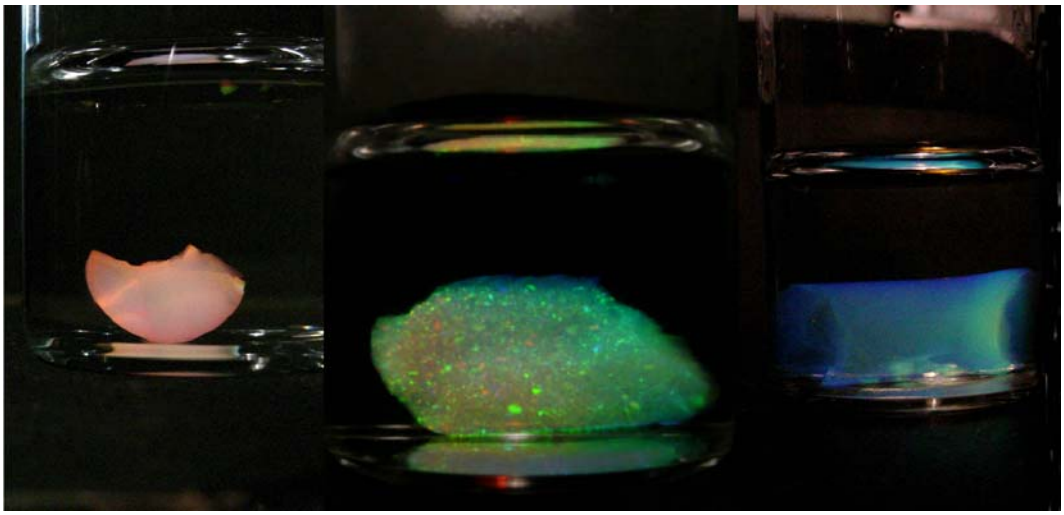

Figure 5.6: Iridescent color of the PNIPAM-allylamine hydrogels with 4 wt% concentration, at different particle sizes. From left to right, 180, 140, 105 nm.

To form a colored gel, the particle concentration and the particle size play an important role. As shown in Figure 5.6, at the same polymer concentration of 4 wt%, the PNIPAM-co-allylamine particles with the size of 140 nm only formed the crystalline phase. If the particle size is bigger, the polymer concentration has to be lowered to give the particles enough freedom to grow crystals. Alternatively, the particle size has to be

decreased so that the dispersion could self-assemble into an ordered array at higher concentration. Compared with the liquid crystalline solution, the Bragg peaks of the hydrogel networks shifted from the longer wavelength to shorter wavelength when the temperature increased. As shown in figure 5.7 (a), the wavelength of the Bragg peak shifted from about 580 to 520 nm when the temperature increased from 19 to 31^{o}C. The crystalline hydrogel at room temperature displays a bright green color. With the increase of temperature, the color of the gel changes from green to blue, and eventually to milky white. above the volume phase transition temperature of the particles. When the temperature is decreased to room temperature again, the gel restored its color and volume. This process is fully reversible. The change of the color is due to the shrinkage of particle size with temperature, which causes the decrease of inter-particle spacing.

For the Bragg diffraction of liquid crystalline dispersions as shown in Figure 5.7 (b), it is found that the Bragg peak position had no significant change as the temperature increased from 21 to 33 ^{o}C. After the temperature was raised above the volume phase transition temperature, the Bragg peak completely disappeared. This suggests that the lattice spacing for the colloidal crystal dispersion doesn't change when the temperature increases. The particles keep the ordered arrangement until the temperature reaches the phase transition point.

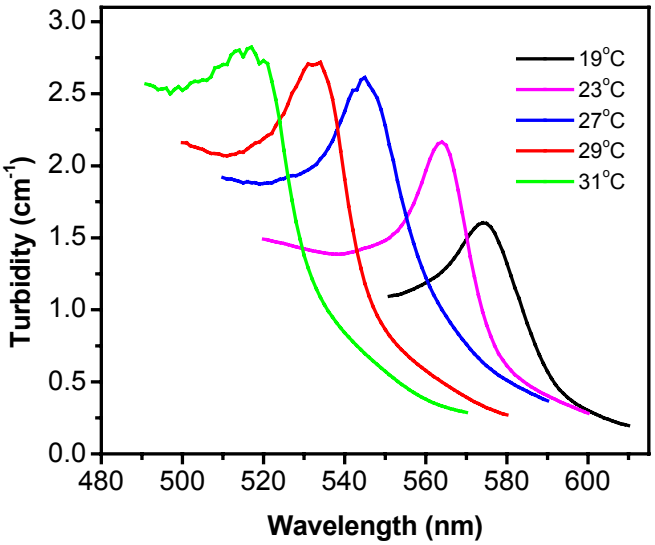

(a)

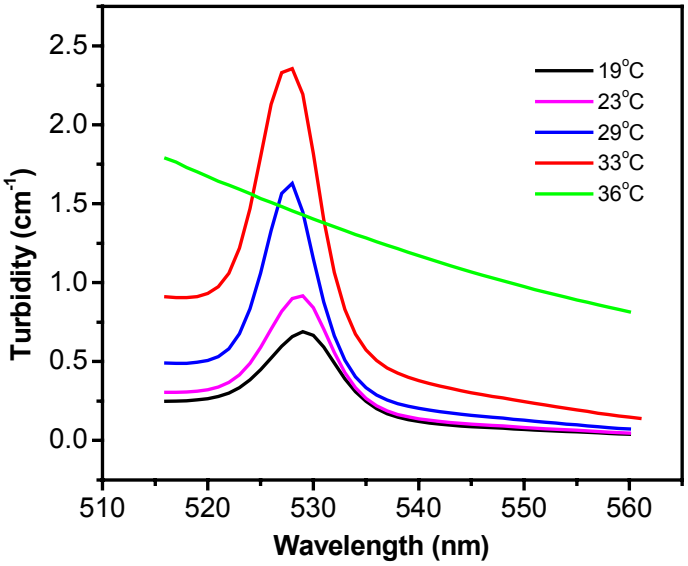

(b)

Figure 5.7: The turbidity versus wavelength curves measured using a UV-visible spectrophotometer. (a) PNIPA-allylamine crystal hydrogels with the concentration of 4.5 wt.-%. (b) PNIPA-allylamine nanoparticle dispersion with the concentration 4.5 wt.-%.

Due to the residues of basic (i.e. $-NH_2$) groups on the PNIPAM-allylamine building blocks, the swelling capacity of the resulting hydrogel can be changed by controlling the pH value of the medium. As a result, the crystal hydrogels could be also used as a pH sensor to monitor the pH change of the surrounding environment. The amine groups on the particles are partially ionized in water at a neutral pH, causing swelling of the particles. At a higher pH, the ionization of the basic groups is inhibited, causing the shrinkage of the particles. This change of the building block size at different pH values causes the lattice spacing to change, resulting in the color change. The color shift is determined by the UV-visible Spectroscopy shown in Figure 5.8 (a). When the pH value changed from 7 to 12, the wavelength of the Bragg peak for the hydrogel shifted from 633 to 556nm. By plotting the diffraction wavelength λ against pH, we can get a linear relationship (λ=747.8-16.6×pH) as shown in Figure 5.8 (b). This change of Bragg peak may be used for monitoring the base environment.

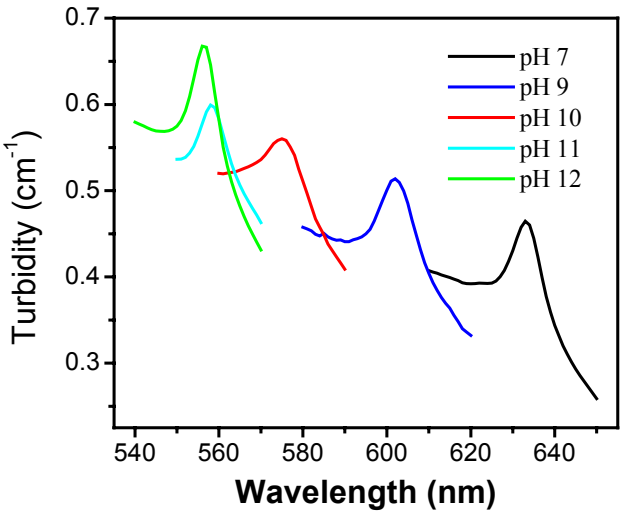

(a)

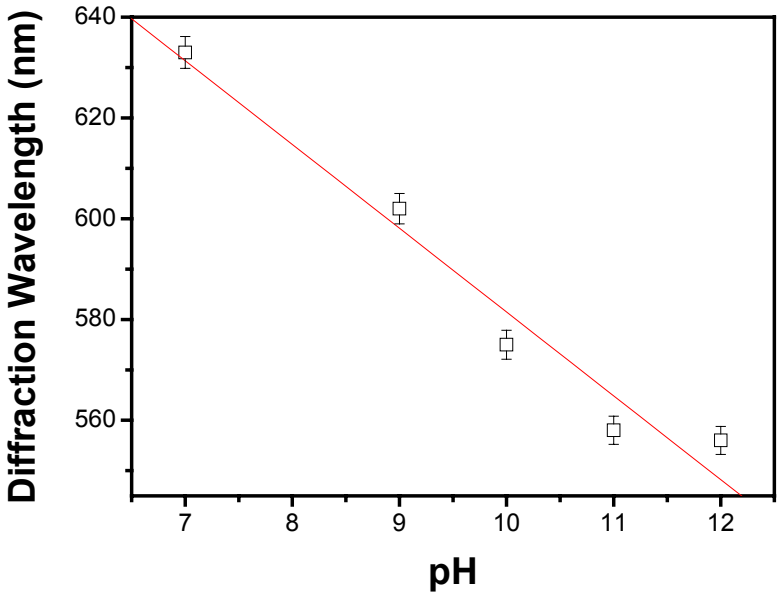

(b)

Figure 5.8: (a) The crystal hydrogel turbidity versus wavelength curves measured using a UV-visible spectrophotometer for different pH values. (b) pH dependence of diffraction from the crystal hydrogel. The solid line is the linear fit to the experimental points.

In addition to being temperature and pH sensors, these hydrogels may also served as a sensor for detecting proteins. Here we used bovine serum albumin (BSA) solution as a model system. Figure 5.9 (a) shows the color change of the crystalline hydrogel immersed in water, 0.1 and 0.5 wt.-% BSA solutions, respectively. Because of the ionic group on BSA, a Donnan potential is built up between the hydrogel phase and the bulk solution phase. In order to reach equilibrium, the hydrogel has to squeeze the water out, causing the shrinkage of the particles in the network. Therefore, the interparticle distance decreased, resulting in the change of color from green to blue. This color change can be quantitatively measured using UV-Visible Spectroscopy as shown in Figure 5.9 (b).

When the concentration of the BSA solution changed from 0 wt.-% to 1 wt.-%, the Bragg Peak shifted from 570nm to 486nm. By plotting the diffraction wavelength λ against the concentration of BSA solution, as shown in Figure 5.9 (c), it is found that when the concentration of the BSA solution is above 0.5 wt%, the Bragg peak position is constant. Between 0 and 0.5 wt%, we can fit the experimental data to make this crystalline hydrogel suitable for the protein sensor system.

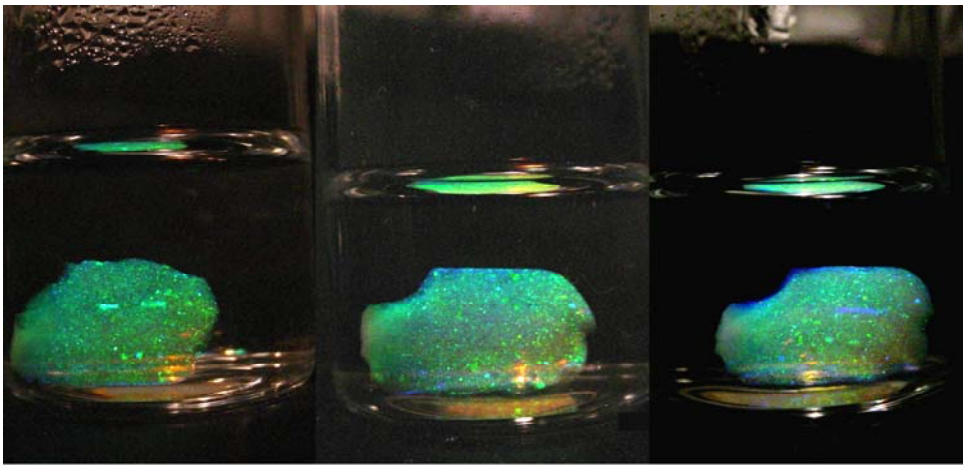

(a)

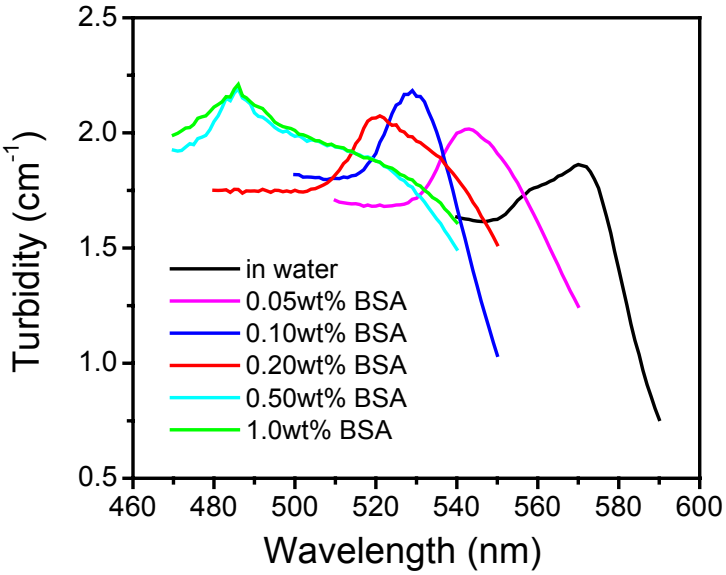

(b)

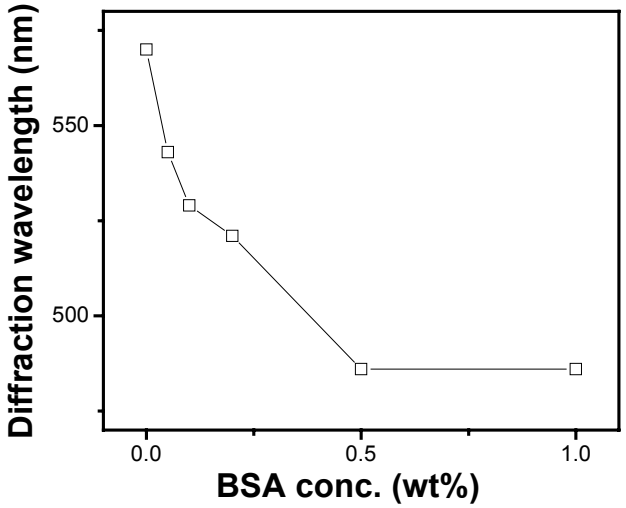

(c)

Figure 5.9: (a) The poly-NIPA-allylamine crystal hydrogels were immersed in the water, 0.1 and 0.5 wt.-% BSA solution, respectively. (b) The crystal hydrogel turbidity versus wavelength curves measured using a UV-visible spectrophotometer under different BSA concentrations. (c) plot of diffraction wavelength vs BSA concentration.

5.4 Conclusions

Crystalline hydrogels have been synthesized using the PNIPAM-co-allylamine microgels as building blocks. The mechanical strength of the hydrogel was significantly improved by using a new heating and cooling process as guided by the phase diagram. This new material shows iridescent color and responds to temperature change. Specifically, by using UV-Visible Spectroscopy, we can quantitatively measure the Bragg peak shift from the crystalline hydrogels as a function of temperature, pH and concentrations of BSA solution. These soft and wet hydrogels with periodic structures may lead to new applications in sensors, devices and displays operating in biological and chemical systems.

Chapter References

1. Holtz, J. H., Asher, S. A. *Nature* **1997**, 389, 829.
2. Blaaderen, A. V., Ruel, R., Wiltzius, P. *Nature* **1997**, 385, 321.
3. Gu, Z., Fujishima, A.; Sato, O. *J. Am. Chem. Soc.* **2000**, 122, 12387.
4. Gao, J., Hu, Z. *Langmuir*, **2002**, 18, 1360.
5. Debord, J. D., Lyon, L. A. *J. Phys. Chem.* **2000**, 104, 6327.
6. Debord, J. D., Eustis, S., Debord, S. B., Lofye, M. T., Lyon, L. A. *Adv. Mater.* **2002**, 14, 658.
7. Xia, Y., Gates, B., Yin, Y., Lu, Y. *Adv. Mater*. **2000**, 12, 693.
8. Xu, X., Majetich, S. A., Asher, S. A. *J. Am. Chem. Soc*. **2002**, 124, 13864.
9. Jones, C. D., Lyon, L. A. *J. Am. Chem. Soc*. **2003**, 125, 460.
10. Senff, H., Richtering, W. *J. Chem. Phys*. **1999**, 111, 1705.
11. Jiang, P., Bertone, J. F., Colvin, V. L. *Science*, **2001**, 291, 453.
12. Pan, G. S., Kesavamoorthy, R., Asher, S. A. *J. Am. Chem. Soc*. **1998**, 120, 6525.
13. Weissman, J. M., Sunkara, H. B., Tse, A. S., Asher, S. A. *Scienc*e **1996**, 274, 959.
14. Asher, S. A., Alexeev, V. L., Goponenko, A. V., Sharma, A. C. *J. Am. Chem. Soc*. **2003**, 125, 3322.
15. Asher, S. A., Sharma, A. C., Goponenko, A. V., Ward, M. M. *Anal. Chem*. **2003**, 75, 1676.
16. Lee, K., Asher, S. A. *J. Am. Chem. Soc*. **2000**, 122, 9534.
17. Sharma, A.C., Jana, T., Kesavamoorthy, R., Shi, L., Virji, M.A., Finegold, D.N.,

Asher, S. A. *J. Am. Chem. Soc*. **2004**, 126, 2971.

18. Reese, C.E. Mikhonin, A.V., Kamenjicki, M., Tikhonov, A. Asher, S.A. *J. Am. Chem. Soc.* **2004**, 126, 1493.

19. Lee, Y., Braun, P. V. *Adv. Mater*. **2003**, 15, 563.

20. Lee, Y., Pruzinsky, S. A., Braun, P. V. *Langmuir* **2004**, 20, 3096.

21. Nakayama, D., Takeoka, Y., Watanabe, M., Kataoka, K. *Angew. Chem. Int. Ed*. **2003**, 42, 4197.

22. Cassagneau, T., Caruso, F. *Adv. Mater*. **2002**, 14, 1629.

23. Hu, Z.B., Huang, G. *Angew. Chem. Int. Ed*. **2003**, 42, 4799.

24. Pelton, R. H., Chibante, P. *Colloids Surf.* **1986**, 20, 247.

25. Wu, C., Zhou, S. Q., Auyeung, S. C. F., Jiang, S. H. *Angew Makromol Chem* **1996**, 240, 123.

26. Hino, T., Prausnitz, J. M. *J Appl Polym Sci* **1996**, 62, 1635.

27. Flory, P. J. *Principles of polymer chemistry*; Cornell University Press: Ithaca, **1953**.

28. Guillermo, A., Addad, J. P. C., Bazile, J. P., Duracher, D., Elaissari, A., Pichot, C. *J Polym Sci B-Polym Phys* **2000**, 38, 889.

29. Israelachvili, J. N. *Intermolecular and Surface Forces*; 2nd ed.; Academic Press: London, **1992**.

30. GilVillegas, A., Galindo, A., Whitehead, P. J., Mills, S. J., Jackson, G., Burgess, A. N. *J Chem Phys* **1997**, 106, 4168.

31. Schosseler, F., Ilamin, F., Candau, S. J. *Macromolecules*, **1991**, 24, 225.

CHAPTER 6

INTER-PARTICLE POTENTIAL AND THE PHASE BEHAVIOR OF TEMPERATURE-SENSITIVE MICROGEL DISPERSIONS*

6.1 INTRODUCTION

Over the past decade colloidal dispersions have been a subject of intensive investigations.[1-3] On one hand, colloidal dispersions provide model systems for studying the long-standing fundamental questions on the nature of liquids, solids, and glasses, while on the other hand, self-assembly of colloidal particles has been extensively used as templates for the fabrication of nanostructured materials.[4,5] Amid numerous conventional colloids, aqueous dispersions of poly-N-isopropylacrylamide (PNIPAM) microgel particles, first synthesized by Pelton and Chibante in 1986,[6] are of special interest for studying the phase transitions and for the fabrication of colloid-based advanced materials.[7,8] Nearly monodispersed PNIPAM particles now can be routinely prepared in a wide range of colloidal sizes (50 nm up to 1 μm) and with a variety of physiochemical characterizations.[7,9] By tuning the preparation conditions and the composition of the aqueous solution, the interaction potential between microgel particles can vary from star-polymer-like to hard-sphere-like potential for short-range repulsion, from electrostatically neutral to highly ionizable for long-range electrostatic interactions, and from essentially no attraction to strong attraction for the van der Waals forces.[8,10] Furthermore, steric

* Figures and tables reproduced with permission from [Wu, J., Huang, G., Hu, Z.B. *Macromolecules;* **2003**; 36, 440] Copyright [2003] American Chemical Society

repulsion can be introduced by grafting polymers on the surface of PNIPAM particles.[11] The versatility in the interaction potential makes PNIPAM microgel particles attractive for studying a broad variety of interesting phenomena in colloidal systems.[12-16]

Like their macroscopic counterparts, PNIPAM particles may undergo a drastic volume change in responding to small variances in the aqueous environment, such as temperature, ionic strength, or pH.[7] The volume transition of the PNIPAM gel is closely related to the coil-globule transition of the PNIPAM chains and has been explained using the Flory-Huggins theory.[17] Because of the unique physiochemical properties, microgel particles are promising for a broad variety of applications. Assembly of microgel particles has been proposed to be used as drug carriers,[18] artificial biomaterials,[19] photonic crystals,[12,20-22] and as separation media.[23,24] While the microgel particles retain the unique physical properties of bulk hydrogels, the swelling/de-swelling kinetics of microgel particles is much faster in comparison to macrogels. For many practical applications, rapid response to environmental stimuli is often of crucial importance.

Although the practical values of PNIPAM particles have been long recognized, most previous studies on the physiochemical properties of PNIPAM dispersions have been focused on the particle preparations, swelling, rheology, and light (neutron) scattering measurements.[7,8,25-27] Little work has been reported on the relationship between the temperature-dependent inter-particle potential and the phase behavior of PNIPAM dispersions. Unlike that in a conventional colloidal system, the inter-particle potential in

aqueous dispersion of PNIPAM microgel particles is sensitive to the temperature changes. Consequently, the phase diagram of PNIPAM dispersions may be noticeably different from those for ordinary colloids where, in most cases, the inter-particle potential is essentially invariant with temperature.

In this work, we report the phase behavior of neutral PNIPAM particles dispersed in pure water. Differing from most previous studies on the phase diagrams of colloidal systems, we start with investigations on the inter-particle potential using both dynamic and static light-scattering measurements. A modified Flory-Rehner theory, that takes into consideration the microgel heterogeneity, is used to correlate the diameter of PNIPAM particles as a function of temperature.[28] The phase diagram is then calculated using a first-order perturbation theory for the fluid phase and an extended cell model for the crystalline solid. Finally, the thermodynamic perturbation theories of the phase behavior of the PNIPAM microgel system will be compared with observations from spectroscopic measurements.

6.2 Experimental

6.2.1 Materials

N-isopropylacrylamide was obtained from Polysciences Inc. and used as received. The crosslinker N,N'-methylene-bis-acrylamide(MBAAm) was purchased from Bio Rad company. The surfactant Dodecyl Sulfate, Sodium (SDS) and the initiator potassium persulfate(KPS) were both bought from Aldrich Chemical Co and used as received.

Distilled and deionized water (resistance of 18 MΩ·cm) was used throughout. A 0.5μm Millipore (Millex LCR25) filter was used to clarify the dilute LLS sample solution.

6.2.2 Sample preparation

Narrowly distributed PNIPAM microgel dispersions were synthesized following the pioneering work by Pelton.[7] Briefly, emulsion polymerization of 1.54g PNIPAM monomer and 0.0262g cross-linking agent MBAAm was performed in 90ml water at 70 ^{o}C. 0.0439g surfactant, Sodium Dodecyl Sulfate (SDS) was added to control the particle size. The solution was stirred and bubbled with nitrogen for about 30 minutes and then heated up to 70 ^{o}C. 0.0624g Potassium Persulfate (KPS) dissolved in 10ml water was added to the reactor to initialize the polymerization. The reaction was kept at 68-70 ^{o}C under nitrogen for 4 hours to ensure that all the monomer was reacted. After cooling to room temperature, the dispersion was exhaustively dialyzed in a dialysis tube for 7 days. The deionized water out of the tube was changed three times every day.

6.2.3 Phase diagram measurement

The PNIPAM particles can self-assemble in water by evaporating the solvent at a temperature higher than 34°C and then allowing the concentrated dispersion to reach an equilibrium state for one week. A quantitative phase diagram of PNIPAM dispersions can be constructed by measuring the UV-visible absorbance spectra on a diode array spectrometer (Hewlett-Parkard, Model 8543) with the wavelength ranging from 190 to 1100 nm. The turbidity of the samples was obtained from the ratio of the transmitted light intensity (I_t) to the incident intensity (I_o) as $\alpha = -(1/L)\ln(I_t / I_0)$, where L was the sample thickness (1 cm). In the crystalline phase, the UV-VIS spectrum exhibits a sharp

attenuation peak due to the Bragg diffraction. Above the crystalline melting temperature, the peak disappears. On the other hand, as the temperature rises to the phase separation temperature, the turbidity increases sharply in the entire range of visible light wavelengths.

6.3 Theory

6.3.1 Volume transition of PNIPAM particles

The classical theory of gel swelling, proposed many years ago by Flory and Rehner,[29] assumes uniform distributions of polymer segments and crosslinking points throughout the polymer network. NMR investigations, however, suggest heterogeneous nature of PNIPAM particles.[30] To take into account the heterogeneity, we use an empirical modification of the Flory-Rehner theory proposed by Hino and Prausnitz.[28] This theory has been applied successfully to describe the volume transition of bulk PNIPAM gels. Because the physics for the volume transition is independent of the particle size as long as the surface effect is unimportant, the same thermodynamic model for bulk polymer gels is also applicable to microgel particles.

At swelling equilibrium, the chemical potential of water is equal inside and outside the microgel particle

$$\mu_{\text{water}}^{\text{gel}} = \mu_{\text{water}}^{\text{pure}}. \tag{6-1}$$

The chemical potential inside the gel includes two contributions, one is the same as that in the aqueous solution of PNIPAM polymer, and the other arises from the cross linking of polymer chains or from the gel elasticity

$$\mu_{\text{water}}^{\text{gel}} = \mu_{\text{water}}^{\text{polymer solution}} + \mu_{\text{water}}^{\text{elasticity}}. \tag{6-2}$$

The chemical potential of water in an aqueous PNIPAM solution can be calculated from the Flory-Huggins theory

$$(\mu_{\text{water}}^{\text{polymer solution}} - \mu_{\text{water}}^{\text{pure}})/(kT) = \ln(1-\phi) + \phi + \chi\phi^2 \quad (6\text{-}3)$$

where ϕ is the volume fraction of PNIPAM polymer, and the Flory polymer-solvent energy parameter χ is given empirically as a function of temperature and composition[28]

$$\chi = \frac{3}{1-0.65\phi}\left[2\ln\left(\frac{5001}{1+5000\exp(2458.867/T)}\right) - \frac{4566.468}{T}\right]. \quad (6\text{-}4)$$

Eq.(6-4) is obtained by fitting the Flory-Huggins theory with the phase-equilibrium data for non-cross-linked PNIPAM polymer in water.[28] For microgels, the volume fraction ϕ in Eq.(6-3) corresponds to that inside of individual particles.

The second term on the right-hand of Eq.(6-2) arises from gel elasticity. This term takes into account the effect of the network formation on the chemical potential of the solvent. According to the modified Flory-Rehner theory by Hino and Prausnitz,[28] the chemical potential of water due to gel elasticity is given by

$$\mu_{\text{water}}^{\text{elasticity}}/(kT) = \frac{\phi_0}{m}\left[\left(\frac{\phi}{\phi_0}\right)^{1/3} - \left(\frac{\phi}{\phi_0}\right)^{5/3} + \left(\frac{\phi}{2\phi_0}\right)\right], \quad (6\text{-}5)$$

where m is the average number of segments between two neighboring crosslinking points in the gel network, and ϕ_0 is the polymer volume fraction in the reference state where the conformation of the network chains is closest to that of unperturbed Gaussian chains. Approximately, ϕ_0 is equal to the volume fraction of polymer within the microgel particles at the condition of preparation.

Substitution of Eqs.(6-5) into Eq.(6-1) yields

$$\ln(1-\phi)+\phi+\chi\phi^2+\frac{\phi_0}{m}\left[\left(\frac{\phi}{\phi_0}\right)^{1/3}-\left(\frac{\phi}{\phi_0}\right)^{5/3}+\left(\frac{\phi}{2\phi_0}\right)\right]=0\,. \tag{6-6}$$

At a given temperature, Eq.(6-6) can be used to find the polymer volume fraction ϕ. Once we have ϕ, the diameter of PNIPAM particles can be found from

$$\frac{\sigma}{\sigma_0}=\left(\frac{\phi_0}{\phi}\right)^{1/3}, \tag{6-7}$$

where σ_0 is the particle diameter at the reference state. In this work, the average chain length m and the volume fraction of polymer ϕ_0 at the reference state are obtained by fitting Eqs.(6-6) and (6-7) to the diameters of microgel particles obtained from static and dynamic light-scattering experiments.

6.3.2 Inter-particle potential and osmotic second virial coefficient

The inter-particle potential $u(r)$ is related to the osmotic second virial coefficient B_2 by

$$B_2=2\pi\int_0^\infty[1-e^{-u(r)/kT}]r^2dr\,, \tag{6-8}$$

where r stands for the center-to-center distance between colloidal particles.

For neutral PNIPAM particles in pure water, we assume that the interaction potential can be represented by a Sutherland-like function that includes a hard-sphere repulsion and a van der Waals attraction. The hard-sphere diameter is related to the swelling of gel particles and can be calculated from Eq.(6-7). The van der Waals attraction beyond the hard-sphere diameter can be represented by

$$u_A(r) = -\frac{H}{r^n}, \tag{6-9}$$

where H is the Hamaker constant. We assume $n = 8$ in considering that the range of attraction between colloidal particles (relative to the particle size) is shorter than that between atomic molecules. The calculated results are not sensitive to a small change in n when the Hamaker constant is obtained by fitting to the osmotic second virial coefficients from static light-scattering experiments.

Approximately, the Hamaker constant of microgel particles is given by[31]

$$H \propto \rho_m^2, \tag{6-10}$$

where ρ_m represents the number density of polymeric groups within each particle. The proportionality constant in Eq.(6-10) is independent of temperature and polymeric group density ρ_m. Following Eqs.(6-9) and (6-10), we obtain the attractive potential due to the van der Waals forces

$$\frac{u_A(r)}{kT} = -k_A\left(\frac{T_0}{T}\right)\left(\frac{\sigma_0}{\sigma}\right)^{6+n}\left(\frac{\sigma}{r}\right)^n, \tag{6-11}$$

where k_A is a dimensionless constant and T_0 is the reference temperature that is introduced for the purpose of dimensionality. In Eq.(6-11), the parameters T_0, σ_0, and k_A are temperature-independent and they can be obtained by fitting Eq.(6-8) to the osmotic second virial coefficients from static light scattering measurements.

6.3.3 Thermodynamic model for the fluid phase

To calculate the phase diagram of microgel dispersions, we need thermodynamic models for both fluid and solid phases. For a dispersion of microgel particles in the fluid

state, a first-order perturbation theory is appropriate because higher order terms are insignificant when the perturbation arises only from short-range attractions.[32] The Helmholtz energy of the fluid phase includes a hard-sphere contribution that is given by the Carnahan-Starling equation of state, and a perturbation that takes into account the van der Waals attraction (Eq.6-11). In dimensionless units, the Helmholtz energy is given by

$$\frac{F}{NkT} = \ln(\eta) - 1 + \frac{4\eta - 3\eta^2}{(1-\eta)^2} + 12\eta \int_1^\infty x^2 g_F^{HS}(x) \frac{u_A(x)}{kT} dx , \qquad (6\text{-}12)$$

where N represents the total number of particles, $\eta = \pi\rho\sigma^3 / 6$ is the particle packing fraction, ρ is the particle number density, and $g_F^{HS}(r)$ is the hard-sphere radial distribution function. For convenience, we correlate the integral in Eq.(6-12) as a function of particle packing fraction using the radial distribution function $g_F^{HS}(r)$ obtained from the Percus-Yevick equation[33]

$$I_F(\eta) \equiv \int_1^\infty x^{-6} g^{HS}(x) dx = 0.027224\eta^2 + 0.1642\eta + 0.2007 , \qquad (6\text{-}13)$$

The quadratic form as given in Eq.(6-13) is applicable to the reduced density $\rho\sigma^3 < 0.6$.

Replacement of the integral in Eq.(6-12) with $I_F(\eta)$ gives

$$\frac{F}{NkT} = \ln(\eta) - 1 + \frac{4\eta - 3\eta^2}{(1-\eta)^2} - 12\eta I_F(\eta)\varepsilon^* , \qquad (6\text{-}14)$$

where

$$\varepsilon^* = \frac{\varepsilon}{kT} = k_A \left(\frac{T_0}{T}\right)\left(\frac{\sigma_0}{\sigma}\right)^{6+n} \qquad (6\text{-}15)$$

Other thermodynamic properties can be derived from Eq.(6-14) following standard thermodynamic relations.

6.3.4 An extended cell model for the solid phase

To describe the thermodynamic properties of the solid phase, we follow a perturbation approach similar to that for the fluid phase. The Helmholtz energy includes a contribution from the reference hard-sphere crystal and a perturbation taking into account the van der Waals attraction

$$\frac{F}{NkT} = \frac{F^{HS}}{NkT} + 12\eta\int_1^\infty x^2 g_S^{HS}(x)\frac{u_A(x)}{kT}dx, \qquad (6\text{-}16)$$

where $g_S^{HS}(r)$ is the radial distribution function of the hard-sphere solid. As in a hard-sphere system, an aqueous dispersion of PNIPAM microgel particles forms a face-centered-cubic (fcc) lattice in the solid phase even when the particles are at low cross-linking density ("softer" particles).[13]

According to an improved cell theory,[34] the Helmholtz energy of the hard-sphere solid is given by

$$\frac{F^{HS}}{NkT} = -\ln\left[\frac{8}{\sqrt{2}}\left((\rho/\rho_0)^{1/3} - 1\right)\right]. \qquad (6\text{-}17)$$

Compared with the original cell model proposed many years ago by Lennard-Jones and Devonshire,[35] the improved cell model introduces a factor of 8, taking into account the fact that the neighboring particles share partially the free space. Unlike the original cell model, the modified cell model provides accurate freezing and melting densities for the fluid-solid transition of uniform hard spheres. As outlined in the additional information

(6.6), the hard-sphere radial distribution function $g_S^{HS}(r)$ can be calculated using a modified Gaussian model for density distributions.

Using the radial distribution function $g_S^{HS}(r)$ for the hard-sphere solid, we numerically integrate the perturbation term in Eq.(6-16). The final expression for the Helmholtz energy of the solid phase is given by

$$\frac{F}{NkT} = -\ln\left[\frac{8}{\sqrt{2}}\left((\rho/\rho_0)^{1/3} - 1\right)\right] - 12\eta I_S(\rho)\varepsilon^*, \tag{6-18}$$

where

$$I_S(\rho) \equiv \int_1^\infty x^{-6} g_S^{HS}(x)dx = 0.451\rho^2 - 0.5253\rho + 0.5514\,. \tag{6-19}$$

Eq.(6-19) is applicable for the solid phase with the reduced density $0.95 < \rho\sigma^3 < 1.27$.

6.3.5 Phase-equilibrium calculations

Once we have an expression for the Helmholtz energy, the chemical potential μ and the osmotic pressure P can be derived following standard thermodynamic relations

$$\mu = \left(\frac{\partial F}{\partial N}\right)_{T,V}, \tag{6-20}$$

$$P = -\left(\frac{\partial F}{\partial N}\right)_{T,N}, \tag{6-21}$$

where V stands for total volume. A fluid-fluid coexistence curve is obtained from the criteria of phase equilibrium

$$\mu^\alpha = \mu^\beta, \tag{6-22}$$

$$P^\alpha = P^\beta, \tag{6-23}$$

where α and β designate two distinguishable fluid phases. To calculate the pressure and the chemical potential in the fluid phase, the Helmholtz energy is given by Eq. (6-14). For each temperature, we solve for equilibrium densities ρ^{α} and ρ^{β} using Eqs.(6-22) and (6-23). If no solution is found, the temperature is above the critical temperature for fluid-fluid equilibrium; in this case, there is only one fluid phase.

For fluid-solid equilibrium, we also use Eqs. (6-22) and (6-23). For phase α we use Eq. (6-14) for the liquid-phase Helmholtz energy while for phase β we use Eq. (6-18) for the solid-phase Helmholtz energy. Again, we search for densities ρ^{α} and ρ^{β} that satisfy both equations of phase equilibrium, i.e., Eqs.(6-22) and (6-23).

6.4. Results and Discussions

Static light scattering was carried out for PNIPAM microgel dilute dispersions with concentrations ranging from 2.5×10^{-6} to 5×10^{-6} to 1×10^{-5}. Figure 6.1 (a), (b) and (c) show the Zimm plots at 25, 31 and 34 ^{o}C respectively. From the extrapolation of $KC/R_{vv}(q)$ in equation 2-10 to the zero angle and zero concentration, the second virial coefficient B_2, and the radius of gyration $<R_g>$ were obtained. Table 1 showed the radius of gyration $<R_g>$ under different temperatures. The positive B_2 coefficient at 25 and 31^{o}C shows that water is a good solvent for the PNIPAM polymer at these two temperatures, while the negative B_2 coefficient at 34^{o}C shows that water becomes a poor solvent when the temperature is above the LCST. The variance in the second virial coefficients indicates that the PNIPAM particles becomes less repulsive as temperature rises (also see Figure 6.4), in contrast to the case for the charged PNIPAM particles as investigated in previous work.[7]

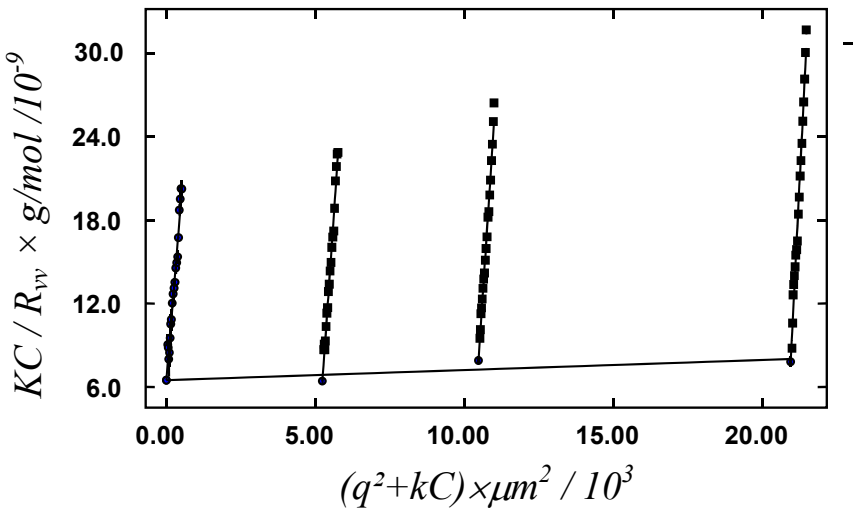
30.0
24.0
18.0
12.0
6.0
0.00
5.00
10.00
15.00
20.00
KC / R_vv × g/mol /10^-9
(q²+kC)×μm² / 10³

(a)

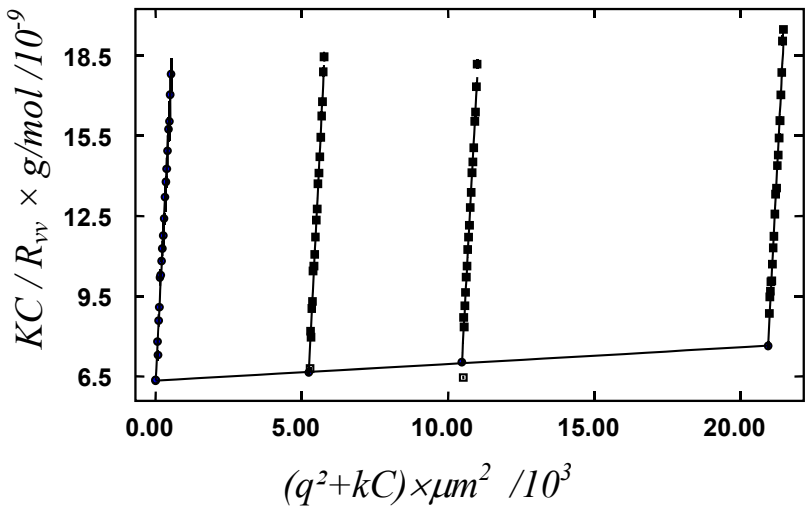
18.5
15.5
12.5
9.5
6.5
0.00
5.00
10.00
15.00
20.00
KC / R_vv × g/mol /10^-9
(q²+kC)×μm² /10³

(b)

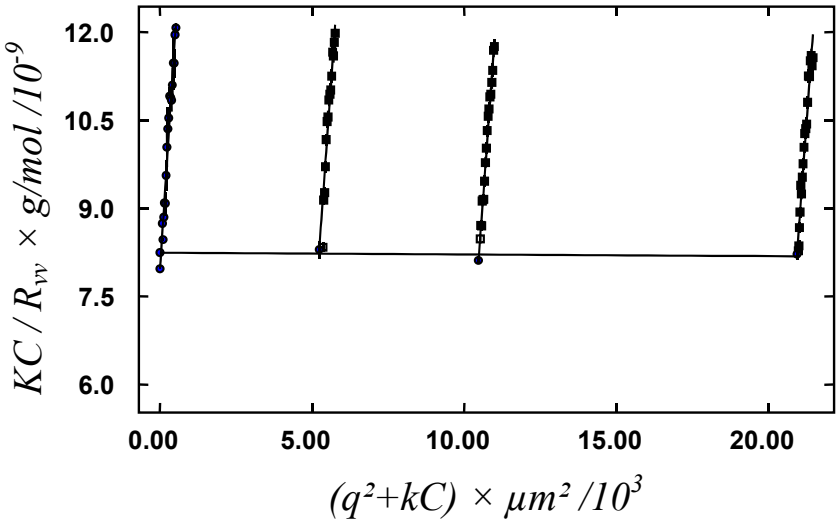

(c)

Figure 6.1: Zimm plots of the PNIPAM microgel particles dispersed in water at various temperatures (a) 25.0 ^{o}C, (b) 31.0 ^{o}C, and (c) 34.0^{o}C, where the concentration ranges from 2.5×10^{-6} to 1.0×10^{-5} g/g.

T (^{o}C)	R_g nm	R_h nm	$(R_h+\sqrt{5/3}R_g)/2$ nm
25	111.85	133.2	139
28	103.88	121	128
31	93.29	110.9	116
33	74.88	107.2	102
34	51.29	79.3	72.8
35	49.92	61.34	62.9
37	45.48	54.09	56.4

Table 6.1: Radius of gyration from SLS, hydraulic radius from DLS, and the average radius from Eq.(6-24).

Figure 6.2 (a) shows the hydrodynamic radius distribution of PNIPAM microgels in dilute dispersions at different temperatures, where dynamic light scattering measurements were made at $\theta = 60^{O}$. At temperatures lower than the phase transition temperature, the microgels are in their swollen state and are narrowly distributed. When the temperature is above the LCST, the microgels shrink sharply, but are still fully dispersed. Table 6.1 shows the size change of the hydrodynamic radius under the different temperatures. Taking temperature as X-axis and R_g, R_h as Y-axis, we can get the plot of temperature-dependent size change vs. radius. Shown in figure 6.2 (b), there is a sharp decrease of radius change when the temperature is close to the low critical solution temperature.

To correlate the radius of PNIPAM gel particles as a function of temperature, we combine the radius of gyration R_g with the hydrodynamic radius R_H from, respectively, static and dynamic light scattering measurements

$$R = (\sqrt{5/3}R_g + R_H)/2 . \qquad (6\text{-}24)$$

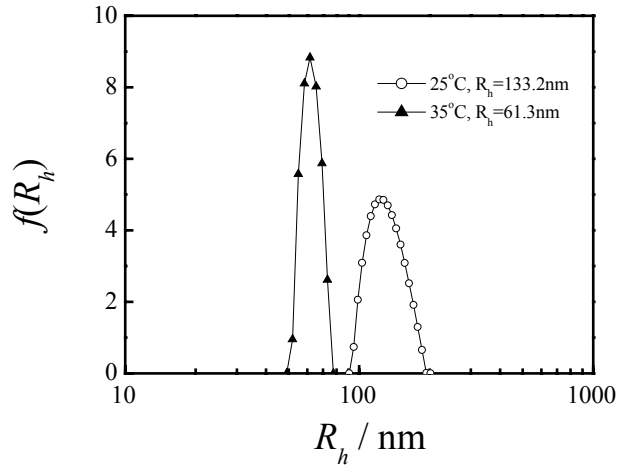

(a)

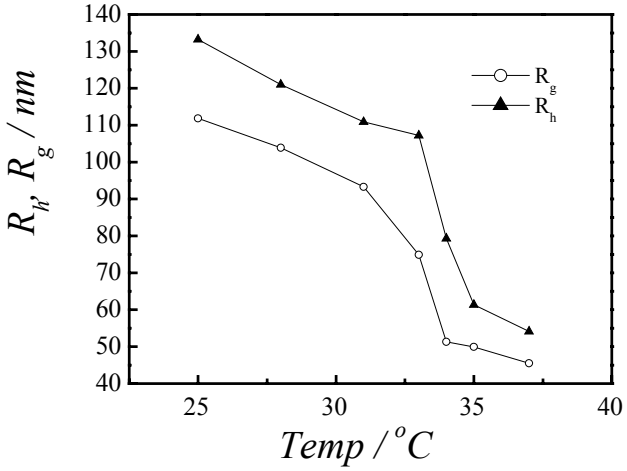

(b)

Figure 6.2: (a) Hydrodynamic radius distributions of PNIPAM microgel spheres in water at T=25 and 35 ^{o}C respectively. Here the microgel concentration is C=5×10^{-6}g/g, and the scattering angle is 60^{o}. (b) Hydrodynamic radius and gyration radius of PNIPAM microgels in water at different temperatures.

Figure 6.3 presents the radius of microgel particles near the microgel volume transition temperature at 34 ^{o}C. The error bars give the difference between hydrodynamic radius and the radius of gyration. The solid line is calculated using the modified Flory-Rehner theory (Eqs. 6-6 and 6-7). In the calculation of the particle radius, the polymer fraction at the condition of preparation $\phi_0 = 0.0884$, the average number of segments between two neighboring cross-linking points $m = 34$, and the particle radius at the preparation condition $R_0 = 125.8$ nm, are obtained by fitting to the experimental data. These model parameters are in good agreement with experiments. Figure 6.3 indicates that the volume transition of PNIPAM particles can be successfully correlated using the modified Flory-Rehner theory.

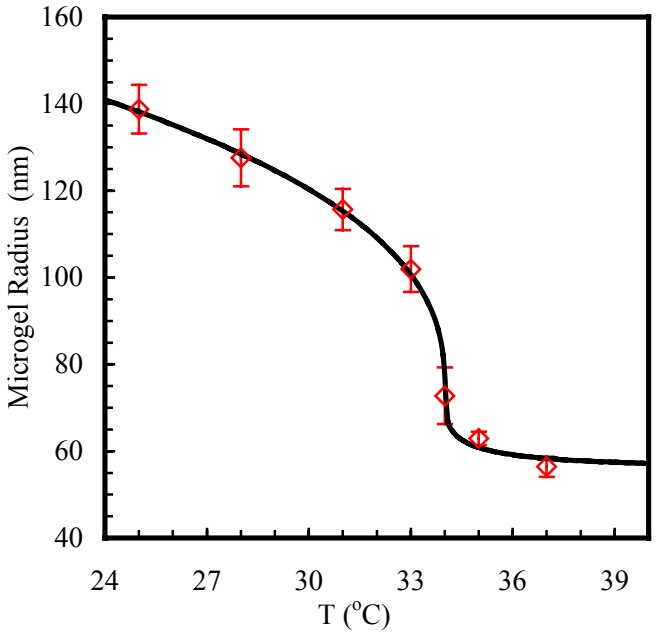

Figure 6.3: Radius of PNIPAM particles vs. temperature. The points are averages from dynamic and static light scattering measurements with the error bars showing the differences between the two. The line is calculated from Eq.(6-6).

Figure 6.4 presents the reduced osmotic second virial coefficients (B_2 / B_2^{HS}) for microgel particles dispersed in water. The hard-sphere second virial coefficient is related to the particle diameter σ by $B_2^{HS} = \frac{2\pi}{3}\sigma^3$. In Figure 6.4, the open circles are data points from static light scattering measurements and the line is calculated using Eqs. (6-8) and (6-11), with the molecular weight $M_W = 1.73 \times 10^7$ g/mol and the proportionality constant is $k_A = 6.43 \times 10^{-5}$ obtained by fitting to the experimental data. A positive osmotic second virial coefficient means that the overall inter-particle potential is repulsive. Figure 6.4 shows that below the volume-transition temperature, the PNIPAM particles behavior essentially like hard spheres. In this case, the microgel particles are in the swollen state and they contain up to 97% of water by volume. The van der Waals attraction between colloidal particles is negligible due to the close match in the Hamaker constants of the particle and the water. The reduced osmotic second virial coefficient exhibits a sharp change at the volume transition temperature, beyond which it turns negative, indicating a rise in the van der Waals attraction as the particles collapse. Figure 6.4 suggests that with temperature-dependent size and energy parameters, the Sutherland-type function captures the essential features of the interaction potential between microgel particles.

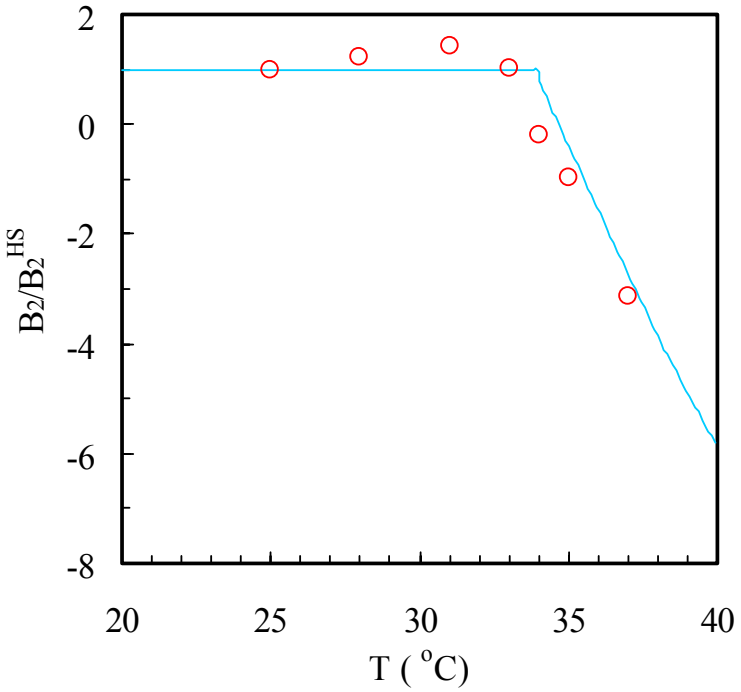

Figure 6.4: The reduced osmotic second virial coefficients (B_2 / B_2^{HS}) for PNIPAM particles dispersed in pure water. Points are from static light scattering and the line is calculated from Eq.(12) normalized by the second virial coefficient $B_2^{HS} = \frac{2\pi}{3}\sigma^3$ for the corresponding hard spheres.

Figure 6.5 shows the reduced energy parameter, $\varepsilon/(kT)$, near the volume transition temperature as obtained by correlation with the osmotic second virial coefficients from experiments. Experimental values for this parameter are not shown here because it is difficult to make a direct or indirect measurement of the reduced energy parameter. Credibility of the calculated results is reflected in the comparison of the osmotic second virial coefficients as shown in Figure 6.4. Remarkably, the energy

parameter increases over six orders of magnitude as the temperature changes from 24°C to 36 °C, with the sharpest increase at the volume transition temperature of 34 °C. Whereas the volume transition of polymer gels has been extensively studied, we are not aware of any published work on the drastic effect of volume transition on the inter-particle potential.

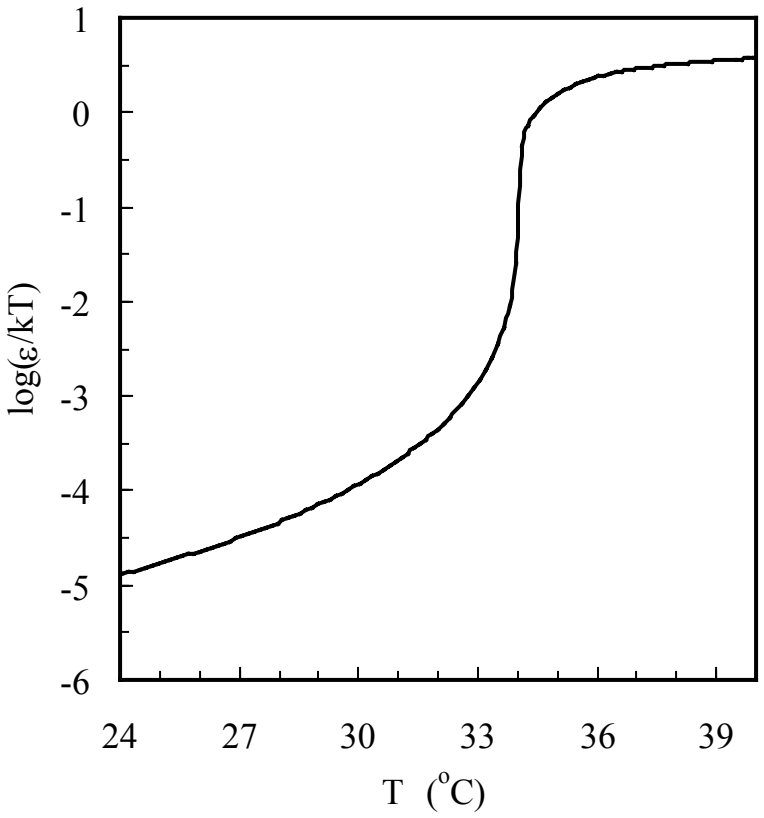

Figure 6.5: The reduced energy parameter (ε / kT) for inter-particle potential between PNIPAM particles near the volume-transition temperature.

Figure 6.6 shows the calculated phase diagram of PNIPAM microgel dispersion using first-order perturbation theory for the fluid phase (Eq.6-14) and the corrected cell

model for the solid phase (Eq.6-18). The inserted plot provides a magnified view of the freezing and melting lines near the volume transition. This phase diagram differs drastically from that for a conventional colloidal dispersion. Below the volume-transition temperature, the coexisting phases at the freezing and melting points have close particle densities, similar to that observed in a hard-sphere system. However, above the volume-transition temperature, the fluid-solid transition spans over a wide gap of particle concentrations. At high temperature, the fluid phase at the freezing point is highly dilute, while the solid phase at the melting point is highly concentrated. Interestingly, this phase diagram indicates that a microgel dispersion can freeze at temperatures both above and below the gel volume-transition temperature. For instance, according to this phase diagram, a microgel dispersion with 7 g/L particle concentration is in the fluid state at 34.5 ^{o}C; it becomes a solid of similar density when the temperature drops to about 34 ^{o}C, and the dispersion will be separated into a dilute solution and a solid of much higher density (about 17g/L) at about 35.3 ^{o}C.

The dashed line in Figure 6.6 shows a metastable fluid-fluid coexistence curve with a low critical solution temperature. This coexistence curve is reminiscent of an aqueous solution of uncross-linked PNIPAM polymer. Because of strong hydrogen bonding with water molecules from CO and NH groups, PNIPAM can be dissolved in water at a low temperature. In this case, the isopropyl groups along the PNIPAM chain are caged by water molecules. When the temperature is increased, the cages of water molecules are partially melted, resulting in an increase in entropy. As a result, upon an increase in temperature, the hydrophobic attraction due to the isopropyl groups and due to

the polymer backbone become more important and the solubility of PNIPAM in water drops.

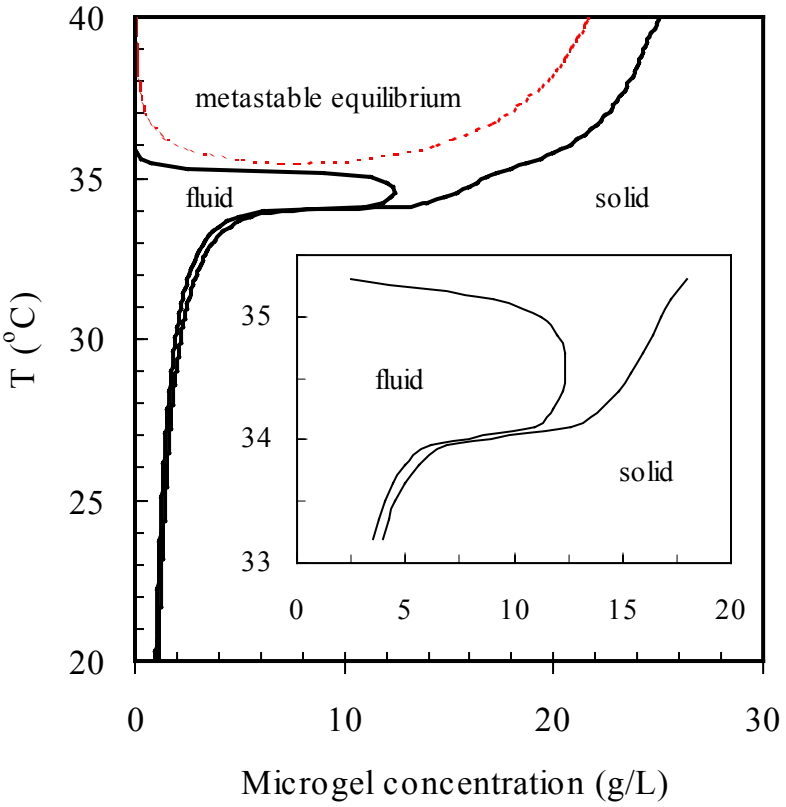

Figure 6.6: Calculated phase diagram for an aqueous dispersion of PNIPAM particles. The inserted plot shows a magnified view of the freezing and melting lines near the volume-transition temperature.

Figure 6.7 shows the phase transitions in aqueous PNIPAM dispersions determined using a UV-VIS spectrometer. In the crystalline phase, the UV-VIS spectrum exhibits a sharp attenuation peak due to the Bragg diffraction. At the crystalline melting temperature (indicated by solid circles), the peak disappears. As the temperature rises to the

phase separation temperature (indicated by open circles), the turbidity increases drastically in the entire visible frequency range, signaling a phase separation. Similar structural changes have been observed from SANS experiments.[36] While at a low temperature the

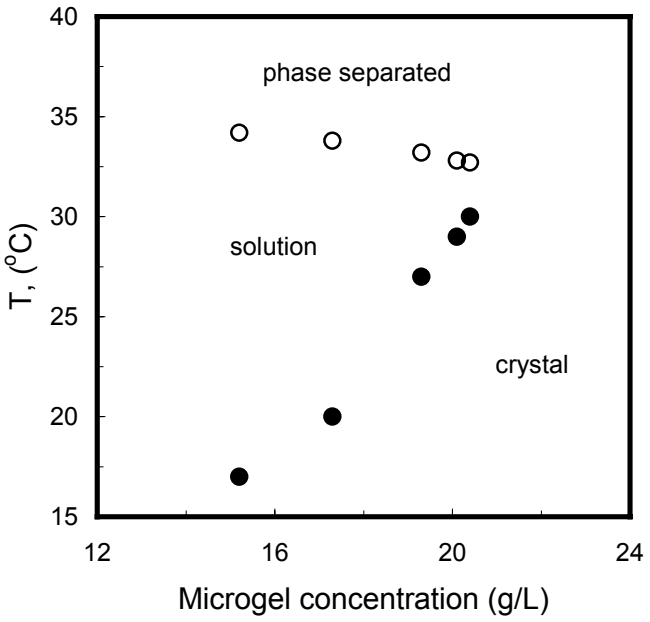

Figure 6.7: Phase diagram of an aqueous dispersion of PNIPAM particles determined from experiments. The open points designate the boundary of phase separation at high temperature and the filled points designate the temperature of colloidal crystallization.

solid phase exhibits apparent characteristics of a colloidal crystal, the phase-separated state at high temperature is much like a glass that is probably related to the metastable fluid-fluid equilibrium. In the presence of a metastable fluid-fluid equilibrium, fast kinetics of fluid-fluid transition leads to an amorphous fluid phase of high particle concentration. Figure 6.7 indicates that the experimental observations agree semi-quantitatively with the main features of the calculated phase diagram.

6.5 Conclusions

We have investigated the volume-transition equilibrium and the interaction potential between neutral PINPAM particles dispersed in pure water using static and dynamic light-scattering experiments. We show that the modified Flory-Rehner theory gives an excellent description of the microgel swelling equilibrium. Using the temperature-dependent size and energy parameters, the Sutherland-like potential provides a reasonable representation of the inter-particle potential for PNIPAM particles in swollen and in collapsed phases. The phase diagram calculated from a first-order perturbation theory and an extended cell model indicates that an aqueous dispersion of PNIPAM particles can freeze at both high and low temperatures. At low temperature, the freezing occurs at large particle volume fraction, similar to that in a hard-sphere system; while at high temperature, the freezing occurs at low particle concentration, driven by the strong van der Waals attraction due to the collapsed microgel particles. The calculated phase diagram has been confirmed semi-quantitatively by experiments.

In many aspects, the phase behavior of colloidal dispersions reassembles that for simple fluids. However, a noticeable difference is that unlike the vapor-liquid equilibrium of a simple fluid, the equilibrium between a dilute and a concentrated colloidal dispersion is often metastable. Whereas that difference, arising for the short-ranged solvent-mediated attraction between colloidal particles, is now well-documented, not much attention has been given to other features that are unique in colloidal systems. The temperature-dependent potential as shown in this work is specific in colloidal systems. Because the inter-particle potential is strongly temperature-dependent, the

phase behavior of PNIPAM dispersions differs remarkably from that for simple fluids or for conventional colloids. In future work it might be interesting to investigate other features that are special to colloidal dispersions, including the multi-body effect on the phase behavior and dissimilarity of inter-particle potential in different phases.

6.6 Additional Information: Radial distribution function of a hard-sphere solid

To obtain the radial distribution function of hard spheres in an fcc lattice, we use a procedure similar to that proposed by Rascon et al.[37] The radial distribution function around an arbitrary tagged particle can be represented by the summation of an empirical exponential function for the first layer, and Gaussian distributions in the remaining layers

$$g_S^{HS}(x) = \frac{A}{x} e^{-\alpha_1 (x - R_1)/2} + \frac{1}{24\eta} \sqrt{\alpha / 2\pi} \sum_{i \geq 2} \frac{n_i}{x R_i} \left[e^{-\alpha (x - R_i)/2} + e^{-\alpha (x + R_i)/2} \right] . \quad \text{(A1)}$$

In Eq.(A1), $x = r/\sigma$, n_i is the number of particles in the i^{th} neighboring layer from the tagged particle, R_i represents the center-to-center distance between a particle in the i^{th} layer and the tagged particle, and A, α_1 and α are yet-to-be determined parameters. For an fcc lattice, the Gaussian parameter α in Eq.(A1) is related to particle density

$$\alpha = \left(\frac{\sqrt{3}\pi}{4} \right)^{2/3} \left[\left(\frac{\sqrt{2}}{\rho \sigma^3} \right)^{1/3} - 1 \right]^{-2} . \quad \text{(A2)}$$

The parameters A, α_1 and R_1 in Eq.(A1) can be determined by requiring that the radial distribution function gives the exact number of particles within the first layer, the exact

mean distance between immediate neighboring particles, and a contact value that is consistent with the corresponding equation of state. By imposing these requirements, the parameters A, α_1 and R_1 can be solved from

$$4\pi\rho A\int_1^\infty xe^{-\alpha_1(x-R_1)/2}dx = n_1, \quad \text{(A3)}$$

$$\frac{4\pi\rho}{n_1}\int_1^\infty x^2 e^{-\alpha_1(x-R_1)/2}dx = R_1, \quad \text{(A4)}$$

$$z = 1 + 4\eta A e^{-\alpha_1(1-R_1)/2}, \quad \text{(A5)}$$

where z stands for the compressibility factor of the hard-sphere solid. According to the modified cell model, the compressibility factor z is given by

$$z = 1/[1-(\rho\sigma^3/\sqrt{2})^{1/3}]. \quad \text{(A6)}$$

In this work, we assume that the correlation beyond the first five lattice layers does not make significant contribution to the thermodynamic properties. The number of particles (n_i) in the first fives layers are given by[38]

$$(12,6,24,12,24) \quad \text{(A7)}$$

and the corresponding distances (R_i) from the central particle, in units of lattice constant a, are

$$(1, \sqrt{2}, \sqrt{3}, \sqrt{4}, \sqrt{5}). \quad \text{(A8)}$$

Chapter References

(1) Pusey, P. N. In *Liquid, Freezing, and the Glass Transition*; Les Houches, J. P., Levesque, H. D., Zinn-Justin, J., Eds.: Elsevier, Amsterdam, 1990.

(2) Poon, W.; Pusey, P.; Lekkerkerker, H. *Phys World* **1996**, *9*, 27.

(3) Frenkel, D. *Science* **2002**, *296*, 65.

(4) Velev, O. D.; Lenhoff, A. M.; Kaler, E. W. *Science* **2000**, *287*, 2240.

(5) Xia, Y. N.; Gates, B.; Yin, Y.; Lu, Y. *Advanced Materials* **2000**, *12*, 693.

(6) Pelton, R. H.; Chibante, P. *Colloids and Surfaces* **1986**, *20*, 247.

(7) Pelton, R. *Advan Colloid Interface Sci* **2000**, *85*, 1.

(8) Saunders, B. R.; Vincent, B. *Advan Colloid Interface Sci* **1999**, *80*, 1.

(9) Kawaguchi, H. *Prog Polym Sci* **2000**, *25*, 1171.

(10) Fernandez-Nieves, A.; Fernandez-Barbero, A.; Vincent, B.; de las Nieves, F. J. *Macromolecules* **2000**, *33*, 2114.

(11) Laukkanen, A.; Hietala, S.; Maunu, S. L.; Tenhu, H. *Macromolecules* **2000**, *33*, 8703.

(12) Gao, J.; Hu, Z. B. *Langmuir* **2002**, *18*, 1360.

(13) Hellweg, T.; Dewhurst, C. D.; Bruckner, E.; Kratz, K.; Eimer, W. *Colloid Polym Sci* **2000**, *278*, 972.

(14) Senff, H.; Richtering, W. *J Chem Phys* **1999**, *111*, 1705.

(15) Debord, J. D.; Lyon, L. A. *J. Phys. Chem.* **2000**, *104*, 6327.

(16) Hu, Z. B.; Wang, C. J.; Chen, Y. Y.; Zhang, X. M.; Li, Y. *J Polym Sci B-Polym Phys* **2001**, *39*, 2168.

(17) Hirotsu, S.; Hirokawa, Y.; Tanaka, T. *J. Chem. Phys.* **1987**, *87*, 1392.

(18) Peppas, N. A.; Huang, Y.; Torres-Lugo, M.; Ward, J. H.; Zhang, J. *Annu Rev Biomed Eng* **2000**, *2*, 9.

(19) Martinez-Rubio, M. I.; Ireland, T. G.; Fern, G. R.; Silver, J.; Snowden, M. J. *Langmuir* **2001**, *17*, 7145.

(20) Weissman, J. M.; Sunkara, H. B.; Tse, A. S.; Asher, S. A. *Science* **1996**, *274*, 959.

(21) Lee, K.; Asher, S. A. *J Am Chem Soc* **2000**, *122*, 9534.

(22) Hu, Z. B.; Lu, X. H.; Gao, J. *Advanced Materials* **2001**, *13*, 1708.

(23) Wu, J. Z.; Sassi, A. P.; Blanch, H. W.; Prausnitz, J. M. *Polymer* **1996**, *37*, 4803.

(24) Ogawa, K.; Wang, B.; Kokufuta, E. *Langmuir* **2001**, *17*, 4704.

(25) Gilanyi, T.; Varga, I.; Meszaros, R.; Filipcsei, G.; Zrinyi, M. *Phys Chem Chem Phys* **2000**, *2*, 1973.

(26) Saunders, B. R.; Crowther, H. M.; Morris, G. E.; Mears, S. J.; Cosgrove, T.; Vincent, B. *Colloid Surface A* **1999**, *149*, 57.

(27) Wu, C.; Zhou, S. Q.; Auyeung, S. C. F.; Jiang, S. H. *Angew Makromol Chem* **1996**, *240*, 123.

(28) Hino, T.; Prausnitz, J. M. *J Appl Polym Sci* **1996**, *62*, 1635.

(29) Flory, P. J. *Principles of polymer chemistry*; Cornell University Press: Ithaca, 1953.

(30) Guillermo, A.; Addad, J. P. C.; Bazile, J. P.; Duracher, D.; Elaissari, A.; Pichot, C. *J Polym Sci B-Polym Phys* **2000**, *38*, 889.

(31) Israelachvili, J. N. *Intermolecular and Surface Forces*; 2nd ed.; Academic Press: London, 1992.

(32) GilVillegas, A.; Galindo, A.; Whitehead, P. J.; Mills, S. J.; Jackson, G.; Burgess, A. N. *J Chem Phys* **1997**, *106*, 4168.

(33) Hansen, J. P.; McDonald, I. R. *Theory of Simple Liquids*; 2nd ed.; Academic Press: London, 1986.

(34) Wu, J. Z.; Prausnitz, J. *Fluid Phase Equilibria* **2002**, *194*, 689.

(35) Lennard-Jones, J. E.; Devonshire, A. F. *Proc. R. Soc. London, Ser A.* **1937**, *163*, 53.

(36) Kratz, K.; Hellweg, T.; Eimer, W. *Polymer* **2001**, *42*, 6631.

(37) Rascon, C.; Mederos, L.; Navascues, G. *Phys Rev E* **1996**, *54*, 1261.

(38) Hirschfelder, J. D.; Curtis, C. F.; Bird, R. B. *Molecular Theory of Gases and Liquids*; Wiley: New York, 1964.

CHAPTER 7

CONCLUSIONS

This dissertation describes on the synthesis and study of novel hydrogel nanoparticle networks, including their application in controlled drug release and sensors.[1-4] In addition, the inter-particle potential in the PNIPAM microgel dispersion has been correlated with particle synthesis conditions.[5] The main conclusions are summerized as follows:

(1) Mono-disperse nanoparticles of poly-N-isopropylacrylamide-co-allylamine and PNIPAM-co-acrylic acid were synthesized. The close packed PNIPAM-co-allylamine and PNIPAM-co-AA nanoparticles were converted into three dimensional gel networks by convalently cross-linking neighboring particles at room temperature and neutral pH using glutaric dialdehyde and adipic acid dihydrazide, respectively. The phase behaviors of both particles were investigated by combining static and dynamic laser light scattering techniques. It was observed that the PNIPAM-co-allylamine particles exhibited a similar phase transition to the homo-PNIPAM particles, and shrank substantially when the temperature increased to 37 °C. In contrast, the phase transition of PNIPAM-co-AA particles occured at a broader and higher temperature range because of the ionization of AA at neutral pH. Controlled release studies were conducted using dextran markers of various molecular weights as model for macromolecular drugs. Release was quantified under various physical conditions, including a range of temperatures and dextran molecular weights. It was found that dextran entrapped between particle cavities in the

nanoparticle network was released with a rate regulated by their molecular weights and the cavity size, compared with the conventional bulk PNIPAM gel. The release of dextran macromolecules from the PNIPAM-co-allylamine networks was much faster at room temperature than that at human body temperature. As to the PNIPAM-co-AA networks, a temperature-independent release profile for the different dextran macromolecules was shown. Creating the PNIPAM derivative nanoparticle networks allowed useful functionality for controlled drug release not only from the constituent building blocks but also from their close-packed particle structures.

(2) A new kind of crystalline hydrogel with high polymer concentration was developed. According to the phase diagram of the PNIPAM-co-allylamine particle dispersions determined by using UV-VIS spectrophotometry, we initiated the crystallinization process near the colloidal crystal melting temperature while subsequently bonding the PNIPAM-co-allylamine particles below the glass transition temperature. The mechanical strength of this crystalline hydrogel was significantly improved. Iridescent color patterns could be observed in the crystalline hydrogels with different polymer concentrations. Because the lattice spacing between the particles could be tunable by external stimuli, this crystalline hydrogel can serve as an optical sensor to visually reveal environmental changes. The color change from green to blue could be observed when the temperature increased from 21 to 34 ºC or the pH value switched from 7 to 11. This process is totally reversible. Such soft and wet hydrogels with periodic structures may lead to new sensors, devices, and displays operating in aqueous solutions that most biological and biomedical systems reside.

(3) UV-VIS spectrophotometry has been used to characterize the potential applications of the crystalline hydrogel as the optical sensors. The mechanical strength of this crystalline hydrogel was demonstrated by measuring the shear modulus of the networks. It was found that their shear moduli were substantially improved, and increased with the concentration of the polymer. The shear modulus also increased upon the decrease of the particle size at a fixed polymer concentration. When increasing the environmental temperature, the Bragg peaks, derived from the diffraction of the crystals inside the hydrogel, shifted to a shorter wavelength. When the pH value of the environment changed from 7 to 12, the wavelength of the Bragg peak shifted from 633 to 556 nm. In addition, this kind of crystalline hydrogel could also respond to protein solutions. When the concentration of bovine serum albumin (BSA) increased from 0.05 to 1 wt%, the Bragg peak shifted from 570 to 486nm, leading to new applications of sensors operating in biological and chemical systems.

(4) The volume transition and the interaction potential between neutral PNIPAM particles dispersed in pure water were investigated by using static and dynamic laser light scattering experiments. The modified Flory-Rehner theory gave an excellent description of the microgel swelling equilibrium. Using the temperature-dependent size and energy parameters, the Sutherland-like potential provided a reasonable representation of the inter-particle potential for PNIPAM particles in swollen and in collapsed phases. The phase diagram calculated from a first-order perturbation theory and an extended cell model indicates that an aqueous dispersion of PNIPAM particles can freeze at both high and low temperatures. At low temperature, the freezing occurs at large particle volume

fraction, similar to that in a hard-sphere system; while at high temperature, the freezing occurs at low particle concentration, driven by the strong van der Waals attraction due to the collapsed microgel particles. The calculated phase diagram has been confirmed semi-quantitatively by experiments.

Chapter References

1. Huang, G., Gao, J., Hu, Z.B., John, J.V., Ponder, B.C., Moro, D. *J. of Controlled release*; **2004**, 94, 303.
2. Hu, Z.B., Huang, G. *Angew Chem Inter. Ed*., **2003**, 42, 4799.
3. Hu, Z.B., Lu, X., Gao, J., Huang, G. " Synthesis and composition of crystal hydrogels" *U. S. Patent*, *Disclosure filed* (November 2001).
4. Huang, G., Hu, Z.B. (to be submitted).
5. Wu, J., Huang, G., Hu, Z.B. *Macromolecules;* **2003**; 36, 440.

APPENDIX

List of Abbreviations

AA	Acrylic acid
BIS	Methylene-bis-acrylamide
CMC	Critical micelle concentration
EDC	1-Ethyl-3-(3-dimethylaminopropyl) carbodiimide hydrochloride
DLS	Dynamic light scattering
LCST	Low critical solution temperature
LLS	Laser light scattering
KPS	Potassium persulfate
PCS	Photon correlation spectroscopy
PNIPAM	Poly-N-isoprpylacrylamide
R_g	Radius of gyration
R_h	Hydrodynamic radius
SDS	Sodium dodecyl sulfate
SLS	Static light scattering

BIBILOGRAPHY

Abbiss, J.b., Smart, A.E. *Photon correlation Techniques and Applications*. **1988**, OSA Proceedings.

Asher, S. A.; Alexeev, V. L.; Goponenko, A. V.; Sharma, A. C. *J. Am. Chem. Soc*. **2003**, 125, 3322.

Asher, S. A.; Sharma, A. C.; Goponenko, A. V.; Ward, M. M. *Anal. Chem*. **2003**, 75, 1676.

Bae, Y.H., Okano, T., Kim, S.W. *Pharm. Res*.**1991**, 8, 531.

Bae, Y.H., Okano, T., Kim, S.W. *Pharm. Res*. **1991**, 8, 624.

Bartsch, E.; Kirsch, S.; Lindner, P.; Scherer, T.; Stolken, S. *Ber. Bunsen-Ges. Phys. Chem.* **1998**, 102, 1597.

Berne, B.J., Pecora, R. *Dynamic Light Scattering*, John Wiley & Sons Press: New York, **1976**

Blaaderen, A. V., Ruel, R., Wiltzius, P. *Nature* **1997**, 385, 321

Brown, W. *Dynamic Light Scattering*, Oxford University Press, Oxford, **1993**

Cassagneau, T.; Caruso, F. *Adv. Mater*. **2002**, 14, No.22, 1629.

Chen, G., Hoffman, A. S. *Nature* **1995,** 373, 49.

Cheng, Z., Russel, W. B., Chaikin, P. M. *Natur*e **1999**, 401, 893

Choi, H.S., Kim, J.M., Lee, K. *J. Appl. Polym. Sci*. **1998**, 69, 895

Chu, B. *Laser Light Scattering*, 2nd edition; Academic Press, **1991**

Dagani, R. *C and EN*, **1997**, 26.

Debord, J.D., Eustis, S., Debord, S.B., Lofye, M.T., Lyon, L.A. *Adv. Mater.* **2002**, 14, 658

Debord, J.D., Lyon, L.A. *J. Phys. Chem*. **2000**, 104, 6327.

Everett, D. H. *Basic Principles of Colloid Science*, London **1998**.

Fernandez-Nieves, A.; Fernandez-Barbero, A.; Vincent, B.; de las Nieves, F. J. *Macromolecules* **2000**, *33*, 2114.

Flory, P. J. *Principles of polymer chemistry*; Cornell University Press: Ithaca,, 1953.

Frenkel, D. *Science* **2002**, *296*, 65-66.

Galaev, I. Y. *Russian Chem. Rev*. **1995**, 64(5), 471.

Gao, J., Hu, Z.B. *Langmuir* **2002**, 18, 1360.

Gilanyi, T.; Varga, I.; Meszaros, R.; Filipcsei, G.; Zrinyi, M. *Phys Chem Chem Phys* **2000**, *2*, 1973-1977.

GilVillegas, A.; Galindo, A.; Whitehead, P. J.; Mills, S. J.; Jackson, G.; Burgess, A. N. *J Chem Phys* **1997**, *106*, 4168.

Gu, Z.; Fujishima, A.; Sato, O. *J. Am. Chem. Soc.* **2000**, 122, 12387.

Guillermo, A.; Addad, J. P. C.; Bazile, J. P.; Duracher, D.; Elaissari, A.; Pichot, C. *J Polym Sci B-Polym Phys* **2000**, *38*, 889.

Gutowska, A., Bae, Y.H., Feijen, J., Kim, S.W. *J. Controlled Release* **1992**, 22, 95.

Hallett, F.R., Watton, J., Krygsman, P.H. *Biophys. J*., **1991**, 59, 357.

Hellweg, T., Dewhurst, C.D., Bruckner, E., Kratz, K., Eimer, W. *Colloid and Polymer Science* **2000**, 278, 972.

Hansen, J. P.; McDonald, I. R. *Theory of Simple Liquids*; 2nd ed.; Academic Press: London, 1986.

Hermanson, G. T. *Bioconjugate Techniques*, 1996, Academic Press: San Diego.

Hino, T.; Prausnitz, J. M. *J Appl Polym Sci* **1996**, *62*, 1635-1640.

Hirotsu, S., Hirokawa, Y., Tanaka, T. *J. Chem. Phys*. **1987**, 87, 1392.

Hirschfelder, J. D.; Curtis, C. F.; Bird, R. B. *Molecular Theory of Gases and Liquids*; Wiley: New York, **1964**.

Hoffman, A.S. *J. Controlled Release* **1987**, 6, 297

Holtz, J.H., Asher, S.A. *Nature*, **1997**, 389, 829

Hu, Z.B. , Xia, X. *Adv. Mater*., **2004**, 16(4), 305

Hu. Z.B., Lu, X., Gao, J. *Adv. Mater*. **2000**, 12, 1173

Hu, Z.B., Lu, X., Gao, J. *Adv. Mater*. **2001**, 13, 1708

Hu, Z.B., Lu, X., Gao, J., Huang, G. " Synthesis and composition of crystal hydrogels" *U. S. Patent*, *Disclosure filed* (November 2001).

Hu, Z.B., Huang, G. *Angew. Chem. Int. Ed*. **2003**, 42, 4799

Hu, Z. B.; Wang, C. J.; Chen, Y. Y.; Zhang, X. M.; Li, Y. *J Polym Sci B-Polym Phys.* **2001**, 39, 2168.

Hu, Z. B., Zhang, X., Li, Y. *Science* **1995**, 269, 525.

Hu, Z. B., Chen, Y., Wang, C., Zheng, Y., Li, Y. *Nature* **1998**, 393, 149.

Huang, G., Gao, J., Hu, Z.B., John, J.V., Ponder, B.C., Moro, D. *J. Controlled Release*; **2004**, 94, 303.

Huang, G., Hu, Z.B. (to be submitted).

Israelachvili, J. N. *Intermolecular and Surface Forces*; 2nd ed.; Academic Press: London, 1992.

Jethmalani, J. M., Sunkara, H. B., Ford, W. T., Willoughby, S. L., Ackerson, B. J. *Langmuir* **1997**, 13, 2633.

Jiang, P., Bertone, J. F., Colvin, V. L. *Science* **2001**, 291, 453

Jones, C.D., Lyon, L.A. *Macromolecules*, **2000**, *33*, 8301.

Jones, C.D., Lyon, L.A. *Macromolecules*, **2003**, *36*, 1988.

Jones, C. D.; Lyon, L. A. *J. Am. Chem. Soc*. **2003**, 125, 460.

Kabra, B. G., Gehrke, S. H., Spontak, R. J. *Macromolecules* 1998, 31, 2166; Gehrke, S. H., in: Amidon, G.L., Lee, P.I., Topp, E.M. (Eds.), *Marcel Dekker* New York, 2000, 473.

Kawaguchi, H. *Prog Polym Sci* **2000**, 25, 1171.

Kratz, K.; Hellweg, T.; Eimer, W. *Polymer* **2001**, 42, 6631.

Laukkanen, A.; Hietala, S.; Maunu, S. L.; Tenhu, H. *Macromolecules* **2000**, *33*, 8703.

Lee, K.; Asher, S. A. *J. Am. Chem. Soc*. **2000**, 122, 9534-9537

Lee, Y.; Braun, P. V. *Adv. Mater*. **2003**, 15, No. 7-8, 563.

Lee, Y. Pruzinsky, S. A., Braun, P. V. *Langmuir* **2004**, 20, 3096.

Lellig, C., Hartl, W., Wagner, J., Hempelmann, R. *Angew. Chem. Int. Ed*. **2002**, 41, 102.

Lendlein, A., Kelch, S. *Angew. Chem. Int. Ed*. **2002**, 41, 2034.

Lennard-Jones, J. E.; Devonshire, A. F. *Proc. R. Soc. London, Ser A.* **1937**, *163*, 53.

Martinez-Rubio, M. I.; Ireland, T. G.; Fern, G. R.; Silver, J.; Snowden, M. J. *Langmuir* **2001**, *17*, 7145-7149.

Murry, M. J.; Snowden, M. J. *Adv. Colloid Interface Sci.* **1995**, 54, 73.

Nakayama, D., Takeoka, Y., Watanabe, M., Kataoka, K. *Angew. Chem. Int. Ed*. **2003**, 42, 4197.

Ogawa, K.; Wang, B.; Kokufuta, E. *Langmuir* **2001**, *17*, 4704.

Okano, T., Bae, Y.H., Jacobs, H., Kim, S.W. *J. Controlled Release* **1990**, 11, 255.

Okuyama, Y., Yoshida, R., Sakai, K., Okano, T., Sakurai, Y. *J. Biomater. Sci. Polym. Ed.* **1993**, 4, 545.

Osada, Y., Gong, J. P. *Adv. Mater.* **1998**, 10, 827.

Osada, Y., Okuzaki, H., Hori, H. *Nature* **1992**, 355, 242.

Osada, Y., Ross-Murphy, S. B. *Sci. Am*. May **1993**, 82.

Ostrowsky, N., Sornette, D., Parker, P., Pike, E.R. *Opt. Acta*., **1981**, 28, 1059.

Pan, G. S.; Kesavamoorthy, R.; Asher, S. A. *J. Am. Chem. Soc*. **1998**, 120, 6525

Pelton, R. *Adv. Colloid Interface Sci.* **2000**, 85, 1.

Pelton, R. H., Chibante, P. *Colloids Surf*. **1986**, 20, 247.

Peppas, N. A.; Huang, Y.; Torres-Lugo, M.; Ward, J. H.; Zhang, J. *Annu Rev Biomed Eng* **2000**, 2, 9.

Peppas, N. A., Langer, R. *Science*, **1994**, 263, 1715.

Poon, W.; Pusey, P.; Lekkerkerker, H. *Phys World* **1996**, 9, 27.

Provencher, S.W. *Biophys. J*. **1976**, 16, 29

Provencher, S.W. *Makromol. Chem*. **1979**, 180, 20

Pusey, P. N. *Liquid, Freezing, and the Glass Transition*, Elsevier, Amsterdam, **1990**.

Qiu, Y., Park, K. *Advanced Drug Delivery Reviews* **2001**, 53, 321.

Rascon, C.; Mederos, L.; Navascues, G. *Phys Rev E* **1996**, 54, 1261.

Reese, C.E. Mikhonin, A.V., Kamenjicki, M., Tikhonov, A. Asher, S.A. *J. Am. Chem. Soc.* **2004**, 126, 1493.

Russel, W. B., Saville, D. A., Schowalter, W.R. *Colloidal Dispersions*, Cambridge University Press, Cambridge **1989**

Saunders, B. R.; Crowther, H. M.; Morris, G. E.; Mears, S. J.; Cosgrove, T.; Vincent, B. *Colloid Surface A* **1999**, 149, 57.

Saunders, B. R.; Vincent, B. *Adv. Colloid Interface Sci*. **1999**, 80, 1.

Schosseler, F.; Ilamin, F.; Candau, S. J. *Macromolecules*, 1991, 24, 225.

Senff, H.; Richtering, W. *J. Chem. Phys.* **1999**, 111, 1705.

Senff, H.; Richtering, W. *Langmuir* **1999**, 15, 102.

Sharma, A.C., Jana, T., Kesavamoorthy, R., Shi, L., Virji, M.A., Finegold, D.N., Asher, S. A. *J. Am. Chem. Soc*. **2004**, 126, 2971.

Siegel, R. A., Firestone, B. A. *Macromolecules* **1988***,* 21, 3254.

Snowden, M. J., Murray, M. J., Chowdry, B. Z. *Chemistry & Industry* **1996**, 531.

Snowden, M.J., Chowdhrym B.Z., Vincent, B. *J. Chem. Soc., Faraday Trans*. **1996**, 92(24), 5013.

Sun, S.T., Nishio, I., Swislow, G., Tanaka, T.J. *J. Chem. Phys*. **1980**, 73, 5971.

Tanaka, T. *Phys. Rev. Lett.* **1978**, 40, 820.

Tanaka, T. *Experimental Methods in Polymer Science*; Academic Press, **2000**

Tanaka, T., Nishio, I., Sun, S. T., Ueno-Nishio, S. *Science* **1982**, 218, 467.

Velev, O. D.; Lenhoff, A. M.; Kaler, E. W. *Science* **2000**, 287, 2240.

Wang, C., Stewart, R. J., Kopecek, J. *Nature*, **1999**, 397, 417.

Weissman, J.M., Sunkara, H.B., Tse, A.S., Asher, S.A. *Science*, **1996**, 274, 959.

Wu, J.Z., Huang, G., Hu, Z.B. *Macromolecules* **2003**, *36*, 440.

Wu, J.Z., Zhou, B., Hu, Z.B. *Phys. Rev. Lett*. **2003**, 90, 048304.

Wu, J. Z.; Sassi, A. P.; Blanch, H. W.; Prausnitz, J. M. *Polymer* **1996**, 37, 4803.

Wu, J. Z.; Prausnitz, J. *Fluid Phase Equilibria* **2002**, *194*, 689.

Wu, C. Chan, K.K., Xia, K.Q. *Macromolecules* **1995**, 28, 1032.

Wu, C.; Zhou, S. Q.; Auyeung, S. C. F.; Jiang, S. H. *Angew Makromol Chem* **1996**, *240*, 123.

Xia, Y.; Gates, B.; Yin, Y.; Lu, Y. *Adv. Mater*. **2000**, 12, 693.

Xia, X., Hu, Z. *Langmuir,* **2004**; *20*(6), 2094.

Xia, Y. *Adv. Mater*. **2001**, 13, 369.

Xu, X.; Majetich, S. A.; Asher, S. A. *J. Am. Chem. Soc*. **2002**, 124, 13864.

Zhang, G., Wu, C. *J. Am. Chem. Soc*. **2001**, 123, 1376.

Zimm, B.H. *J. Chem. Phys*. **1948**, 16, 10